"Investigation of Selective Binding Interactions for Analytical Separation and Determination of Pharmaceuticals and Toxins"

By

Wayne M. Mullett, B.Sc.

A dissertation submitted to the Faculty of Graduate Studies in partial fulfillment of the requirements for the degree of Doctor of Philosophy

Department of Chemistry
Ottawa, Ontario, Canada
K1S 5B6

April 2000

ABSTRACT

The technique of molecular imprinting was employed to produce a polymer material that was utilized as a chromatographic stationary phase and solid phase adsorbent for the improved separation of the asthmatic drug theophylline and interferents from human serum samples. The molecular imprinting technique was based on creating cavities, in a highly cross-linked polymer matrix, which corresponded to the size and shape of the print molecule. Removal of theophylline print molecule by solvent extraction left behind monomer functional groups at defined positions in a spatial arrangement that was complementary to the structure of theophylline. The MIP material possessed an inherent selectivity for the print molecule and was resistant to mechanical stress, heat, acids, bases, water and organic solvents.

The ground polymer particles were packed into a column. Solvents with ranging chemical properties such as polarity and protic nature eluted theophylline through the MIP column and the degree of theophylline retention was determined. These studies elucidated the molecular recognition process that provided the selective binding of theophylline. More specifically, the roles of intermolecular interactions such as hydrogen bonding and electrostatic forces between the theophylline molecule in a sample solution and the functional groups of the MIP cavities were implicated in the molecular recognition process.

The molecular recognition of theophylline by the MIP column was optimized in the presence of non-polar and aprotic solvents, which were unable to interfere with the hydrogen bonding and electrostatic interactions. This resulted in the complete retention of theophylline

while interfering compounds were flushed through the column by the solvents. The bound theophylline could rapidly be desorbed from the column with a very small volume (20 μL) of a polar and protic solvent for quantification by UV detection. The developed approach was labeled molecularly imprinted solid phase extraction – pulsed elution (MISPE-PE). The MISPE-PE technique also allowed for analyte enrichment or preconcentration through injection of a relatively large volume of dilute sample solution, thus improving the detection limit of theophylline.

A micro-column was evaluated for faster analysis times and more complete removal of the theophylline from the column. In addition, the roles of solvent flow rate and column temperature were investigated to ensure maximal diffusion of theophylline to the selective cavities of the MIP particles. Any non-specifically bound compounds were removed by an intermediate 20-μL wash with an appropriately chosen solvent before theophylline removal from the column. Application of this analytical method, MISPE- differential pulsed elution (DPE), is demonstrated for accurate determination of theophylline in human blood serum over a linear range of 2 μg/mL to at least 20 μg/mL. The MISPE-DPE approach was also validated with MIP micro-columns prepared for the selective determination of nicotine and 4-aminopyridine.

Surface plasmon resonance (SPR) was successfully incorporated into an immunosensor format for the simple, rapid and non-labeled assay of fumonisin FB_1 (a mycotoxin). Polyclonal antibodies produced against FB_1 were adsorbed onto a thin gold film substrate, which was coupled to a glass prism in the Kretschmann configuration. The output beam of a

planar light emitting diode was focused through the prism to excite SPR at the surface of the gold film. When a sample containing FB_1 was added to a cell on the outside of the gold film, the angular profile of the reflected light intensity shifted. This changed the resonance angle and the reflected light intensity at a selected angle, both of which were proportional to the FB_1 concentration. After optimization of the antibody overlayer, a detection limit of 50 ng/mL was obtained for the direct assay with an analysis time of under 10 min. Multiple sample additions and large-volume sample circulation can be used with the high-affinity antibodies to achieve lower detection limits.

PUBLICATIONS and PRESENTATIONS

Publications

1. Mullett, W.M., Mohammed, I., Lai, E.P.C. and Yeung, J. "Peanut Allergen Detection in Food by Surface Plasmon Resonance Immunoassay". In preparation.

2. Mullett, W.M., Dire, M.F., Lai, E.P.C., He, X.W. "Determination of 4-Aminopyridine by Selective Solid Phase Extraction with a 2-Aminopyridine Molecularly Imprinted Polymer Micro-column". (2000) Analytica Chimica Acta, 414, 123-131.

3. Mullett, W.M., Lai, E.P.C. and Yeung, J. "Development of Surface Plasmon Resonance Based Immunoassays - A Critical Review". (1999) Methods, A Companion to Methods in Enzymology, in press.

4. Mullett, W.M., Lai, E.P.C. "Rapid Determination of Theophylline in Serum by Selective Extraction using a Heated Molecularly Imprinted Polymer Micro-column with Differential Pulsed Elution". (1999) Journal of Pharmaceutical and Biomedical Analysis, 21, 835-843.

5. Mullett, W.M., Lai, E.P.C. and Sellergren, B. "Determination of Nicotine in Tobacco by Molecularly Imprinted Solid Phase Extraction with Differential Pulsed Elution". (1999) Analytical Communication, 36, 217-220.

6. Mullett, W.M. and Lai, E.P.C. "Molecularly Imprinted Solid Phase Extraction Micro-column with Differential Pulsed Elution for Theophylline Determination in Serum". (1999) Microchemical Journal, 61,143-155.

7. Mullett, W.M. and Lai, E.P.C. "Determination of Theophylline in Serum by Molecularly Imprinted Solid-Phase Extraction with Pulsed Elution". (1998) Analytical Chemistry, 17, 3636-3647.

8. Mullett, W.M. and Lai, E.P.C. "Immunoassay of Fumonisins by a Surface Plasmon Resonance Biosensor". (1998) Analytical Biochemistry, 258, 161 - 167.

9. Owega, S., Lai, E.P.C and Mullett, W.M. "Laser Desorption Ionization of Gramicidin S on Thin silver Films with Matrix Isolation in Surface Plasmon Resonance Excitation". (1998) Journal of Photochemistry and Photobiology, 119, 123-136.

Conference Presentations

1. 83rd Canadian Society for Chemistry Conference and Exhibition, University of Calgary, Calgary, AB, Canada. May 27-May 31, 2000. "Investigation of Selective Binding Interactions for the Rapid Determination of Various Pharmaceutical Compounds by Molecularly Imprinted Solid Phase Extraction – Differential Pulsed Elution". Mullett, W.M. and Lai, E.P.C.

2. 82nd Canadian Society for Chemistry Conference and Exhibition, Zerox Research Center of Canada, Toronto, ON, Canada. May 30-June 2, 1999. "Determination of Theophylline in Serum by Solid Phase Extraction with Differential Pulsed Elution Using a Molecularly Imprinted Micro-column". Mullett, W.M. and Lai, E.P.C.

3. 81st Canadian Society for Chemistry Conference and Exhibition, Simon Fraser University, Whistler, BC, Canada. May 31-June 1, 1998. "Molecularly Imprinted Polymer Column for HPLC Separation and Pulsed-elution SPE of Theophylline in Serum Analysis". Mullett, W.M. and Lai, E.P.C.

4. 80th Canadian Society for Chemistry Conference and Exhibition, University of Windsor, Windsor, ON, Canada. June 1-4, 1997. "Immunoassay of Fumonisins and Base-Hydrolysis Products by a Surface Plasmon Resonance Sensor". Mullett, W.M. and Lai, E.P.C.

5. Varian Day Lecture, Carleton University, Ottawa, ON, Canada. April 14,1997. "Immunoassay of Fumonisins by a Surface Plasmon Resonance Biosensor". Mullett, W.M and Lai, E.P.C.

Poster Presentations

1. 219th American Chemical Society National Meeting, San Francisco, California, USA. March, 2000. "Is Biosensor a Viable Method for Food Allergen Detection?" Yeung, J. M., Lai, E.P.C. Lai and Mullett, W.M.

2. 6th Ottawa Life Sciences National Conference and Exhibition, Ottawa ON, Canada. November, 1999. "Development of Plastic Antibodies for the Selective Solid Phase Extraction and Rapid Determination of Various Pharmaceuticals." Mullett, W.M and Lai, E.P.C.

3. Ottawa-Carleton Chemistry Institute Symposium, Ottawa, ON, Canada. May 1999. "Rapid Determination of Theophylline in Serum by Selective Extraction using a Molecularly Imprinted Polymer Micro-column." Mullett, W.M and Lai, E.P.C.

4. 5th Ottawa Life Sciences National Conference and Exhibition, Ottawa, ON, Canada. November, 1998. "Molecularly Imprinted Solid Phase Extraction Micro-column with Differential Pulsed Elution for Theophylline Determination in Serum." Mullett, W.M and Lai, E.P.C

5. Ottawa-Carleton Chemistry Institute Symposium, Ottawa, ON, Canada. May 1998. "Molecularly Imprinted Polymer Column for SPE-Pulsed Elution of Theophylline in Serum Analysis." Mullett, W.M and Lai, E.P.C.

6. Ottawa-Carleton Chemistry Institute Symposium, Ottawa, ON, Canada. May 1997. "Immunoassay of Fumonisins by a Surface Plasmon Resonance Biosensor". Mullett, W.M and Lai, E.P.C.

ACKNOWLEDGEMENTS

There are numerous people, over the years, who have brought me to this point but due to space limitations, I shall only highlight a few.

I would like first to acknowledge my thesis supervisor, Dr. E.P.C. Lai. From his initial guidance, during my summer employment at Carleton many years ago, he has fostered my growth as a scientist. I am deeply appreciative of his inspirational words, patience, and interest in me over the last several years.

During my thesis research, several productive research collaborations have been initiated and have flourished. Dr. Jupiter Yeung, at the National Food Processors Association in Washington, USA, has provided me with valuable advice and many free supplies during the SPR immunoassay studies. Likewise, Dr. Sellergren, at the Johannes Gutenberg University in Mainz, Germany and Dr. Xiwen He at Nankai University in Tianjin, China, have kindly offered reagents allowing me to test further the developed MIP methods. Dr. Hindmarch at the Ottawa General Hospital, Ottawa, Canada was also kind enough to contribute the human serum samples. I respect this collaborative "wealth of knowledge" and hope to maintain these ties for productive future relationships.

I would also like to thank Dr. Burk, Dr. Wigfield, Dr. Hollebone and Dr. Buist, from the Chemistry Department, for providing me with valuable information and advice. I cannot forget the technical staff, namely Fred Cassalman, Jim Logan, Tony O'Neil and Wayne Archer, for helping me through the setup of many experiments, Robert Kehle my supplier of

chemicals and Luc Lalande, from Carleton's Office of Technology & Research Development, for showing me the way towards the commercial potential of my research. My time at Carleton was also made easier with graduate scholarships from Agriculture and Agrifood Canada and the Ontario Graduate Scholarship Program.

On a lighter note, I would like to thank my colleagues, Sandy Owega for his unusual but helpful discussions and Meredith Curren for the lunches, gossip and supply of cheap American purchases that always kept my friends and I smiling.

My parents, Peter and Alice Mullett, whose patience, love and financial support have enabled me to reach my goals. I'm not sure words can describe what they have given me throughout this long (and costly) educational journey. I owe them everything and would therefore like to dedicate this thesis to them.

I will certainly not forget all my friends outside the lab who provided a "mental release" from the world of chemistry. Stan and Ellie for their hospitality and friendship; Rick, Wayne and Terry for our Friday night fun. Weekends just wouldn't be the same without you guys. Finally, Anik, who has also been there for me. I hope I can always be there for her.

I shall leave the last word to Isaac Newton who, after reflecting on his life in science, profoundly stated:

"I do not know what I may appear to the world, but to myself I seem to have been only like a boy playing in the seashore, diverting myself in now and then finding a smoother pebble or a pretty shell than ordinary, whilst the great ocean of truth lay undiscovered before me."

LIST OF TABLES

LIST OF FIGURES

LIST OF SYMBOLS

Symbol	Description
α	relative retention
Ab	antibody
θ	angle of incidence
Ag	antigen
AIBN	azo-bis(isobutyronitrile)
BSA	bovine serum albumin
ε	dielectric constant
CEC	capillary electrochromatography
EDMA	ethylene glycol dimethacrylate
ELISA	enzyme-linked immunosorbent assay
HBP	hydrogen bond parameter
HETP	height equivalent of a theoretical plate
HPLC	high performance liquid chromatography
Ig	immunoglobulin
2,4-D	2,3-dichlorophenoxyacetic acid
k	capacity factor
MAA	methacrylic acid
MIP	molecularly imprinted polymer
MISPE-DPE	molecularly imprinted solid phase extraction – differential pulsed elution
MISPE-PE	molecularly imprinted solid phase extraction –pulsed elution
n	number of points
η	refractive index
NMR	nuclear magnetic resonance
PBS	phosphate buffered saline
SPE	solid phase extraction
SPR	surface plasmon resonance
STP	standard temperature and pressure
T	temperature (°C)
TDM	therapeutic drug monitoring
THF	tetrahydrofuran
TLC	thin layer chromatography
TEA	triethylamine
TFA	trifluoric acid
TRIM	trimethylolpropane trimethacrylate
UV	ultra-violet

CHAPTER 1: GENERAL INTRODUCTION

1.1.1 Molecular Recognition in Nature

In nature, molecular recognition plays a very decisive role. The molecular building blocks of living organisms such as DNA and proteins all participate in various levels of molecular recognition. These processes are governed by the physical and chemical ability of molecules to distinguish the structures they encounter. This ability is essential to maintain control and order in living systems and has enabled life to evolve. Although nothing is certain about the origin of life, it has become widely accepted that life evolved from the interplay of small organic species. Selective interaction among these molecules gave rise to larger and more ordered biological systems possessing extensive molecular recognition capability.

Although most biological molecules are held together by strong covalent bonds, the level of molecular recognition is dictated by non-covalent forces. The individual magnitudes of non-covalent binding interactions are relatively small. However, their impact is unparalleled because of their immense numbers. In addition to the large number of individual forces, the variety of non-covalent interactions enables an unlimited capacity for recognition at the molecular level.

1.1.2 Molecular Recognition in Chemical Analysis

Analytical chemists have been able to exploit the power of molecular recognition for the better design of chemical analysis. Stable, easily available molecular recognition compounds are very useful in the development of rapid and sensitive analytical methods. Since

advancements in technology have enabled detection sensitivities in the attomole range[1], the challenge to the modern analytical chemist is the enhancement of analyte selectivity. More specifically, the progression of health and environmental care is becoming more dependent on the development of specific chemical analysis methods.[2] The ability to selectively recognize a target analyte is therefore an important parameter in chemical analysis, especially for trace analysis. Complex matrices, such as biological samples, often require time-consuming and error-prone cleanup steps to remove interferents prior to analysis. Although commercially available solid phase adsorbents provide sample pretreatment solutions, they impart little analyte selectivity. We have to look no further than our own body's immune systems to witness powerful recognition systems capable of highly specific interactions.

1.1.2.1 Natural Molecular Recognition for Chemical Analysis

In classical bioanalytical techniques, the selective recognition element is the antibody. This represents one of the best examples of molecular recognition. The machinery responsible for antibody production, the β-cells, is able to give rise to 10^7-10^9 different species.[3] They are the most common recognition structures in practical use today. The versatility was demonstrated by their use in therapeutics, diagnostic assays and purification systems. The mechanism responsible for the natural selectivity of antibodies has been a curiosity since their discovery, and consequently several theories emerged. The template theory of antibody synthesis was initially hypothesized by Pauling[4] and was since supported by other researchers[5,6]. The theory explained how the great diversity in antibody production and high selectivity were due to the formation of different three-dimensional configurations

of the antibody polypeptide chain induced by the interaction with antigens. Thus, the antibody combining sites were "molded" with the antigen as a template in a casting procedure, i.e. they were molecularly imprinted with the antigens.

The increasing knowledge base surrounding the antibody-antigen reaction has led to an explosion of analytical techniques. By combining the selectivity of antibody-antigen interactions with the vast array of antibodies that can be naturally produced, immunoassays can be designed for a variety of analytes. This technique is the fastest growing analytical technology in use for the detection and quantification of biomolecules in the diagnosis and management of disease.[7] Immunoassays are routinely used for the recognition of small molecules (such as drugs) through peptides, to large macromolecules and whole cells. However, monitoring the binding interaction between the antibody and analyte is essential for quantification purposes and several labels have been developed to meet this requirement. The most common labels include radioisotopes[8,9], enzymes[10] and fluorophors.[11] However due to preparation difficulties, time consumption and disposal costs for radioactive materials, there has been a new emphasis placed on non-labeled immunoassays. An apparent leader in this area is the optical phenomenon of surface plasmon resonance (SPR). SPR is a highly sensitive method for following optical changes at a metal surface in real time. It has shown potential as a transducing element for biosensors (or immunosensors) based on antibody–antigen interactions. Since SPR does not require labelling of the analytes under study, its potential for simplicity and reagentless immunoassays is a "Holy Grail" of immunosensor development.

Antibodies also suffer from certain limitations for their practical application in bioanalytical processes (see Table 5.1). They are relatively expensive to produce in a large

scale, their preparation is time consuming and they posses thermal and chemical limitations. However, since antibodies are at the heart of a wide range of analytical procedures, the development of synthetic counterparts is highly desirable and researchers have been working for decades to mimic the unique recognition properties of these molecules.

1.1.2.2 Alternatives to Natural Molecular Recognition for Chemical Analysis

The initial serendipitous discovery of crown ethers by Pedersen initiated the research field of host-guest interactions in supramolecular chemistry[12,13] Crown ethers possess an inner cavity that exhibits partial selectivity for certain sizes of cations. Since this time several other structures were synthesized with various levels of inherent selectivity as highlighted in a review by Lehn in 1988.[14] Although these materials evolved past the stage of scientific curiosity, their entry into practical applications has been confined due to their limited selectivity and lengthy multistep synthesis.

To date, the most successful approach for producing synthetic recognition sites has been the technique of molecular imprinting. The imprinted polymer material is composed of a three dimensional network that has a memory of the shape and functional group positions of the template molecule. This concept, inspired by Pauling's early antibody formation theory, has started a renaissance in the field of synthetic receptor sites. Although the MIP theory is incompletely, it has become obvious that forming a three-dimensional structure around a template for preparing synthetic analogues of antibodies to recognize target molecules with a similar selectivity is possible. These materials are inexpensive to prepare and easy to scale up, making them ideally suited for industrial applications.[15,16]

1.1.3 Objectives of the Thesis

The work underlying this thesis was aimed at improving our understanding of molecular recognition for the development of better chemical analysis methods. The first, larger component of the research work entailed investigations into molecularly imprinted polymers. This new class of materials was utilized as a stationary phase for the selective recognition of chosen analytes. The developed method was validated on several MIP materials selective for different pharmaceutical analytes. The second section involved an immunoassay method using natural antibodies and the optical phenomenon of surface plasmon resonance for the unlabelled detection of the fumonisin FB_1 mycotoxin.

CHAPTER 2: MOLECULAR IMPRINTING

2.1 Introduction

2.1.1 History

The concept of molecular imprinting has a long history with its roots in the area of immunology. As briefly outlined in the General Introduction, the preparation of a natural antibody may result from its structural units being selected and oriented to fit the local configuration and features of the antigen surface. Following these "instructive" theories on antibody diversity, the antibodies would be able to change their 3-D structure in order to form as many interaction points as possible with the epitomes of the antigen. As a consequence of these theories about antibodies, the idea arose that the same concept of antibody imprinting by the antigen, could be utilized in synthetic matrices. Scattered attempts were performed in the 50s, 60s, 70s and 80s but it was not until the late 80s that a real breakthrough for the technology was seen. The laboratories of Wulff[17] and Klotz[18], prepared the first organic material that possessed a predetermined selectivity. Since this time, much research interest has occurred and the versatility of MIPs becomes ever more apparent.

2.1.2 Preparation of MIPs

Currently, two basic approaches to molecular imprinting may be distinguished. The pre-organized approach entails assembly of the monomer and template species in solution

by reversible covalent bonds prior to polymerization. In the more common, self-assembly approach, the pre-arrangement between the print molecule and the functional monomers is formed by non-covalent or metal coordination interactions. Although the covalent approach will not be discussed here, both imprinting procedures make use of a high percentage of cross-linker resulting in polymers that are very rigid and insoluble.

An outline of the protocol used for the preparation of a molecularly imprinted polymer (MIP) is highlighted in Figure 2.1.2.1. Functional monomers arrange themselves around the theophylline template via non-covalent interactions and are "frozen" into position by polymerization with a high degree of cross-linking. Subsequent removal of the template leaves cavities with a complementary size, shape and arrangement of functional groups.

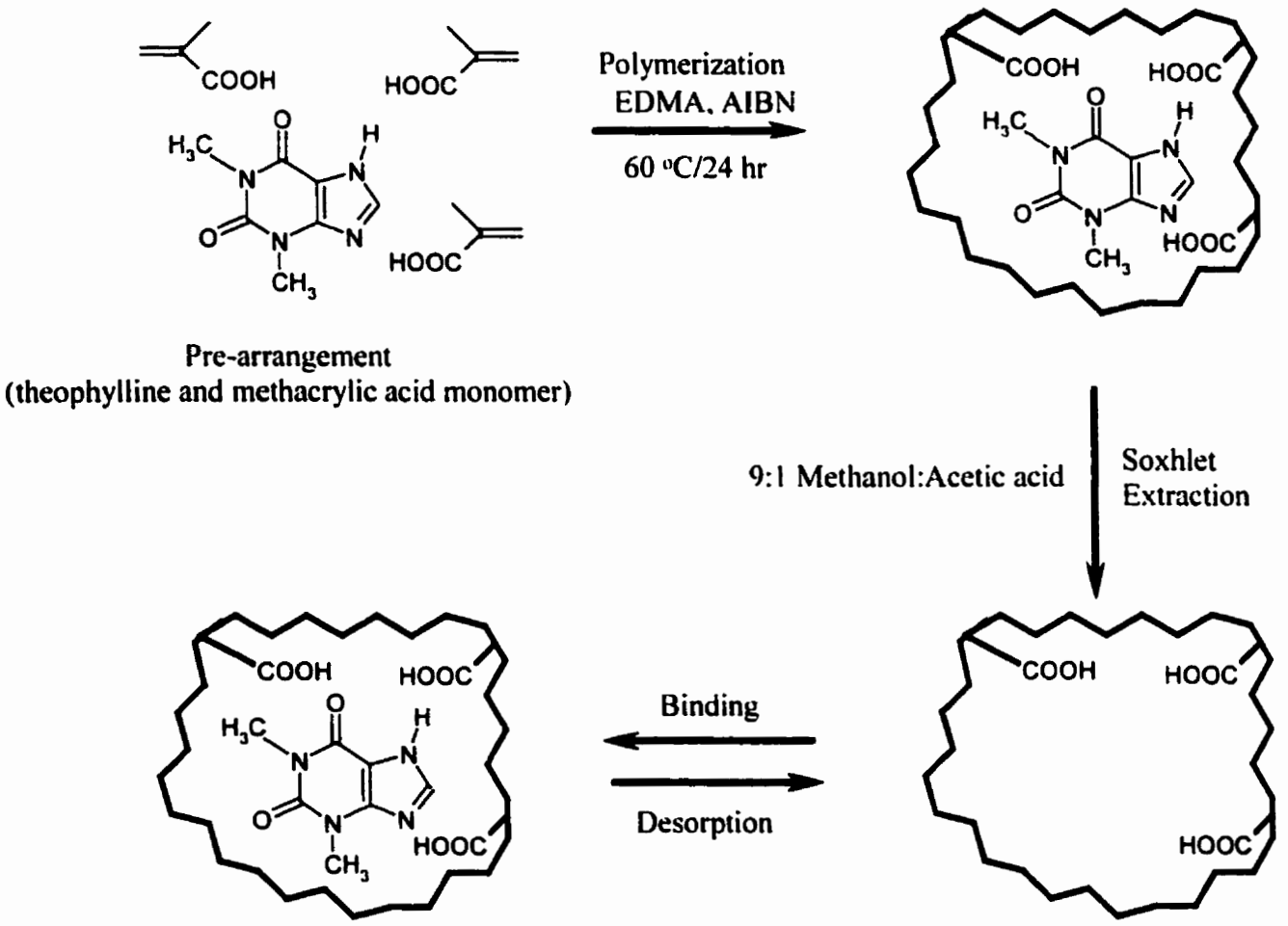

Figure 2.1.2.1: Preparation of a theophylline MIP and binding vs. desorption.

Removal of the print molecule by Soxhlet extraction leaves behind functional monomer groups at defined positions in a spatial arrangement that is complementary to the structure of the original print molecule. Intermolecular interactions (such as hydrogen bonding, dipole-dipole and ionic forces) between the print molecule in a sample solution and the functional groups of the MIP can subsequently drive the specific molecular recognition binding process.

A plethora of print molecules has been used in various imprinting protocols. A comprehensive selection of different substances is listed in Table 2.1.2.1. Compounds such as drugs, amino acids, carbohydrates, proteins, nucleotide bases, hormones, pesticides and co-enzymes have been successfully used for the preparation of selective recognition matrices. Of the imprinting strategies used, it has become evident that the use of non-covalent interactions between the print molecule and the functional monomers is the more versatile. The apparent weakness of these interaction types when considered individually may be overcome by allowing a multitude of interaction points simultaneously. Together with the fast association and dissociation kinetics of these bond types, so that in a short time many possible combinations can be checked before the correct partners associate, this protocol has proven advantageous. Furthermore, the use of non-covalent interactions in the imprinting step closely resembles the recognition process observed in nature.

Table 2.1.2.1: Compounds Employed as Templates for the Preparation of MIP Materials.

Compound Class	Examples		Compound Class	Examples
Drugs	caffeine[19]		Carbohydrates	galactose[115]
	chloramphenicol[20]			glucose[115]
	cyclobarbital[21]			fructose[115]
	diazepam[22]			Z-aspartame[23]
	ephedrine[24]			
	7-hydroxycoumarin[25]		Nucleotide bases	adenine[26]
	metoprolol[27]			1-cyclohexyl uracil[30]
	morphine[28]			1-propyl cytosine[30]
	naproxen[29]			1-propyl thymine[30]
	nicotine[31]			
	oleandomycin[32]		Protein	chymotrypsin[33]
	pentamidine[34]			Rnase A[35]
	propranolol[36]			Urease[115]
	ropivacaine[37]			
	sameridine[38]		Alkaloids	cinchonidine[39]
	tylosin[32]			cinchonine[39]
	timolol[40]			quinine[41]
	theophylline[22]			hydroquinine[42]
	xanthine[19]			
Hormones	castasterone[43]		Biologically Active Compounds	2-aminopyridine[44]
	cholesterol[45]			corynanthine[46]
	corticosterone[47]			creatinine[48]
	β-estradiol[49]			methylpyrazines[50]
	11-α-hydroxyproges-terone[51]			
	hexestrol[52]		Herbicides	ametryn[53]
	enkephalin			atrazine[54]
	tamoxifen[55]			bentazone[56]
	testosterone[57]			cynazine[53]
				2,4-D[58]
Amino Acids	phenylalanine[115]			prometryn[53]
	typtophan[115]			triazine[59]

2.1.3 Approaches to Molecular Imprinting

MIPs have been prepared and used in several configurations. The most common configuration involves the preparation of bulk polymer monoliths, which after fragmentation and particle sieving (giving particles of about 25 μm) are used in separation applications. For chromatographic purposes, alternative configurations have been developed. For example, polymers have been prepared in situ in chromatography columns[20] and in capillary electrophoresis systems[60] eliminating the requirement of particle sizing and leaving sites that are undamaged from any fragmentation process. Attempts have been made to enhance the flow properties of the MIP particles through preparing polymer particles homogeneous in dimensions and morphology.[61] Leading the research is the laboratory of Hosoya *et. al* who have accomplished this task in either of two ways: the polymer is grafted on pre-formed particles such as silica or poly-(trimethylolpropane trimethacrylate) particles.[62] or preparation of beads through suspension, emulsion or dispersion polymerization.[63,64] Spherical MIP particles with narrow size distribution can be obtained, providing good flow performances in chromatography.

For analytical or sensor-device applications, thin layers or polymer membrane configurations have been developed and recently reviewed in the literature.[65] In this case, the MIP is either directly cast as a thin layer[66] on a surface or chip, or alternatively, MIP particles[67] are glued together using a particle binding agent.

The last configuration, surface imprinting, is performed by forming adducts with functional monomers in solution and the formed complexes are subsequently allowed to

bind to an activated surface such as silica wafers or glass surfaces. This technique, usually reserved for large molecules, yields a physical footprint of the template on the surface.

2.1.4 Applications of MIPs

The inherent selectivity of MIPs, in addition to their chemical and physical robustness, endows them with a tremendous potential for applications in chemical analysis. The imprinted polymer material has shown promise in many fields of analysis; however, the most common usage is liquid chromatography (LC). Utilizing the synthesized polymer as a stationary phase packing in LC columns is one of the most simplistic ways to evaluate the material for its binding selectivity. Fairly extensive success has been illustrated with MIP chiral stationary phases, both in LC columns and on thin layer chromatography (TLC) plates[68,69] There is an ever-increasing demand, especially in the pharmaceutical industry, to more efficiently purify and analyze chiral compounds.[70] Presently, several commercially available chiral stationary phases and mobile phase combinations have to be evaluated before separation is, if at all, accomplished. In contrast, the predetermined and custom-made selectivity of MIPs is ideally suited for predictable separation of chiral molecules. To enhance pharmaceutical analysis, MIP materials have been utilized for drug screenings[71] and as selectors in combinatorial libraries.[51] The use of a MIP stationary phase material has been further exploited to produce imprinted capillary electrochromatography (CEC) columns.[72] Nilsson *et al.* were the first to accomplish this approach through in-situ dispersion polymerization.[73]

Unfortunately, MIPs operated in the chromatographic mode suffer from several disadvantages. Often, the template molecule will exhibit a very broad elution profile because of heterogeneous binding sites, relatively few strong binding sites and inconsistent size and shape of the MIP particles.[74]

However, the advantages of imprinted polymer materials have driven researchers to exploit a variety of other applications. Because MIPs are chemically and physically robust, simple and inexpensive to prepare, maintain the recognition capacity over extended periods and possess a predetermined selectivity, they have been useful for various types of sensing devices. The rebinding of the print molecule by the MIP material has been combined in several signaling or transduction methods. These include capacitance measurements,[75,76] differential-pulse voltammetry,[77] fluorescent groups in the polymer,[78,79] and surface plasmon resonance (SPR).[19] Desorption of the fluorescently labeled chloramphenicol print molecule from the MIP material by a sample analyte also forms the basis of a displacement type sensor.[80]

2.1.5 Solid Phase Extraction

Most recently, MIPs have shown significant promise as solid phase extraction (SPE) sorbents.[81,82,83,84] SPE is a commonly employed sample preparation approach that relies on the preconcentration of the analyte(s) on a stationary phase, followed by elution and collection of the fractions containing the analyte(s). The goal of traditional SPE is to enhance the analyte - sorbent interactions. This will enhance the binding capacity and

selectivity of the material. Selectivity in SPE is the degree to which an extraction technique can separate the analyte(s) from interferences in the original sample. This enrichment step allows analysis of samples with very low concentrations and forms an essential part of any analytical method. However traditional SPE is expensive, time consuming and demand a large volume of solvent (> 0.5 mL).[85] There are also several chemical limitations, including pH sensitivity of the silica-based sorbent and requirement of a wetting solvent that must not evaporate.

Consequently, development of new approaches for the inexpensive, selective and rapid cleanup to preconcentrate sample analytes is an important area of research. Again, the high binding capacity, chemical stability and physical robustness of the MIP make it an ideal packing material for use in SPE. The high selectivity of the MIP employed for the SPE yields an efficient way for the removal of interferents and this application appears to be one of the most promising.

MIP columns can be used for on-line selective SPE of the template molecule. An appropriately chosen mobile phase composition can provide exceptionally strong binding of the print molecule to the MIP column. Subsequent injection of a 20-μL aliquot of a protic polar solvent onto the column will produce a rapid, pulsed elution (PE) of the analyte molecule for direct UV detection. This PE band is very narrow, thus providing great analytical sensitivity. The present technique, molecularly imprinted solid-phase extraction with pulsed elution (MISPE-PE), also allows for analyte enrichment or preconcentration through injection of a relatively large volume of dilute sample solution, thus further improving the detection limit. These online procedures do not involve sample manipulation

between preconcentration and analysis, so loss and contamination risk are avoided and reproducibility can be further improved, with minimal consumption of organic solvents and more potential for automation. Previous MISPE methods were not on-line techniques and therefore disadvantaged in terms of time and sample handling requirements.[86]

The high binding capacity of the MIP material enable micro-columns to be used for the selection extraction of trace analyte(s) in the hopes to further decrease analysis time, solvent use while increasing analyte sensitivity. The small amount of MIP in the micro-column will permit more effective desorption of the bound analyte by a single PE. The narrow column diameter will prevent peak broadening due to radial diffusion of the injected sample, resulting in greater analytical sensitivity. A new MISPE-differential pulsed elution (DPE) method, as represented in Figure 2.1.5.1, can utilize an intermediate solvent wash possessing the appropriate polarity to remove the interferents while leaving the print molecule bound to the column. This novel microanalysis technique, MISPE-DPE, offers the advantage of micro-scale performance for sample introduction, chemical interference removal and spectrometric analyte determination.

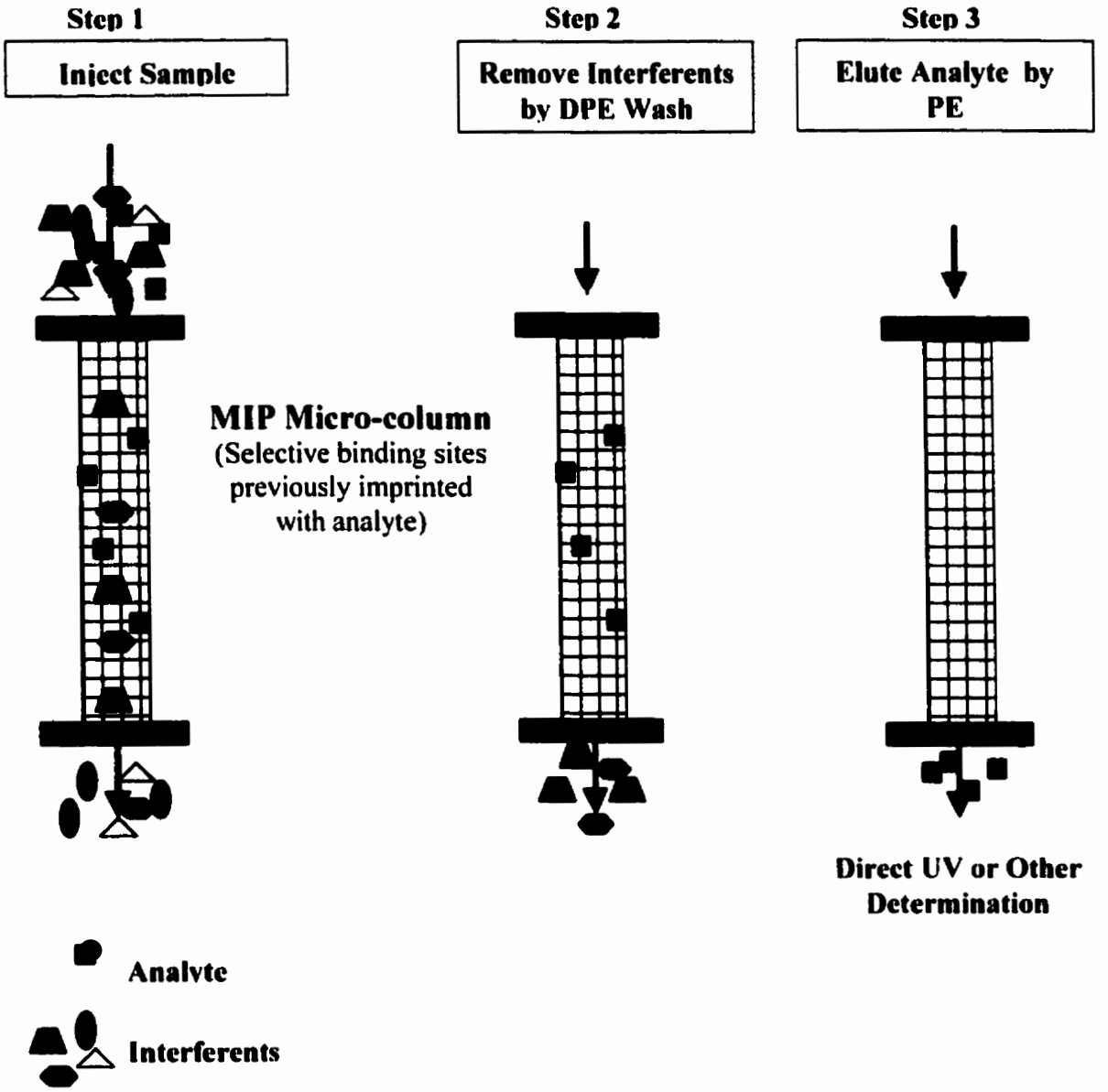

Figure 2.1.5.1: Summary of Molecularly Imprinted Solid Phase Extraction – Differential Pulse Elution (MISPE-DPE) method.

2.1.6 Pharmaceutical Analysis

The field of pharmaceutical development is highly dependent on sample preparation techniques. The complexity of pharmaceutical and/or biological matrices demands a highly effective cleanup approach, and the high selectivity of the MIP material employed for SPE yields an efficient way for the removal of interferents.

2.1.6.1 Theophylline

Theophylline was chosen as a template (or print) molecule for MIP synthesis and MISPE-PE/DPE method development mainly due to its pharmacological importance. Chemically, theophylline acts a powerful bronchodilator and has long been used to treat asthmatic symptoms in children and adults as well as apnea in premature infants.[87] It is considered to be the most commonly prescribed pharmaceutical[88] and was one of the three drugs most frequently monitored by pharmacokinetics services in the U.S. Veterans Affairs medical centers.[89] The drug has also demonstrated the ability to inhibit the repair of potentially lethal DNA lesions[90] and its pharmacokinetics has recently seen a resurgence of interest in the development of new oral macrolide and fluoroquinolone antibiotics.[91]

Biological samples such as urine[92] plasma or serum[93,94] and tissue[95] have been used in theophylline doping control investigations, clinical pharmacokinetic experiments[96], and human liver metabolism studies.[97] Many physiological factors will cause variable theophylline clearance rate in plasma.[98] Hence, careful dosage adjustment based accuract and consistent therapeutic drug monitoring of theophylline levels in serum is necessary.

However, considering theophylline belongs to a class of compounds known as methylxanthines (including caffeine and theobromine), which are ubiquitous in biological samples, its analysis can be seriously impaired by these and other constituents in complex sample matrices. Often a lengthy sample extraction of approximately 30 min is necessary before the analysis can be performed followed by traditional separation techniques such as high performance liquid chromatography (HPLC) to assay theophylline and other methylxanthines.[91,99] However, HPLC methods were generally disadvantaged in terms of analysis time and sample handling requirements. As for immunoassays, an international health control survey showed that commercial immunoassay kits were comparable in performance to reverse-phase HPLC (coefficient of variation = 7.5%, accuracy = 3.2%) when measuring theophylline in serum.[100] One shortcoming of immunoassays is the availability and relatively short working life of antibodies. A significant cross-reactivity of 6.7% was also found when theophylline was measured by fluorescence polarization immunoassay (FPIA) in the presence of caffeine.[101] Such cross-reactivity with caffeine may have important consequences in the monitoring of premature newborns.

2.1.6.2 Nicotine

The versatility of the MISPE-DPE approach was assessed for a second MIP that had been imprinted for nicotine. Nicotine makes up 98% of the total alkaloids in tobacco, which is a member of the Nicotiana genus.[102] Since nicotine is rapidly absorbed in humans to exert a number of physiological and therapeutic[103] effects, strict health and environmental

regulations have demanded nicotine monitoring.[104] Therefore, reliable determination of nicotine in tobacco and pharmaceutical formulation (such as nicotine gum and transdermal patches) is important. The most common method for the analysis of nicotine in tobacco is either GC using a nitrogen specific detector or HPLC with UV detection. Similar to typical theophylline analysis, these methods require expensive mobile phase solvents, time-consuming extractions or long analysis times (>10 min).[105,106] Other quantitative analysis techniques for nicotine (including capillary electrophoresis,[107] ion chromatography[108] and flow injection photometry[109]) also suffer similar disadvantages of time-consuming extractions and long analysis times.

2.1.6.3 4-Aminopyridine

The last MIP material to be validated was imprinted with 2-aminopyridine. This column was used as a surrogate column for the selective binding and determination of the structural analogue 4-aminopyridine. The objective of this validation was to further extend the practical application of the MISPE-DPE approach, for the rapid determination of this potassium channel blocker. This drug compound is used to treat several neurological conditions (including myasthenia gravis[110] and Lambert-Eaton syndrome[111]) and acts as a potent convulsant at high dosages.[112]

2.2 Theory

2.2.1 Preparation of MIP

There are three principal steps in the preparation of a MIP: prearrangement, polymerization, and extraction of template. The first step, the non-covalent interaction between the functional monomer and the template molecule, forms the basis of molecular recognition in the synthesized MIP. Typically, the specific interactions involved in the molecular imprinting process include charge-charge, charge-dipole, dipole-dipole or hydrogen bonding. The potential range of these and other non-covalent interactions and their energies in relation to distance is summarized in Table 2.2.1.1.

Table 2.2.1.1: Summary of Non-covalent Interactions.

Type of Interaction	Dependence of Energy on Distance
hydrogen bonding	fixed bond length
charge-charge	$1/r$
charge dipole	$1/r^2$
dipole-dipole	$1/r^3$
charge-induced dipole	$1/r^4$
dipole-induced dipole	$1/r^5$
dispersion	$1/r^6$

Obviously, there is a significant effect of distance on the energy of non-covalent interactions except for hydrogen bonding. Since, molecular interactions between monomer and template molecules are only prominent at close distances, steric hindrance can have a large influence

on the complex formation and must be minimized. During the prearrangement step, the orientation of bonds that dictates the imprinting process are under thermodynamic control. For example, when placed in the electric field produced by an ion, the dipole will orient itself so that the end with opposite charge to that of the ion will be directed toward the ion, and the other repulsive end directed away. Similarly, the H bond donor tends to point directly at the acceptor's electron pair. Comparable to biological systems, hydrogen bonding plays a very significant role in molecular imprinting. The energy of a hydrogen bond is on the order of 50 kJ/mol, making it the strongest non-covalent interaction. This apparently small magnitude of bond energy is offset by the large number of individual hydrogen bonds that can co-exist, yielding a strong overall interaction.

2.2.2 Thermodynamics Basis of Intermolecular Interaction

Chemical interaction is a very dynamic process, with bonds being continually broken and reformed. The interaction between a receptor (A) and a ligand (B) to form a complex (AB) therefore exists as an equilibrium process as shown below:

$$A + B \underset{k_d}{\overset{k_a}{\rightleftharpoons}} AB \qquad \textbf{Equation 2.2.2.1}$$

The association equilibrium constant, K_{ass}, governs the extent of complex formation and can be written as:

$$K_{ass} = \frac{[AB]}{[A][B]} = \frac{1}{K_{diss}} = \frac{k_a}{k_d} \qquad \textbf{Equation 2.2.2.2}$$

where K_{diss} is the dissociation equilibrium constant, k_d is the dissociation rate constant and k_a is the association rate constant. Although the K_{ass} value provides useful information about the position of the equilibrium, a better understanding of the factors responsible for the binding process can be represented by the thermodynamic spontaneity of the complex formation. The value of thermodynamic spontaneity, as represented by a negative Gibbs free energy value (ΔG), is logarithmically related to K_{ass} via the Gibbs free energy equation as shown below:

$$\Delta G_{ass} = -RT \ln K_{ass} \qquad \textbf{Equation 2.2.2.3}$$

where R is the gas constant and T is the absolute temperature. This equation represents the sum of energies, which may have both positive and negative effects on the complex formation. A negative value of ΔG predicts the spontaneous formation of the complex.

More importantly, a model put forth by Williams[13] highlights the individual energies involved with intermolecular interactions. Although the specific energies associated with this model are beyond the scope of this thesis, a brief overview of the model is noteworthy. The critical parameters of this model are summarized by Equation 4.

$$\Delta G = \Delta G_{t+r} + \Delta G_{rotor} + \Delta G_{conf} + \Delta G_{vib} + \Delta G_{vdW} + \Delta G_h + \sum \Delta G_p \qquad \textbf{Equation 2.2.2.4}$$

where ΔG_{t+r}, is the free energy loss associated with translational and rotational freedom upon association of the ligand and receptor, ΔG_{rotor} denotes the energy loss when internal rotors are immobilized. ΔG_{conf} is the result of adverse conformational changes necessary for binding. ΔG_{vib} is the residual of soft vibrational modes, and ΔG_{vdW} represents the energy loss from unfavorable van der Waals interactions. The last two terms, ΔG_h, the energy gain

from hydrophobic interactions, and $\sum\Delta G_p$, the sum of interactive polar group contributions, are both favorable interactions.

As a brief overview, the value of ΔG_{t+r} results from a loss of entropy as the molecule's freedom is restricted. This energetic term is similar to ΔG_{rotor}, which arises from the restriction or freezing of the rotation around internal bonds. A third term compensating for the restricted motion of the bound complex is ΔG_{vib}. This type of motion is separate from the rotation and is dictated by temperature and molecular size. Often the binding process may cause the bound molecule to adopt a slightly different structural conformation and this energetic penalty is reflected in the ΔG_{conf} term. The binding process requires the ligand and receptor to approach each other within close vicinity. This can be an unfavorable situation due to effect of van der Waals repulsion. These forces are electrostatic in nature and are highly distance dependent as previously shown in Table 2.2.1.1. The van der Waals energy, ΔG_{vdW}, can be approximated by the equation:

$$\Delta G_{vdW} = -\frac{a}{r^6} + \frac{b}{r^{12}} \qquad \textbf{Equation 2.2.2.5}$$

where a and b are constants for each atom and r is the distance between their nuclei. Therefore, at very short distances atoms will experience strong repulsion.

The positive influences on binding include the hydrophobic effect, as represented by ΔG_h. This is the driving force behind the association of non-polar groups in polar media. Lastly, the energy resulting from polar bonds in a complex is denoted by the term, $\sum\Delta G_p$.

2.2.3 Monomer

The functional monomer is the key building block in the molecular imprinting process. 24 monomers that have been employed in non-covalent molecular imprinting schemes are shown in Figure 2.2.3.1. Several functional groups such as carboxylic acids, sulphonic acids and heteroaromatic bases have been utilized. However, MAA is by far the most frequently used monomer, likely due to its ability to participate in ion-ion, ion- dipole, dipole-dipole and hydrogen bonding interactions. The success of a monomer is entirely dependent on both the chosen template and limitations such as solubility in the pre-polymerization mixture.

Acidic

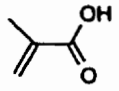

methacrylic acid

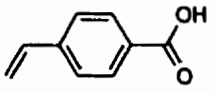

p-vinylbenzoic acid

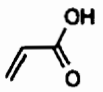

acrylic acid

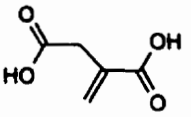

itaconic acid

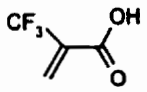

2-(trifluoromethyl)-acrylic acid

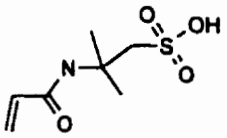

acrylamido-(2-methyl)-propane sulfonic acid

Basic

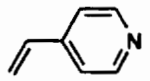

4-vinylpyridine

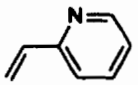

2-vinylpyridine

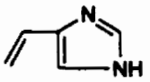

4-(5)-vinylimidazole

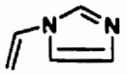

1-vinylimidazole

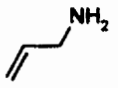

allylamine

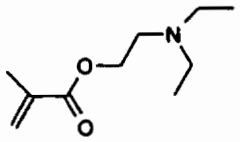

N,N'diethyl aminoethylmethacrylamide

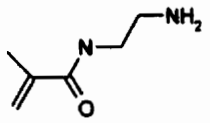

N,(2-aminoethyl) methacrylamide

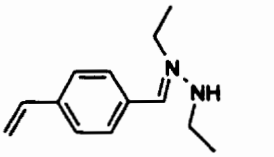

N,N'-diethyl-4-styrylamine

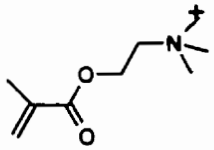

N,N,N-trimethyl aminoethylmethacrylate

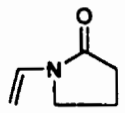

N-vinylpyrroline

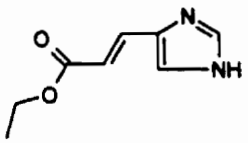

l-urocanic ethyl ester

Neutral

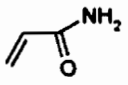

acrylamide

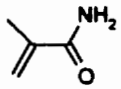

methacrylamide

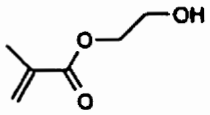

2-hydroxyethyl methacrylate

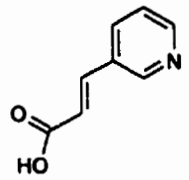

2-trans-3-(3-pyridyl)-acrylic acid

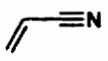

acrylonitrile

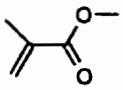

methyl methacrylate

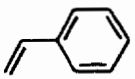

styrene

Figure 2.2.3.1: Typical monomers used in the non-covalent MIP approach.

2.2.4 Crosslinker

A very high degree of cross-linking, between 70-90%, is necessary for achieving specificity in addition to chemical and physical rigidity in the MIP material. The cross-linkers can also play an important role in the porosity and the hydrophobicity of the MIP. As illustrated in Figure 2.2.4.1, only 20 cross-linkers have been utilized as the solubility of the crosslinker itself and the solubility of the monomerised template species in the pre-polymerization solution reduce the number of possibilities. Nevertheless, several different crosslinkers have been tried with different degrees of success. Most commonly, ethylene glycol dimethacrylate (EDMA) and trimethylolpropane trimethacrylate (TRIM) are employed in several systems.

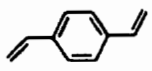

p-divinylbenzene

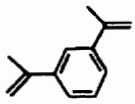

1,3-diisopropenyl benzene

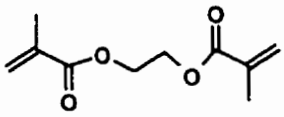

ethylene glycol dimethacrylate

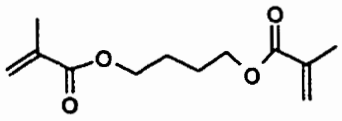

tetramethylene dimethacrylate

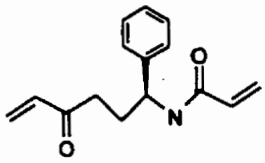

N,O-bisacryloyl-L-phenylalaninol

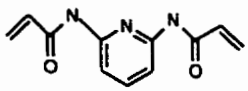

2,6-bisacryloylamidopyridine

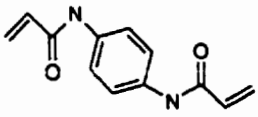

1,4-phenylene diacrylamide

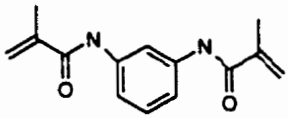

N,N'-1,3-phenylenebis(2-methyl-2-propenamide)

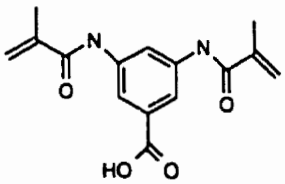

3,5-bisacrylamido benzoic acid

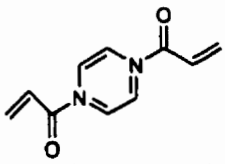

1,4-diacryloyl piperazine

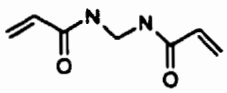

N,N'-methylene bisacrylamide

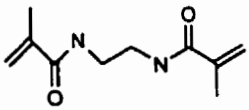

N,N'-ethylene bisacrylamide

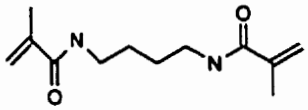

N,N'-tetramethylene bisacrylamide

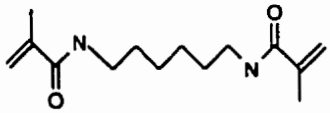

N,N'-hexmethylene bisacrylamide

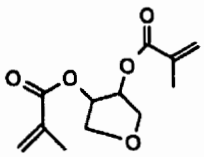

anhydroerythritol dimethacrylate

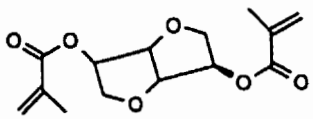

1,4,3,6-dianhydro-D-sorbital-2,5-dimethacrylate

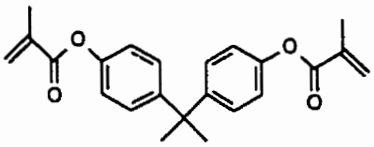

isopropylenebis(1,4-phenylene) dimethacrylate

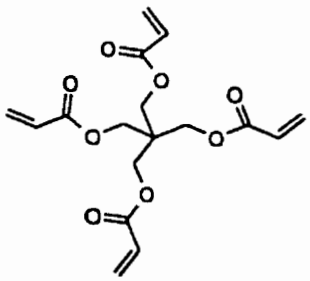

pentaerythritol tetraacrylate

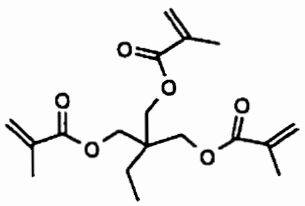

trimethylolpropane trimethacrylate

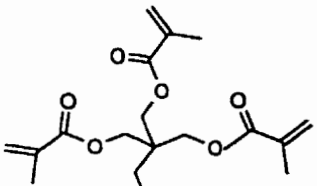

pentaerythritol triacrylate

Figure 2.2.4.1: Selection of crosslinkers utilized in MIPs.

2.2.5 Porogen

The porogen or pre-polymerization solvent plays an important role in the outcome of a molecular imprinting process. Its main role is to solubilize the reagents and influence porosity and surface area in the resultant polymer. As porogen in the polymerization, the solvent governs the strength of non-covalent interactions in addition to its influence on the polymer morphology. Generally, the more polar the porogen, the weaker the resulting recognition effect becomes, as a consequence of the influence of the solvent polarity on non-covalent interactions. A general relationship between the polarity of the solvent, expressed as dielectric constant, ε, and the ability to disrupt coulombic complexes can be given by Coulomb's law below:

$$F = \frac{Q_1 Q_2}{r^2 \varepsilon} \qquad \textbf{Equation 2.2.5.1}$$

where F is the force of attraction between two charges, Q_1 and Q_2, at a given distance r.

Therefore, the presence of high dielectric (high polarity) solvents weakens electrostatic interactions. Consequently, the best imprinting porogens for accentuating the binding strengths are solvents of very low dielectric constant, such as toluene and chloroform. The use of more polar solvents will inevitably weaken the interaction forces between the print molecule and the functional monomers, resulting in poorer recognition. Protonicity can also be an important factor in classifying porogens. Protic solvents are able to act as hydrogen bond donors and can influence the stability of the complex. Hydrogen bonds, a main driving force behind molecular recognition, are directionally dependent and distortions of these bond angles will greatly influence complex formation. The hydrogen

bond parameter, HBP, is a measure of this distortive effect of a particular solvent on hydrogen bonds. This factor is derived from the infrared shift of the -OD band of MeOD in the solvent in question to the position of the same band in *n*-heptane.[114] Table 2.2.5.1 summarizes the ε and HBP values for several common solvents.

It is important to realize that a higher polarity porogen can positively influence the structure of the MIP, compensating for the reduction in complex interaction. For example, acetonitrile leads to more macroporous polymers than chloroform.[115] A lower surface area and a lower macroporosity may lead to diminished recognition, because of lower accessibility to the sites. The solvent used in the recognition process is also critical due to its effect on the MIP's morphology, since the swelling of the polymer is dependent on the surrounding medium. Thus, swelling can change the three-dimensional configuration of the functional groups taking part in the recognition in the sites, resulting in poorer binding capability. In general, the best choice of recognition solvent is often identical to the imprinting porogen.

Table 2.2.5.1: Dielectric Constants and Hydrogen Bond Parameters[114] (HBP) of Common Solvents at STP.

Solvent	Dielectric Value (ε)	HBP
acetone	21	7.5
acetonitrile	36.2	7.0
benzene	2.3	3.1
carbon tetrachloride	2.4	1.1
chloroform	4.8	1.8
dichloromethane	9.1	2.2
diethyl ether	4.3	10.7
DMSO	49	15.5
ethanol	24.3	-
ethyl acetate	6	6.5
hexane	1.9	-
methanol	32.6	-
n-heptane	1.9 (20 °C)	0
nitromethane	39	2.7
TEA	2.4	-
TFA	39	-
THF	7.4	11.5
toluene	2.5	3.6
water	78.5	-

2.2.6 High Performance Liquid Chromatography

The molecular interactions taking place during a chromatographic separation may appear to be quite simple. However, the details of the mechanism of retention are not completely understood.[116] The principle of separation in liquid chromatography is the distribution of the solutes between a liquid mobile phase and a solid stationary phase. Those solutes that are preferentially distributed in the stationary phase remain in the column longer than those that are preferentially distributed in the mobile phase. Consequently, the

individual solutes will be eluted from the column in the order of their increasing distribution coefficients.

To control the retention of a solute, different molecular forces have to be exploited in the mobile and stationary phases. Typically, in MIP, non-covalent forces are responsible for increasing the imprinted molecule's distribution coefficient as described previously. The distribution coefficient for a solute travelling in the mobile phase can be represented by a capacity factor, k and is defined as:

$$k = \frac{t_r - t_m}{t_m}$$ **Equation 2.2.6.1**

where t_r is the retention time for the solute and t_m is the time required for the mobile phase to travel through the column. For one or more eluting solutes, a relative retention, α, can be calculated as follows:

$$\alpha = \frac{t_{r2}}{t_{r1}}$$ **Equation 2.2.6.2**

where t_{r1} and t_{r2} are the calculated retention times for the two eluting peaks.

2.2.7 HPLC Column Performance Measures

For comparison purposes, several measures of chromatographic performance have been established. Two quantities widely used are height equivalent of a theoretical plate (HETP) and resolution (R). HETP is determined by dividing the column into N segments, where one equilibration of the solute between the mobile and solid phase occurs. For a column of length, L the HETP value is simply denoted by:

$$HETP = \frac{L}{N}$$ **Equation 2.2.7.1**

The effect of flow rate on the solute equilibration process is better represented by the van Deemter equation for plate height:

$$HETP = A + B/u + Cu$$ **Equation 2.2.7.2**

where u is the linear flow velocity of the mobile phase. A, B and C are constants that pertain to a specific dispersion process each. For example, the term A refers to the multiple paths of different lengths traveled by the solute, B is the longitudinal diffusion term, and C is the speed of equilibration, also called the mass transfer term. A plot of HETP versus flow velocity yields a hyperbola, which can be used to determine the optimal flow rate for the best column efficiency.

A direct measure of the ability of a column to separate two compounds is resolution. In order to ensure proper quantification of the individual components, resolution values greater than 1.0 are necessary. The value of resolution is calculated according to:

$$R = \frac{t_{r2} - t_{r1}}{(w_1 + w_2)/2}$$ **Equation 2.2.7.3**

where w_1 and w_2 are the peak widths at half height.

2.2.8 Solid Phase Extraction

The mechanism of extraction in MISPE is highly dependent on the functional groups present in the monomer and target molecule. However, a range of non-covalent interactions have been implicated in the MIP binding process. The partitioning of the solute between the

mobile phase and the MIP binding sites is stabilized by hydrogen bonding, dipole-dipole and induced dipole interactions. These forces are also responsible for adsorption in normal phase SPE. Figure 2.2.8.1 represents a typical hydrogen bonding interaction between theophylline and the theophylline MIP binding site.

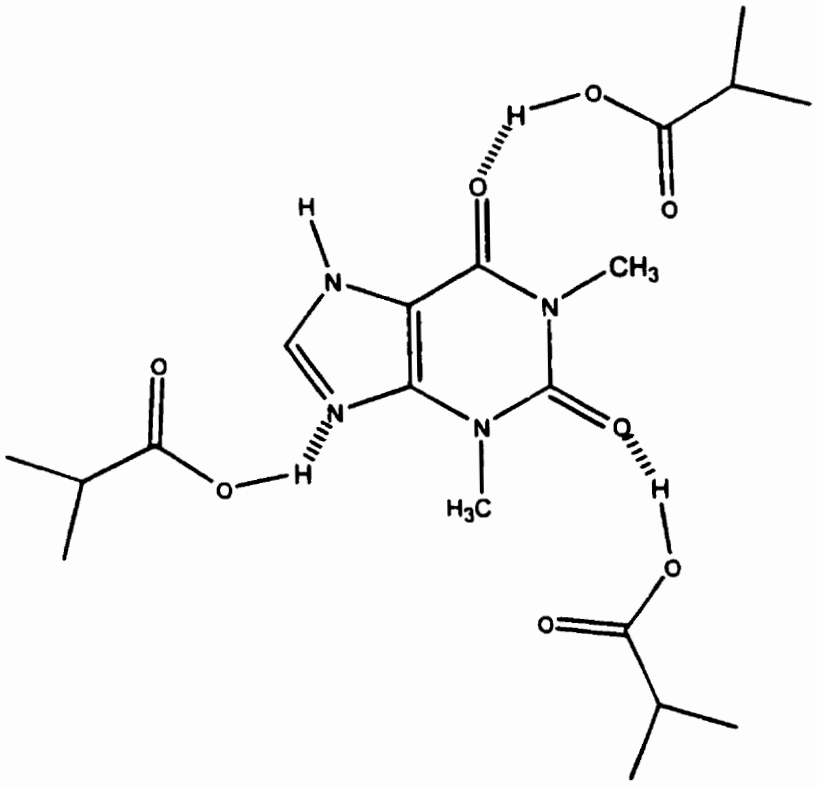

Figure 2.2.8.1: Typical hydrogen bond interactions between theophylline (target) and MIP binding site are depicted by broken lines.

The target molecule is adsorbed onto the MIP particles via an equilibrium process. Therefore, a distribution coefficient, K_d, can be expressed to describe the relative concentration of the print molecule in the mobile phase and adsorbed to the MIP particles at a given temperature.

$$K_d = \frac{P_s}{P_{mp}} \qquad \textbf{Equation 2.2.8.1}$$

where P_s is the print molecule concentration in the MIP sorbent phase and P_{mp} is the print molecule concentration in the mobile phase. A plot of the P_s versus P_{mp} at a constant temperature is referred to as an isotherm. As illustrated above, the slope of the line is equal to the distribution constant.

Similar to HPLC columns, the MISPE column can be divided into a number of theoretical plates. The number of plates and the magnitude of K_d is critical for determining the binding capacity of the column, as each plate is responsible for one equilibration of the print molecule with the MIP sorbent. As the solution moves down the column, now depleted in the print molecule, the equilibration process is repeated at the next plate. Since the value of the distribution coefficient is the same at each plate, the print molecule can become completely adsorbed on the column of MIP sorbent, provided there are enough plates present. The imprinted nature of the MIP material plays an important role in increasing the K_d value. The molecular recognition process provides the MIP material with a preferential affinity for the print molecule and therefore enhances the binding capacity of the sorbent.

The theory of plate numbers can be useful to explain several parameters that affect the performance of SPE columns. For example, flow rates that are too rapid do not allow equilibrium to be reached, which reduces the plate number and column efficiency. The efficiency is also influenced by particle size, as smaller particles will increase plate number. Likewise, increasing column length increases the plate number. Lastly, increasing the temperature of the sorbent can be employed to maximize the plate number.[117]

Increasing the number of plates in a SPE column is also important during the elution step. The higher the number of plates, the more efficiently the analyte(s) will be eluted from the column, requiring a lower volume of elution solvent. This is evident because a column with high plate count (and therefore small HETP value) will have less dispersion of the adsorbed solute. The elution of the solute from a MIP column is typically a function of the polarity and protic nature of the elution solvent. Typical values for both of these parameters are listed in Table 2.2.5.1. The elution solvent must effectively break the bonding interactions between the MIP sites and the bound target molecule.

2.3 Experimental

2.3.1 Chemicals and Standards

All solvent and reagents used were either analytical or HPLC grade and only deionized water (Milli-Q Water System, Millipore) was used. The chemicals were used as received by the supplier with the exception of methacrylic acid, which was purified by vacuum distillation just prior to use.[118] A list of suppliers for all reagents used in provided in Appendix B.

2.3.2 Instrumentation

The prepared columns were connected to an Eldex 9600 solvent delivery system (San Carlos, CA) as illustrated in Figure 2.3.2.1. A Rheodyne 7125 switching valve (Cotati, CA), containing a 20-μL sample loop was used for sample injection and pulsed elution (PE). A Gilson 115 UV detector (Middleton, WI) set at the wavelength of maximum absorption for each template molecule was used to monitor the absorbance of the column's eluate. Retention time and peak area measurements were recorded with a Dionex 4270 integrator (Sunnyvale, CA).

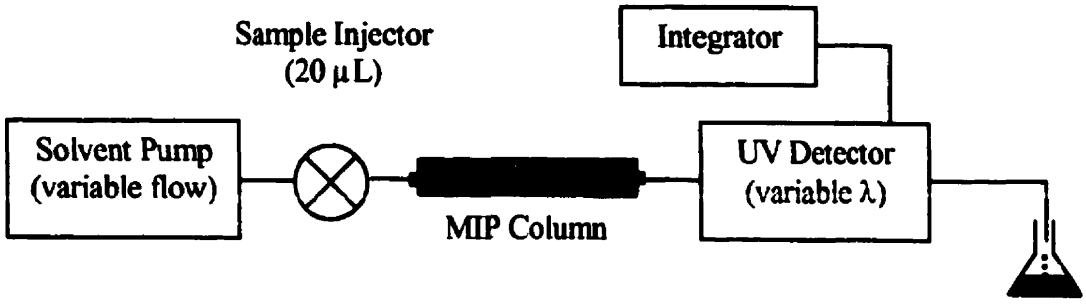

Figure 2.3.2.1: Experimental setup for HPLC, MISPE-PE and MISPE-DPE studies with MIP columns.

2.3.3 MIP Preparation

2.3.3.1 Theophylline

The polymer preparation was previously reported by Mosbach and co-workers.[22] The monomer MAA (0.90 g), the print molecule theophylline (0.47 g) and 25 mL of chloroform were placed in a 100-mL three-necked round bottom flask. The mixture was allowed to pre-organize until equilibrium overnight. The cross-linkerlinker EDMA (9.4 g) was then added, followed by the reaction initiator AIBN (0.12 g). The mixture was degassed under vacuum in a sonicating water bath while being purged with nitrogen for a period of 5 min. While maintaining a flow of nitrogen, the reaction flask was removed from the sonicating bath, fitted with a condenser and placed inside a 60 ^{0}C water jacket to begin

the reaction. Under these conditions, the reaction was continued for 24 hours. The product polymer, after drying in air overnight, was white in color and possessed a rigid structure. It was ground into fine particles using a mortar and pestle.

A control polymer was also prepared when polymerization was carried out in the absence of theophylline. This control polymer was used to determine the presence of any non-specific binding of the target molecule. Both the imprinted and control polymers were sieved and the ≤ 63 μm size fraction collected.

2.3.3.2 Nicotine

Zander and co-workers previously reported the polymer preparation.[119] A typical procedure involved dissolving the nicotine print molecule (4.37 mmol), monomer MAA (27.8 mmol), cross-linkerlinker TRIM (27.8 mmol) in 20 mL of methylene chloride. The solution was transferred to a thick-walled glass polymerization tube, degassed by sparging with nitrogen gas for 20 min, and then sealed with Parafilm. The tube was then immersed into a 10 °C water bath and equilibrated for ten minutes. The tube was irradiated using the UV lamp for 24 hr, rotating the tube periodically to ensure even polymerization. The polymer monolith was ground in wetted state by means of a mechanical ball mill. The 25-35 μm size fraction was isolated by sieving and used for column packing.

A control polymer was also prepared when polymerization was carried out in the absence of nicotine. This control polymer was used to determine the presence of any non-specific binding of the target molecule.

2.3.3.3 2-Aminopyridine

Zhou and He previously reported the preparation of a 2-aminopyridine MIP.[44] The 2-aminopyridine print molecule (2 mmol) and functional monomer MAA (8mmol) were dissolved in 25 mL of chloroform in a glass ampoule. The EDMA cross-linker (60 mmol) and the AIBN initiator (130 mg) were added to this mixture and sparged by nitrogen for 5 minutes. The ampoule was sealed under vacuum and placed in a shaker bath at 60 °C for 24 h. The product polymer was ground into fine particles using a mortar and pestle and passed through a 75 μm sieve.

2.3.4 Extraction of Theophylline from the MIP

Removal of the theophylline print molecule from the MIP particles was accomplished through a Soxhlet extraction. A sample of the theophylline-imprinted polymer (5.500 g) was placed inside the cellulose extraction thimble. The extraction solvent (150 mL) was a mixture of methanol and acetic acid (9:1). Heat was applied to the flask containing the solvent, at a rate that caused a filling and eventual emptying of the extraction chamber every 45 min. The extraction was continued for 24 hours, to produce the anti-theophylline polymer particles. Quantification of the extracted theophylline was accomplished by HPLC using UV detection at 270 nm. Soxhlet extraction was not performed on the control polymer particles.

2.3.5 Column Preparation

The polymer material was sieved and the specified size fraction was suspended in ~ 1 mL of methanol. A small volume of methanol was added to the MIP particles, and the slurry was dispensed into a 1/16" stainless steel tubing (1.0 mm i.d., 80 mm long). The fully-packed column was capped at both ends by a 1/16" zero-volume union fitted with a 2-μm screen (Chromatographic Specialties, Brockville, ON). For comparison purposes, two larger MIP columns were also packed using 1/8" (1.6 mm i.d., 50 mm long) and 1/4" (3.0 mm i.d., 80 mm long) stainless steel tubings and corresponding end column fittings from Chromatographic Specialties.

2.3.6 Extraction of Nicotine and 2-Aminopyridine from the MIP

Removal of the nicotine and 2-aminopyridine print molecules was accomplished by extensive washing of the MIP columns with a 10 % acetic acid in methanol solution, at a flow rate of 0.5 mL/min. This treatment was continued until the print molecule could no longer be detected in the column eluate.

2.3.7 Batch Binding Assay

0.100 g each of the theophylline MIP and control polymer particles were placed in separate glass vials containing 5.00 mL of a 20 μg/mL theophylline standard solution prepared in either methanol or chloroform. Each suspension was magnetically stirred for 24 hours and then passed through a 0.45-μm filter. The concentration of theophylline in the

filtrate was analyzed by HPLC using UV detection at 270 nm and compared to the original standard concentration.

2.3.8 High Performance Liquid Chromatography

HPLC analyses, using the anti-theophylline polymer column (3.0 mm i.d., 80 mm long), were performed isocratically at room temperature with 1.0% methanol in chloroform at a mobile phase flow rate of 1.0 mL/min. Various mixtures of theophylline, caffeine, xanthine, dyphylline and β-hydroxyethyltheophylline (all prepared in acetonitrile) were analyzed on the column. The void time, t_0, was determined by injection of acetonitrile. UV detection of the eluting peaks was performed at 270 nm.

2.3.9 MISPE

Injections of a 100-μg/mL theophylline solution in chloroform were tested with several mobile phases ranging in polarity at a flow rate of 0.5 mL/min. The break through peak was recorded and the remaining analyte bound to the MIP micro-column was removed with a successive 20 μL pulsed elutions (PE) with methanol. Various mixtures of theophylline, caffeine, xanthine, theobromine, acetaminophen, dyphylline, hydrochlorothiazide, β-hydroxyethyltheophylline, nicotinic acid and phenylbutazone in chloroform were analyzed by MISPE-PE. Approximately 1 min after the sample solvent peak and matrix components were detected, 20 μL of a selected polar and protic solvent was injected through the same Rheodyne valve to cause PE of any bound analyte(s).

2.3.10 Effect of Solvent Polarity

The effect of solvent polarity in the molecular recognition process of MISPE-PE was investigated by injection of 50-μg/mL standard solutions of theophylline and theobromine in chloroform, under mobile phase conditions ranging from 0% to 100% chloroform in acetonitrile. Both the break-through and pulsed-elution fractions were quantified by UV absorbance detection at 270 nm.

2.3.11 MISPE–DPE

Under isocratic mobile phase conditions of 100% chloroform, a 100-μg/mL sample of drug compound was injected onto the MIP micro-column. After rapid elution of the initial peak, three intermediate 20-μL injections of acetonitrile were used to wash off any drug remaining on the micro-column. To test if the wash removed the drug quantitatively, the column was subjected to three 20-μL injections of methanol.

2.3.12 Temperature Effect on MISPE-PE

The micro-column was either at room temperature or submerged in a Haake Instruments variable-temperature circulating water bath (Paramus, NJ) set at 40°C or 60°C. Various standard solutions of structural analogues of theophylline in chloroform were analyzed by MISPE-PE. After 1-2 min of waiting time was allowed for the detection of any

break-through peak, a 20-μL pulse of methanol was injected through the Rheodyne valve to cause PE of any bound 2-aminopyridine or non-specifically bound drug compounds.

2.3.13 Serum Analysis

A 1-mL sample of human serum was extracted with an equal volume of chloroform, vortexed for 10 s and centrifuged at 4000 rpm for 5 min. The chloroform layer was removed and spiked with theophylline (in chloroform) to provide a series of working standard solutions over the concentration range of 0-20 μg/mL. A calibration curve was constructed by triplicate 20-μL injections of these standard solutions onto the micro-column for analysis by MISPE-DPE at 60 °C. **Safety considerations**: Human serum samples are a potential biohazard. Unused serum samples should be treated with Javex before disposal as hazardous waste.

2.4 Results and Discussion

2.4.1 Soxhlet Extraction of Theophylline from the MIP

A total of 210 mg of theophylline was extracted from 5.500 g of the MIP. Therefore, the % by weight extracted was calculated to be 3.8%. By comparison, the maximum possible extraction would be 4.3% assuming all the theophylline was taken up by the MIP. The extraction efficiency was therefore 89%, which was sufficiently high to ensure the presence of selective cavities in the theophylline MIP.

2.4.2 Batch Binding Assay

The functionality of the theophylline MIP was confirmed in a batch binding assay. Table 2.4.2.1 summarizes the theophylline concentration in the filtrate and the percentage of theophylline bound to the MIPs in methanol and chloroform.

Table 2.4.2.1. Batch Binding Assay of 20 μg/mL Theophylline in Methanol and Chloroform with Theophylline MIP and Control Polymer.

Binding meduim	Theophylline Concentration in Filtrate (μg/mL)	% Theophylline Bound	% Cavities binding Theophylline
		Theophylline MIP	
Methanol	16.5	17.5	0.18
Chloroform	0.42	97.9	2.27
		Control polymer	
Methanol	19.78	1.1	0.02
Chloroform	19.54	2.3	0.05

Since the binding occurred over a 24-hour period, the percentage of theophylline bound would represent the maximum binding. This binding capacity was highly dependent on the sample solvent used in the assay, with an almost quantitative uptake of theophylline occurring in chloroform. This observation agrees well with previous results for a methacrylic acid MIP in its ability to bind atrazine.[120] Under batch binding conditions, the theophylline uptake was smaller in methanol, due to the solvent's polar and protic nature. The target molecule binding property of a MIP is known to be influenced by the solvent used in the polymer synthesis and the solvent used in the binding application of the MIP.[121] Since chloroform provides maximal interactions between the theophylline print molecule and the MAA functional monomers during the pre-organization, specific binding of theophylline can be expected when chloroform is used as the binding medium. If a polar solvent such as methanol serves as the binding medium, the binding of theophylline is greatly weakened. A small amount of non-specific binding (1.1-2.3%) was elucidated by the control polymer.

With a theoretical number of 1.31×10^{20} cavities/g of MIP, the percentage of cavities binding the print molecule was determined to be 2.27% in chloroform and 0.18% in methanol. These percentages should be evaluated in consideration of the theoretical number of cavities calculated, which assumes that every print molecule added to the synthesis produces a useful binding site. In practice, extensive cross-linking around each print molecule must occur in order to produce one cavity of the correct size and shape. Since there is a potential for the production of sites containing varying degrees of cross-linking, sites of lower recognition ability or accessibility may result.

2.4.3 HPLC

Various solvents that stretch across a rather broad range of polarities were evaluated for use as the mobile phase in the HPLC separation of theophylline from different drug molecules on the theophylline MIP column. Generally, all the experimental results confirmed that a retention mechanism typical of normal-phase chromatography ruled the separation. Chloroform was found to enhance the specific molecular recognition to such an extent that total retention of theophylline occurred on the column. Conversely, other mobile phases that are more polar and protic than chloroform could not generate adequate retention to even separate theophylline from the solvent peak. As illustrated in Table 2.4.3.1, the best mobile phase composition was a mixture of 1% methanol and 99% chloroform.

Table 2.4.3.1: HPLC Mobile Phase vs. Theophylline Capacity Factor for a Theophylline MIP Column.

HPLC Mobile Phase	Capacity Factor (k)
Acetone	0
Ethanol	0
Methanol	0
Water	0
1% Methanol in Chloroform	5.0
Chloroform	∞

It was also observed that theophylline solutions could not be prepared in any protic solvent to result in a good separation. This observation suggests that protic solvent molecules would effectively compete for the hydrogen bonding and ionic interactions with imprinted sites on the MIP stationary phase.[122] A recent paper by Baggiani *et al* evaluated the chromatographic performance of a MIP, selective for theophylline, in aqueous buffers and reached a similar conclusion.[123]

Theophylline (1,3-dimethylxanthine) was successfully separated from caffeine (1,3,7-trimethylxanthine) on the theophylline MIP column under mobile phase conditions of 1.0% methanol in chloroform. Similar results were observed for the separation of theophylline and xanthine. A typical chromatogram illustrating the separation of theophylline from a mixture with caffeine is shown in Figure 2.4.3.1.

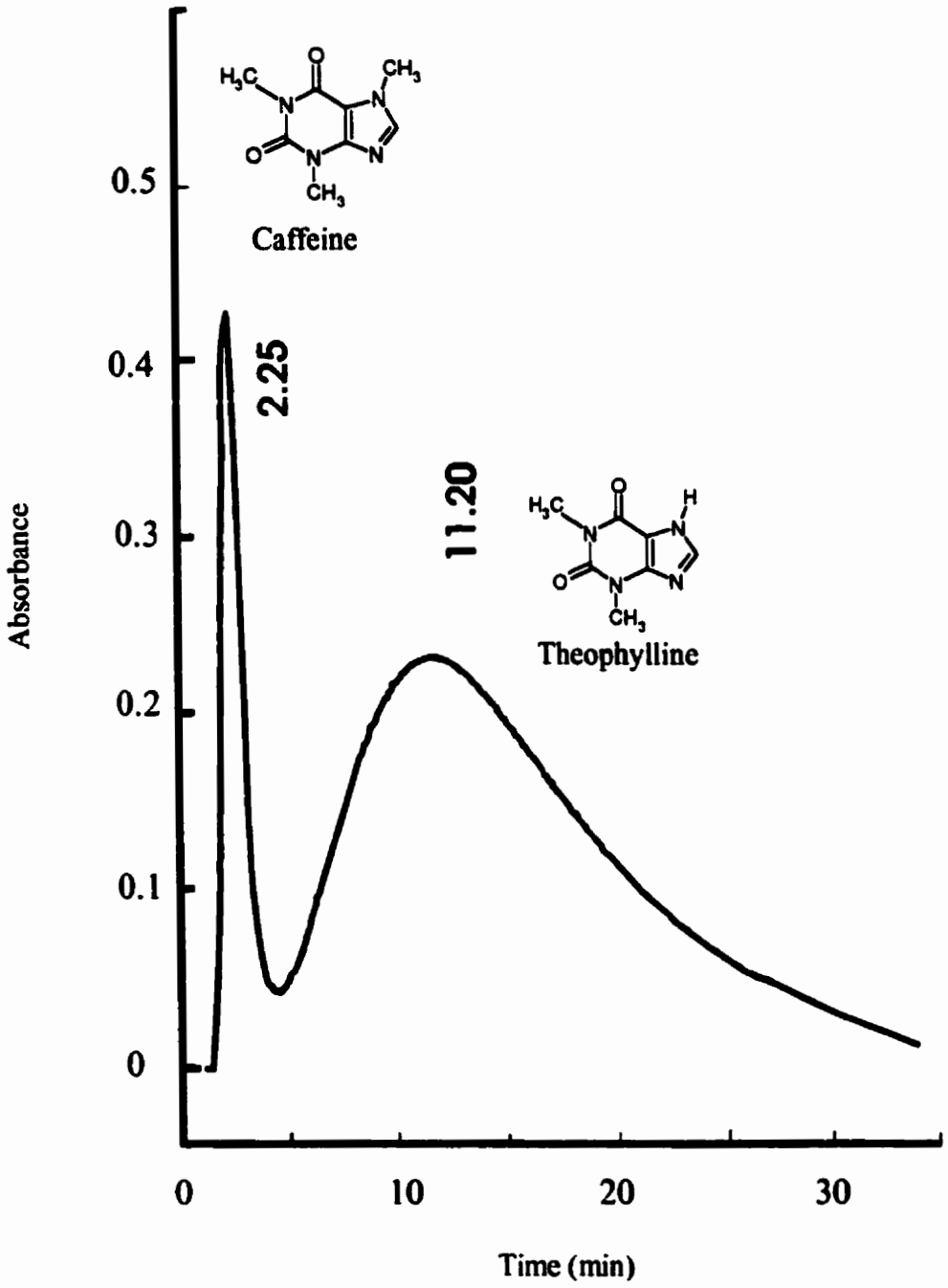

Figure 2.4.3.1: HPLC separation of theophylline from caffeine using a theophylline MIP column. Theophylline MIP column (8.0 cm X 0.4 cm i..d); mobile phase = 1% methanol in chloroform; flow rate = 0.5 mL/min; sample volume = 20 μL; detection λ = 270 nm.

The peak profile for theophylline elution was characterized by a prolonged average retention time of 12.4 ± 2.4 min accompanied by extensive peak broadening. When the control polymer was packed in a column for the HPLC, it was unable to retain theophylline, caffeine or xanthine. The overall HPLC performance characteristics of the theophylline MIP column are summarized in Table 2.4.3.2 for comparison with those for the control column.

Table 2.4.3.2: Chromatographic Performance of Theophylline MIP and Control Polymer Columns.

Analyte	Capacity Factor (k)		Selectivity Factor (α)	
	Theophylline MIP Column	Control Column	Theophylline MIP Column	Control Column
Theophylline	5.0	0.3	26.5	0.8
Caffeine	0.2	0.4	-	-

There was a very high capacity factor (k) for theophylline and a good separation factor (α) between theophylline and the hardly retained caffeine. Therefore, quantification of the individual drug molecules was readily attained with good linearity (R^2 = 0.9999 for peak areas and 0.9955 for peak heights) up to 2.0 mg/mL, as shown in Table 2.4.3.3.

Table 2.4.3.3: Peak Heights, Areas and Retention Times for the HPLC of Theophylline and Caffeine Standards using Theophylline MIP Column.

Concentration (mg/mL)	Peak Area (10^6 arbitrary units)	Peak Height (cm)	Retention Time (min)
	Theophylline		
2	745	12.5	9.68
1	366	5.6	12.3
0.5	184	2.5	14.5
0	0.0	0.0	0.0
	Caffeine		
0.1	60	8.8 ± 0.2	2.3 ± 0.1
0	0.0	0.0	0.0

HPLC results were also obtained for caffeine, xanthine, β-hydroxyethyltheophylline and dyphylline, all of which were rapidly eluted from a smaller theophylline MIP column close to the solvent peak (at 0.58 min) as presented in Table 2.4.3.4.

Table 2.4.3.4: Retention of Structurally Similar Drugs on Theophylline MIP Column.

Sample	Concentration (μg/mL)	Retention Time (min)
Caffeine	50	0.61
Xanthine	50	0.62
β-hydroxyethyltheophylline	100	0.60
Dyphylline	200	0.58
Theophylline	50	3.70

These findings signify the ability of the theophylline MIP column to selectively bind and retain only theophylline, thereby separating the target molecule from a mixture of closely related compounds with similar chemical structures.

Unfortunately, the HPLC separation efficiency in the isocratic mode was unacceptably low as indicated by calculated value 0.75 for resolution (R). The theoretical plate number, N, was determined to be 4. The elution of theophylline was slow and diffuse leading to a lengthy analysis time and poor detection limits. Column efficiency depends on a number of variables such as particle size, morphology, packing homogeneity, and pore size of the stationary phase. [117] A recent report by Hosoya[124] has outlined a method for the molecular imprinting polymerization of methacrylic acid that produces a uniform particle distribution. This new method of polymerization should be advantageous for HPLC applications.

Another significant cause of peak broadening is the possibility of different types of binding sites found within the MIP. The heterogeneous binding affinity of the MIP resulted in a decreasing HPLC retention time for increasing theophylline concentrations as illustrated in Figure 2.4.3.2. Theophylline molecules, from a standard injection, would initially interact with the strong binding sites of the MIP column, resulting in an extended retention time. However, as the number of theophylline molecules increases, these sites become saturated and interaction with sites of weaker binding affinity would predominate and yield a decreased retention time. Therefore, the linearity of the line ($R^2 = 0.980$) in Figure 2.4.3.2 provides experiential evidence to the effect of MIP binding site heterogeneity.

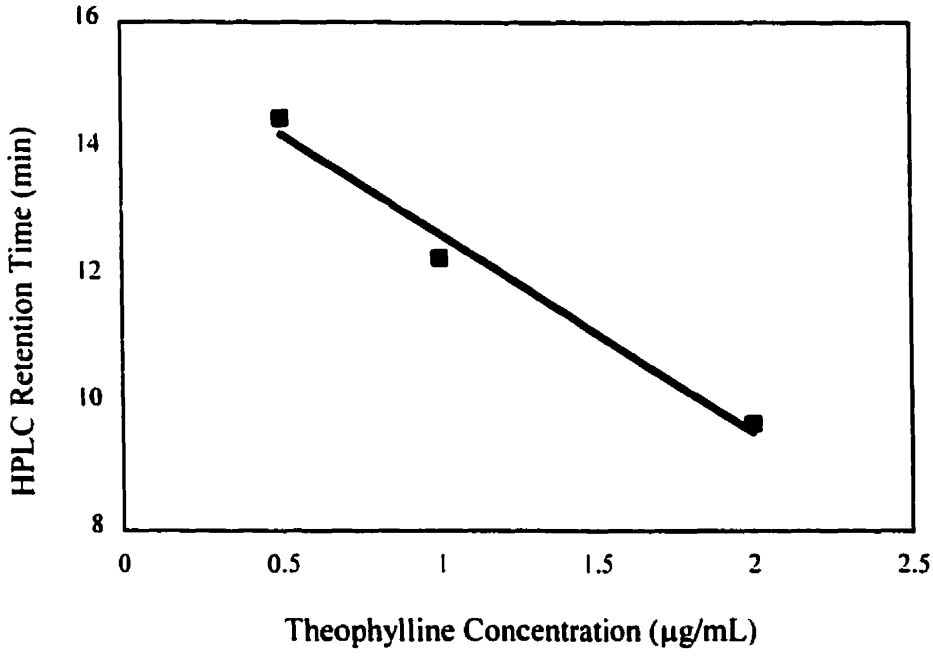

Figure 2.4.3.2: HPLC retention time vs theophylline concentration using a theophylline MIP column.

Such a heterogeneous binding characteristic of MIPs is due to the weak non-covalent (electrostatic) interactions between the target molecules and the functional monomers. which lead to the formation of sites with a wide range of binding affinities in the MIP.[125] In other words. the nature of the pre-organization process may give rise to the formation of different modes of interaction between the theophylline molecule and the

functional groups on the monomer molecules. This will result in the creation of different recognition sites in the polymer.

The variable binding energies or sorption kinetics of these sites would produce retention of theophylline to different extents and hence an overall of peak broadening. Comparable peak broadening was also displayed in a previous work that prepared a rod type affinity medium for liquid chromatography[126]. Similar broad peaks were also observed by Sellergren *et al* in the elution profile of D,L-PhNHPh enantiomers on a L-PhNHPh MIP column.[127] They addressed this issue in terms of dissociation constants; it was determined that the anti-polymer contained binding sites which exhibited a variety of affinities for the print molecule.

However, the use of a different cross-linker, trimethylolpropane trimethacrylate (TRIM), can improve column performance. TRIM has been shown to be superior in terms of load capacity, selectivity, and resolving capability of the resulting MIP stationary phases for liquid chromatography.[128,129] Also, the temperature at which the polymerization is carried out affects the molecular imprinting process. The stability of the monomer and print molecule at low temperatures, due to a more favorable entropy term, can result in a MIP with superior recognition properties.[130]

2.4.4 Molecularly Imprinted Solid Phase Extraction – Pulsed Elution (MISPE-PE)

The anti-theophylline MIP was applied to the specific SPE of theophylline, in order to provide maximum separation of theophylline from different drug molecules.

The selective retention of theophylline on the anti-theophylline column was controlled by electrostatic interactions and hydrogen bonding. Therefore, complete retention of theophylline could be achieved by using an aprotic, non-polar solvent such as chloroform. Conventionally, elution of the analyte from a SPE cartridge requires several aliquots of 0.5-mL or larger volume of solvent. For on-line UV detection of the eluting analyte, even 0.5-mL of sample is too large a volume to be handled efficiently by the 8-μL flow cell. The detection sensitivity will be greatly enhanced if the sample elution volume can be decreased. In the case of MISPE, this is feasible since the electrostatic and hydrogen bonding interactions can be effectively disrupted with a very small volume of protic and polar solvent. A novel elution technique, coined pulsed elution, was designed whereby a 20-μL aliquot of the polar protic solvent was injected directly through the switching valve onto the anti-theophylline column. Upon testing different solvents for pulsed elution, methanol was found to produce quantitative elution of the theophylline in one single injection.

Apparently, when this methanol solvent band was carried quickly down the column by isocratic chloroform, it ran into the theophylline solute zone where displacement of the analyte molecules from the binding sites in the stationary phase occurred. As the methanol solvent had sufficient polar and protic strength, it could keep the free theophylline molecules in the band for fast elution off the column. Due to the powerful elution strength of methanol only a small volume of solvent was required. This small elution band volume produced a large peak height and hence large signal-to-noise ratio, thereby resulting in a low detection limit. Pulsed elution of theophylline could

begin after the sample solvent and other component peaks were eluted. This could be as short as 4 minutes, and therefore the overall analysis time would be <6min/sample. This approach eliminated the previous difficulty with binding site heterogeneity as the interaction between theophylline and weak binding sites was enhanced with the use of an aprotic and nonpolar solvent to ensure quantitative SPE. Conversely the interaction between theophylline and strong binding sites, which normally resulted in peak tailing during analyte elution, was annihilated by the use of a 20-μL aliquot of protic and polar solvent to result in rapid desorption of the bound theophylline.

A successful separation of theophylline from caffeine is illustrated in Figure 2.4.4.1. Baseline separation between theophylline and other sample components is guaranteed through a delay of the pulsed elution. For selective theophylline determination, the speed of MISPE-PE analysis cannot be attained by either MIP or non-MIP columns operating in the HPLC mode.[126,131] After each MISPE-PE analysis, little had to be done to condition the theophylline MIP column. No significant differences in peak height were observed for ten consecutive runs of the same theophylline standard solution, without column conditioning in between.

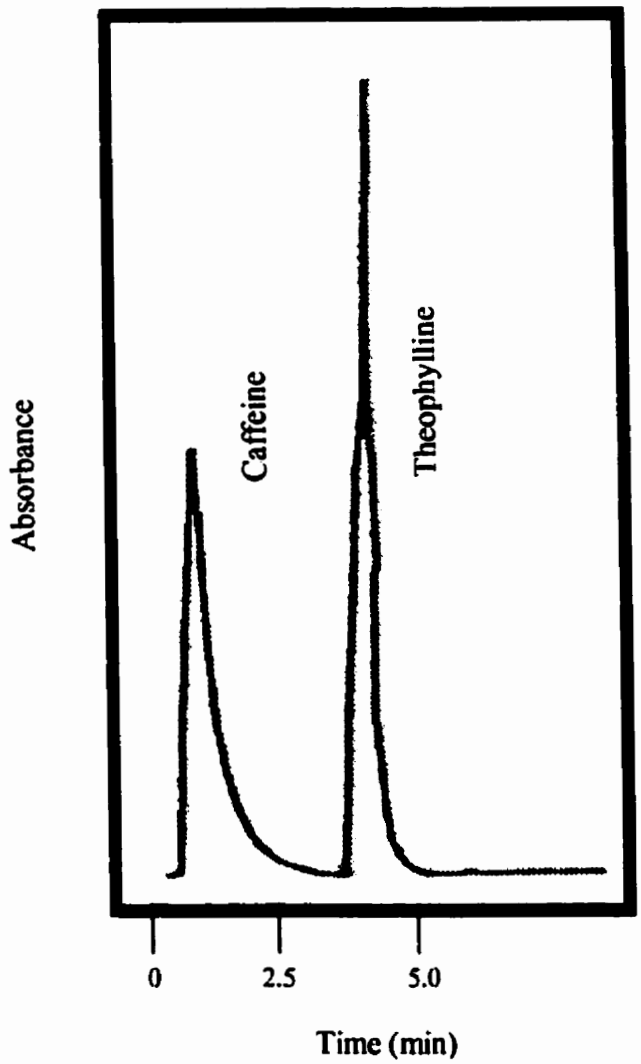

Figure 2.4.4.1: MISPE-PE of a 500 ng/mL theophylline and 50 ng/mL caffeine mixture on a theophylline MIP column. Theophylline MIP column (8.0 cm X 0.4 cm i..d); mobile phase = 100% chloroform; flow rate = 0.5 mL/min; sample volume = 20 μL; PE volume 20 μL; detection λ = 270 nm.

The efficacy of various protic solvents for the elution of theophylline in MISPE-PE was studied to optimize this technique for quantitative accuracy and to confirm the nature of specific interactions between the target molecule and the binding sites. Figure 2.4.4.2 illustrates the effect of normalized solvent polarity on elution efficacy (in terms of normalized peak area relative to that for methanol, which resulted in the quantitative elution of theophylline). A general trend can be seen of increasing elution efficacy with greater solvent polarity. This data provides clear guidance to the choice of a suitable elution solvent and can further provide insight on the pulsed elution process. With the use of less polar (and weaker) solvents, additional injections of 20-μL solvent aliquots were necessary in order to remove any remaining quantity of theophylline from the column.

When two aprotic solvents (acetonitrile and chloroform) were studied, neither produced any elution of the bound theophylline. Although acetonitrile is very polar, it proves to be a total exception to the trend observed for protic solvents. This contradiction suggests that the theophylline molecule is bound to the binding sites through hydrogen bonding, which cannot be disrupted through injection of an aprotic polar solvent. Therefore, only protic solvents are able to compete, through hydrogen bonds, with the binding sites for the theophylline causing the rapid desorption of the bound molecule.

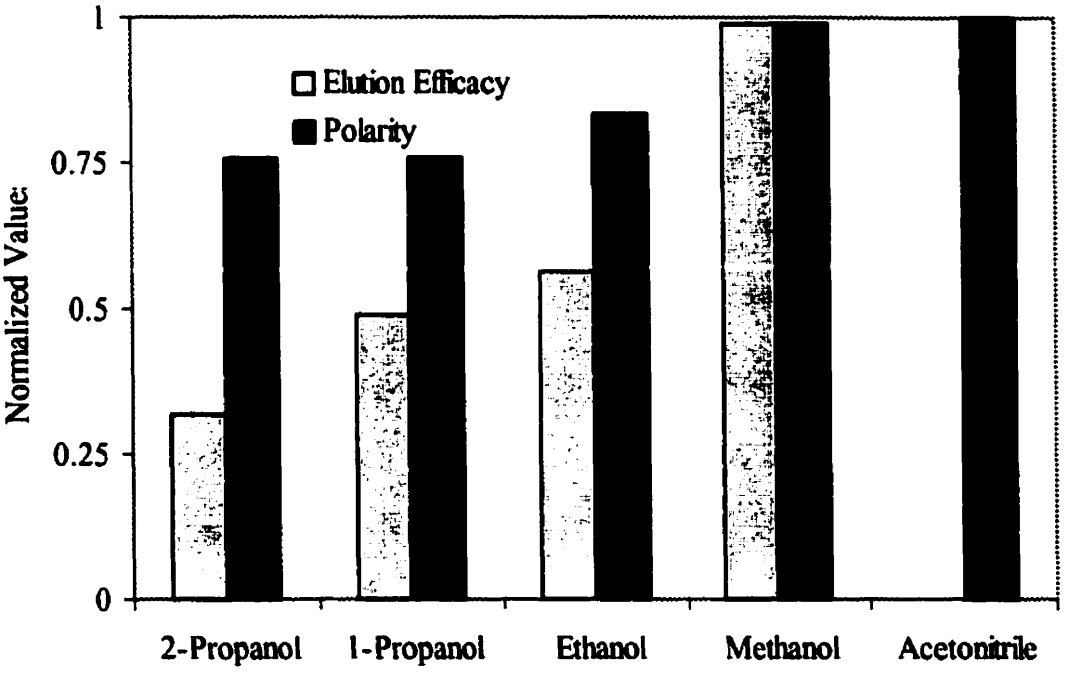

Figure 2.4.4.2: Correlation between normalized solvent polarity and normalized elution efficacy of 400 ng/mL theophylline from a theophylline MIP column.

Under the optimized conditions of mobile phase (chloroform) and pulsed elution solvent (methanol), a standard calibration curve was generated for theophylline over a large range of concentrations (0.25-1000 μg/mL). As shown in Figure 2.4.4.3, the curve had excellent linearity as indicated by a R^2 value of 0.997. The concentration detection limit was 120 ng/mL, corresponding to an absolute quantity of 2.4 ng, which falls well below the required detection limit of 10 μg/mL for serum analysis.[132]

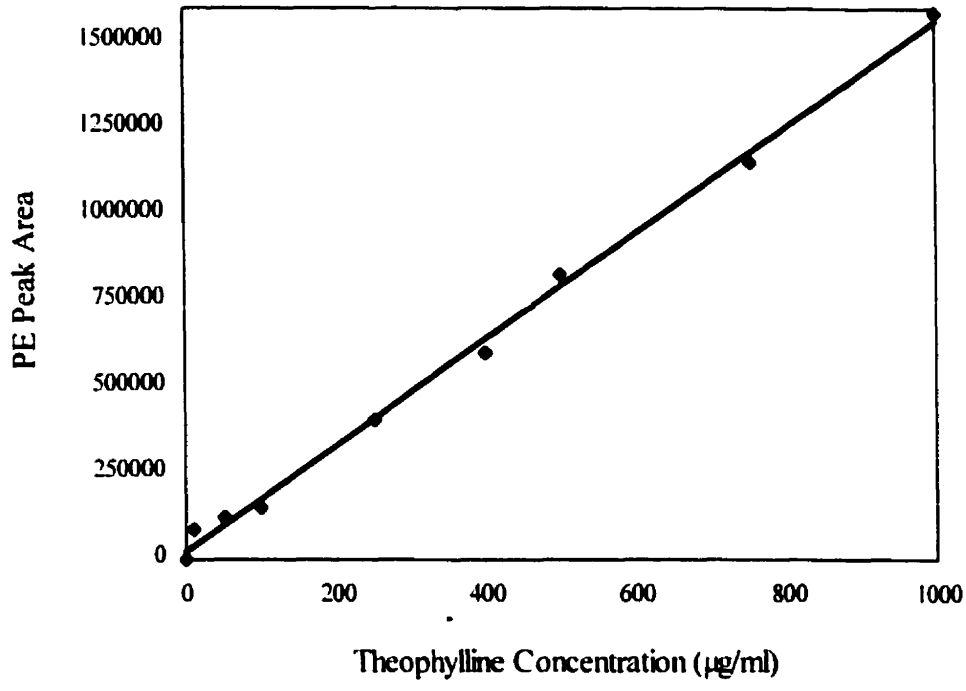

Figure 2.4.4.3: MISPE-PE theophylline calibration curve.

Furthermore, preconcentration of a 40-ng/mL sample on the MIP column by performing 5 injections before pulsed elution provided an improved detection limit of 25 ng/mL. In comparison with existing HPLC methods of theophylline analysis, the MISPE-PE technique offers a very competitive detection limit and greatly reduced time requirements.[21] Automation of a similar sample enrichment procedure has been recently illustrated using a solid-phase microextraction tube.[133] Automated MISPE-PE will prove itself to be a powerful technique for the routine analysis of dilute theophylline samples.

2.4.5 Preparation of Micro-columns

The MIP could be reproducibly prepared with small batch-to-batch variations. Binding sites could be created using MAA as the functional monomer and theophylline as the basic template equipped with proton-accepting (or hydrogen-bonding) functional groups. After crushing, grinding and Soxhlet extraction with methanol-acetic acid (9:1 v/v), the MIP particles contained vacant sites (or cavities) which could bind theophylline up to a maximum capacity of 35.2 mg/g, as determined in a batch binding measurement over 24 hours. As a consequence of the high binding capacity of the polymer, the development of a micro-column was possible as only a very small amount of material was required for the successful separation of trace quantities of theophylline from its structural analogues. The relatively large particles (≤63 μm) and small dimensions of the micro-column generated low back pressures (< 500 psi), which allowed the use of high flow rates for rapid equilibration with the chloroform mobile phase and for fast MISPE-PE determination of theophylline. The particles were so durable that the MIP micro-column could be used repeatedly over a prolonged period of months without any apparent loss of performance. Possible settling of these particles, resulting in a void volume at the entrance of the column, was not a concern due to the size of HPLC tubing used to construct the micro-column. The normal peak broadening associated with a void volume is eliminated due to the small size of the micro-column's inner diameter relative to the 20-μL injected volume of sample.

In addition, when compared to larger columns, the reduced mass of polymer in the micro-column, provides better desorption of bound theophylline for a standard volume of 20 μL of the pulsed elution solvent as the ratio of elution solvent molecules to binding sites is

increased. The micro-column (63 μL) was compared to two columns of larger volumes, 100 μL and 565 μL, for its pulsed elution efficacy. A 20 μL standard theophylline solution was injected onto each column followed by desorption of the bound theophylline by 4 successive pulsed elutions of methanol. The percent relative standard deviation (% RSD) of the total theophylline peak area for second, third and fourth pulse elution was calculated for each column and is presented in Figure 2.4.5.1. In terms of sensitivity, accuracy, reproducibility and simplicity complete desorption of the theophylline by the first addition of methanol is essential.

The calculated % RSD for the micro-column (~ 2 %) was much lower than those for the larger columns therefore indicating the complete removal of the bound theophylline with the first pulsed elution. As mentioned above, the inability of a 20-μL aliquot of methanol to quantitatively remove theophylline from the 100 and 565 μL columns was due to the decreased volume ratio of elution solvent to polymer material. In addition, the increased inner diameter of the larger columns provide a reduced linear flow rate that enhances the amount of theophylline diffusing into the porous cavities of the MIP, resulting in a greater number of available binding sites for theophylline adsorption during sample injection.

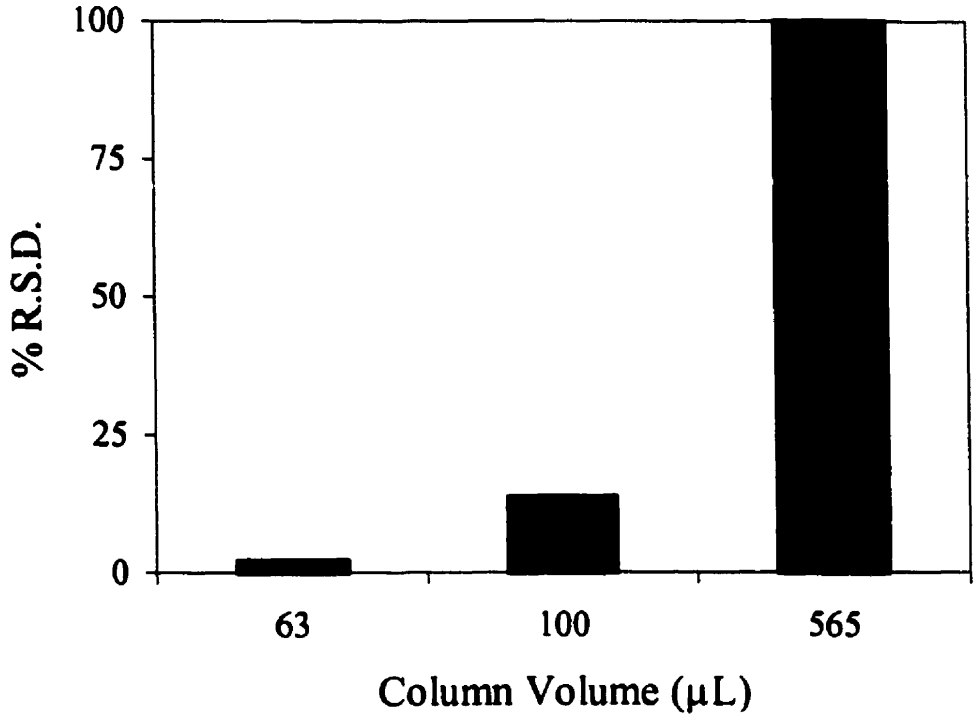

Figure 2.4.5.1: Percentage relative standard deviation of total theophylline peak area for second, third and fourth pulsed elution from 65, 100 and 565 µL MIP columns.

2.4.6 MISPE-PE with Micro-column

The affinity of theophylline molecules to the MIP micro-column results from complex interactions between their complementary chemical functionalities, which are strongly dependent on the surrounding solvent medium.[134] Chloroform is a low (to medium) polarity, non hydrogen-bonding (aprotic) solvent which was found to be suitable for theophylline determination by MISPE-PE. Under these mobile phase conditions, a theophylline standard concentration below the load capacity of the MIP micro-column, will yield complete retention of theophylline. However, this acid-base interaction between the polymerized methacrylic acid monomer and theophylline print molecule can be effectively disrupted by a 20-μL injection of methanol. Standard calibration curves, over a fairly wide concentration range of 1-250 μg/mL theophylline in chloroform, were constructed at two flow rates in Figure 2.4.6.1 for evaluation of the micro-column performance in MISPE-PE.

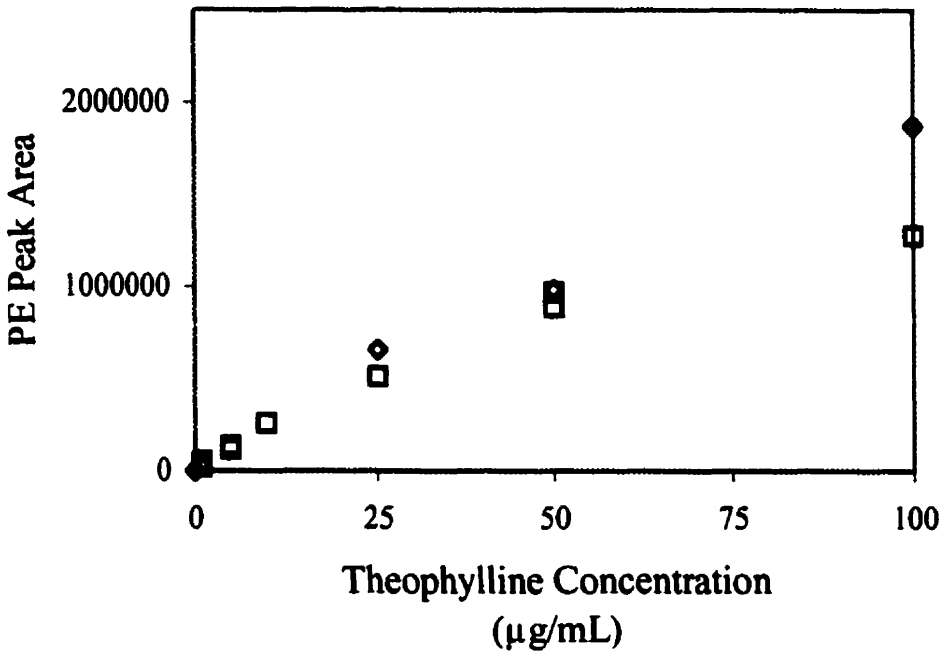

Figure 2.4.6.1: MISPE-PE standard calibration curve for theophylline, using mobile phase flow rates of 0.5 (◊) and 1.0 mL/min (□).

Excellent linearity was observed (average R^2 = 0.997) over the 0-10μg/mL concentration range for both curves. However, the binding capacity of the micro-column was saturated at the 100-μg/mL theophylline level for the 0.5-mL/min flow rate, and 70 μg/mL for 1.0 mL/min. These saturation levels are relatively high but not unrealistic, considering the high sample load capacity of MIP materials. Although the curve shapes were identical for both flow rates, the peak areas for the saturation levels were quite different. For instance, the peak area measured for 100-μg/mL theophylline at a flow rate of 0.5 mL/min was 46% larger than that at 1.0 mL/min. This suggests an important role of diffusion in the accessibility of binding sites. Since the MIP material is very porous,

the slower flow rate enabled the theophylline molecules to better permeate the cavities to interact with more binding sites. Therefore, at this slower flow rate, the micro-column also had an increased binding capacity and the MISPE-PE method exhibited a larger linear dynamic range. However the capacity of the micro-column to bind theophylline will not be a serious concern, as the saturation level of 100 μg/mL is already 5 times larger than the upper therapeutic limit for theophylline.

The binding capacity of the micro-column was further evaluated by comparison to two larger columns. Figure 2.4.6.2 shows typical chromatograms from the three columns to contrast their peak shapes. As expected, the peak width at half maximum decreases with smaller column diameter due to less lateral (radial) diffusion of the injected theophylline. Since the micro-column was constructed from HPLC tubing with an inner diameter close to that of the in-take tubing, the extent of diffusion is negligible as the sample entered the column resulting in an optimal peak shape. The narrow peaks observed in MISPE- PE on a micro-column provide better analytical sensitivity than on the larger conventional HPLC-type columns. The calibration curves constructed for the two larger columns indicated no saturation up to the 100-μg/mL theophylline level. The slopes of the linear portions over the lower concentration range were very similar to those observed for the micro-column.

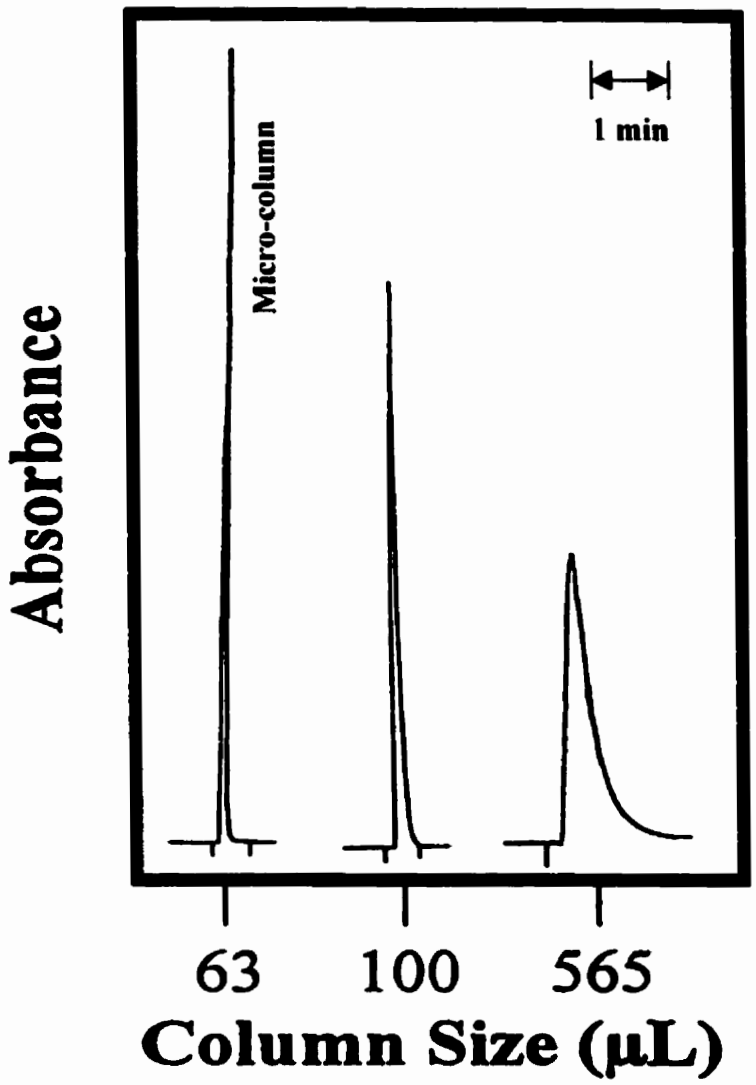

Figure 2.4.6.2: Typical MISPE-PE chromatograms for 63, 100, and 565 µL MIP columns. Mobile phase = 100% chloroform; flow rate = 0.5 mL/min; sample volume = 20 µL; PE volume 20 µL; detection λ = 270 nm.

A rigorous comparison of their analytical sensitivities is complicated by differences in solvent flow velocity and analyte radial diffusion. The detection limit for the micro-column is 0.5 μg/mL, which is comparable to those determined for the larger columns.

2.4.7 Effect of Solvent Polarity

The selection of an appropriate solvent polarity for MISPE-PE was an important parameter in the present method development. Essentially, the solvent carried the sample through the column, where the theophylline molecules underwent a multitude of binding interactions including hydrogen bonding. A polar solvent with high dielectric constant could reduce the Coulombic attraction to weaken the binding. Hypothetically, many theophylline molecules would be carried out of the SPE column leaving only a few retained for PE. Such an effect of solvent polarity on MISPE-PE was investigated by adding acetonitrile (polarity = 5.8) to the chloroform (polarity = 4.1) in varying percentages. The results verified a trend of increasing peak areas for the break-through portion (or analyte eluted through column by mobile phases without retention) with the addition of acetonitrile, and decreasing peak areas for the PE portion, as shown in Figure 2.4.7.1.

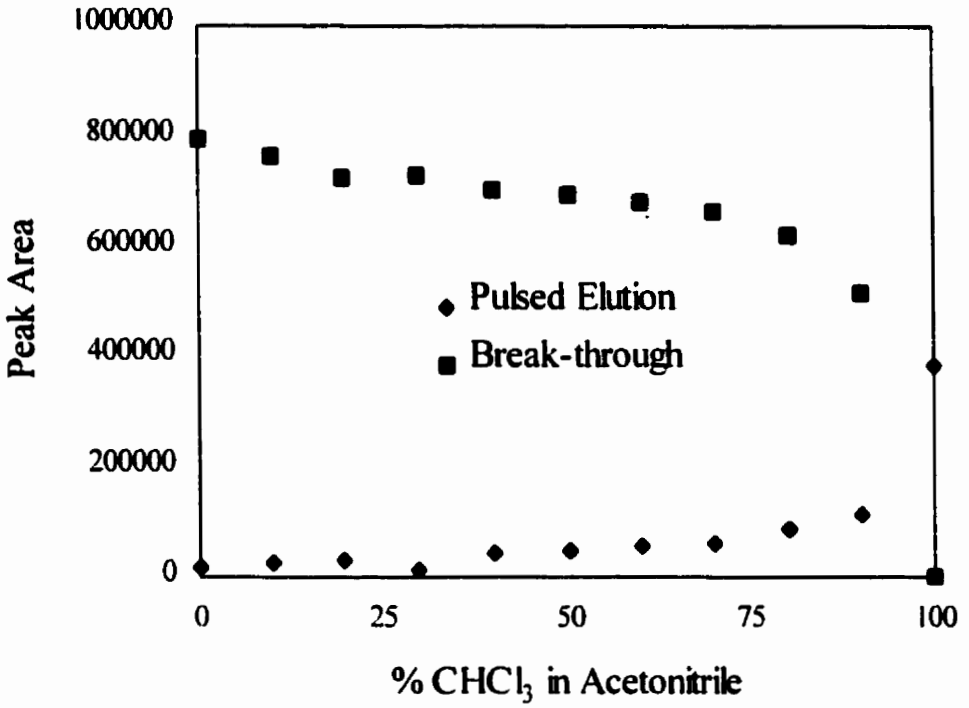

Figure 2.4.7.1: Solvent polarity effect on MISPE-PE of theophylline with micro-column.

Chloroform clearly was the best solvent for theophylline determination by MISPE-PE, when the theophylline injected was quantitatively retained on the MIP column for PE. As the percentage of acetonitrile was increased, the amount of retained theophylline rapidly decreased to as low as 2.2%. At 100% acetonitrile, the polarity of the solvent was so high that the molecular recognition capabilities of the MIP could not be maintained.

2.4.8 Interference of Various Drugs

The selectivity of the theophylline MIP material had been previously evaluated.[135,136,137] In all instances, the material showed selectivity for theophylline, but interference evaluation was limited to caffeine and/or xanthine. Vlatakis *et al* had determined the cross-reactivity of the theophylline MIP with ten structural analogues of theophylline.[22] This was accomplished by incubating the polymer particles with each analogue in acetonitrile/acetic acid (99:1) for 15 hours. Poor binding (<1%) of the theophylline MIP with the analogue was demonstrated in all cases by radioactivity measurements, except for 3-methylxanthine which produced a 7% cross-reaction. Although the same theophylline MIP preparation was used in the present MISPE-PE work, a different degree of selectivity was observed when eight drug compounds were tested on the theophylline MIP micro-column and their interference effects are summarized in Table 2.4.8.1.

Table 2.4.8.1: Percent Interference of Various Drug Compounds on Theophylline MIP Micro-column.

Drug	Concentration (μg/mL)	% Interference	
			Vlatakis[22]
Dyphylline	200	97.6	
β-hydroxyethyltheophylline	200	12.0	
Theobromine	200	35.8	< 1
Caffeine	200	0.0	< 1
Acetaminophen	200	100	
Phenylbutazone	200	1.2	
Hydrochlorothiazide	100	17	
Nicotinic acid	100	90.7	

The percent interference was calculated as a ratio of the pulsed eluted peak area to the sum of the break-through and pulsed eluted peak areas. Apparently, the binding selectivity increased with the number of proton-accepting (or hydrogen-bonding) sites on the drug molecule, as previously reviewed by Sellergren.[138] One notion was that the % interference was governed by some strong interaction between the basic nitrogen(s) in a drug molecule and the acidic carboxylic moieties in the MIP matrix. Indeed, a relationship exists between the % interference and the basicity (or pK_a) for the drug molecules tested, as seen in Figure 2.4.8.1. The % of interference increases sharply with pKa, until reaching and maintaining the maximum value at ~ pKa = 9 (theophylline). The empirical or calculated pK_a values were obtained from the ACD/Ilab Web service, version 3.06 (http://www.acdlabs.com/ilab/).

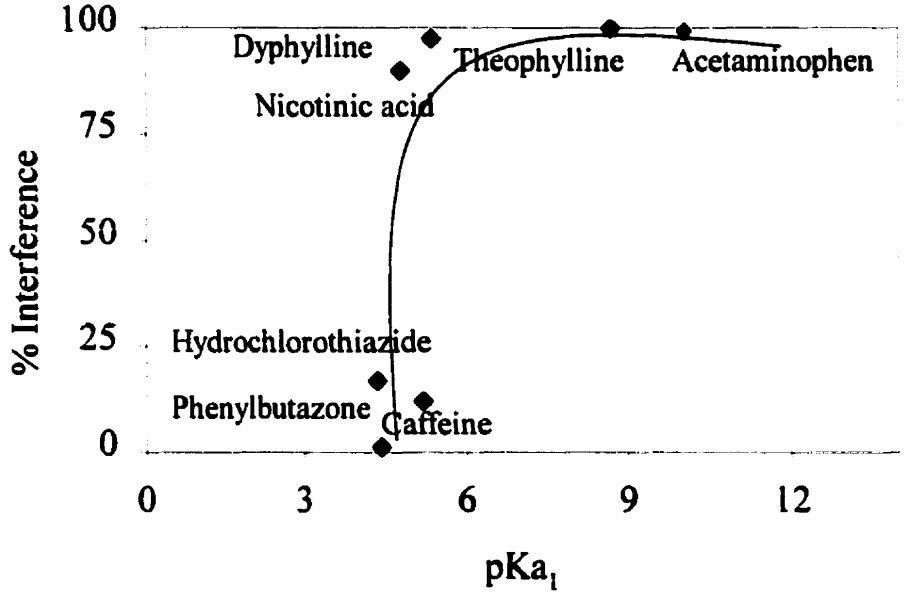

Figure 2.4.8.1: Percentage interference vs pKa_1 for several drug compounds.

The interference occurred as a result of non-specific acid-base interactions between drug molecules and the MIP particle surfaces under fast solvent flow velocity conditions. A contrast can be made between 21.2 mm/s and 1.3 mm/s for the linear solvent flow velocities through this micro-column and a MIP column with a larger inside diameter of 4 mm, assuming the same solvent flow rate of 1 mL/min through each. If the non-specific nature of basic drug interference can be confirmed, one practical solution, as discussed below, would b performing the MISPE step at reduced solvent flow velocities to promote analyte

diffusion into the selective cavities inside the MIP particles. Another partial solution would be solvent pH adjustment which eliminates all interference by those drugs having a pK_a greater than the solvent pH. These now protonated drug molecules are unable to undergo the non-specific acid-base interactions. However, for the intended protocol of rapid MISPE-PE, a more selective elution technique using differential pulses was investigated as detailed below.

2.4.9 Molecularly Imprinted Solid Phase Extraction Differential Pulsed Elution (MISPE-DPE)

The effect of solvent polarity, as studied above, represents a convenient parameter for controlling theophylline versus interference binding on the MIP column. By adjusting the polarity of the PE solvent, the non-specific adsorption of drugs could be selectively removed in consecutive pulses. For example, after a 100-μg/mL sample of hydrochlorothiazide was injected onto the MIP micro-column, rapid elution of an analyte peak by isocratic chloroform was observed. Three intermediate injections of 20-μL acetonitrile were next performed to wash off any hydrochlorothiazide remaining on the micro-column due to non-specific adsorption. To confirm if the wash removed the hydrochlorothiazide quantitatively, three pulsed elutions with 20-μL methanol were carried out. The overall results indicated that acetonitrile was successful in removing 95% of the hydrochlorothiazide, while the other 5% was eventually eluted by methanol. For comparison purposes, a 100-μg/mL theophylline standard was also evaluated in the same

manner. No analyte peak was initially eluted, and only 43% of the bound theophylline was removed by the acetonitrile wash. This percentage may be interpreted as the theophylline molecules which were non-specifically bound to the MIP surface sites. In terms of eliminating interference, the polar acetonitrile was effective in removing all non-specifically bound species. Such a differential pulsed elution (DPE) approach allows the determination of theophylline after interference removal, even though the sensitivity of the MISPE-DPE method may be sacrificed. Consequently, the detection limit for theophylline will be increased from 0.5 μg/mL to 1.0 μg/mL, a level that still satisfies theophylline's therapeutic range of 10.0 –20.0 μg/mL.

2.4.10 Flow Rate Dependence at 20°C

The selective binding of theophylline to the micro-column had to be further optimized in order to circumvent a decreased sensitivity of the MISPE-DPE technique. For enhanced theophylline selectivity in the MISPE binding process, accessibility to the binding sites inside the porous MIP particles by molecular diffusion was essential. The problem of accessibility was exacerbated by the small diameter of the micro-column which generated a high solvent flow velocity, thereby kinetically limiting the access of theophylline molecules to the inner selective cavities.[139,140] Consequently, the kinetic selectivity of the MIP suffered when compared to its thermodynamic selectivity under batch binding conditions, as recently reported for the slow kinetics of equilibrium sorption in packed-bed experiments[141]. Since the solvent flow velocity dictated the time available for diffusion, analyte selectivity

of MISPE was evaluated by varying the solvent flow rate over a range of 0.05-1.00 mL/min. Standard solutions of 50 μg/mL theophylline and acetaminophen (prepared in chloroform) were separately injected onto the micro-column, followed by desorption of the bound analyte by PE with methanol. This PE peak area was used to determine the amount of theophylline or acetaminophen bound to the MIP at each flow rate, as illustrated in Figure 2.4.10.1.

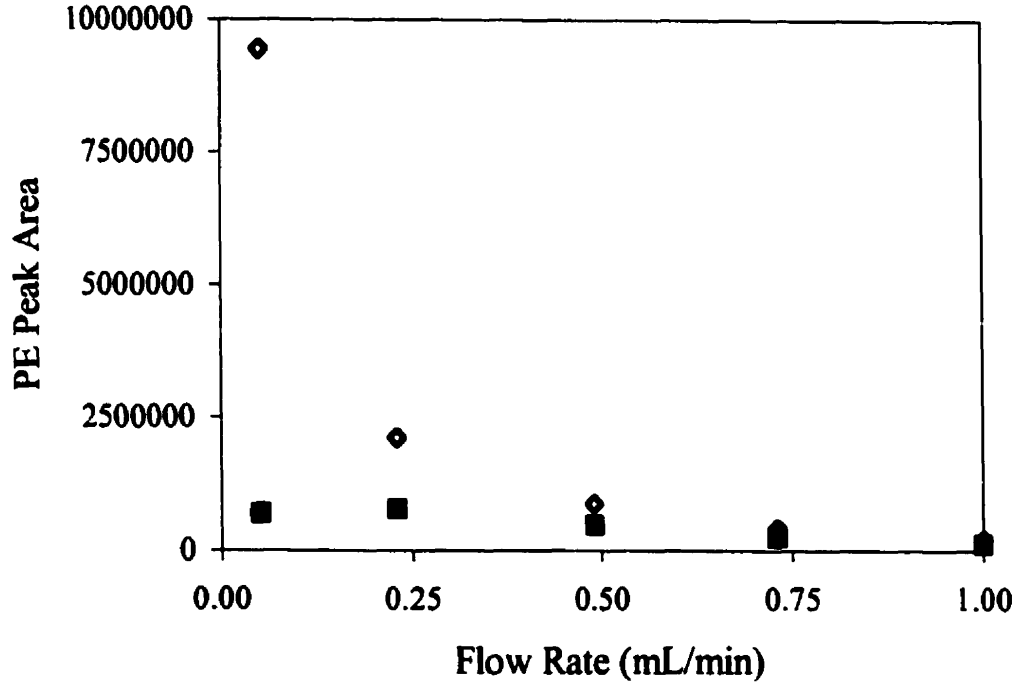

Figure 2.4.10.1: PE peak areas for theophylline (◊) and acetaminophen (■) at various flow rates.

Theophylline displayed a trend of increased binding efficiency with decreasing flow rate, which provided more time for the diffusion of theophylline molecules to the strong and selective binding sites inside the MIP particles. This confirmed the critical role of diffusion in the binding process. Such molecular recognition was not shared by acetaminophen, as evidenced in its fairly constant amount bound over the evaluated flow rates. A ratio of PE peak areas, theophylline to acetaminophen, now provides in Table 2.4.10.1 a theophylline

binding selectivity factor for the micro-column at each flow rate after the UV molar absorptivities of theophylline and acetaminophen at 270 nm are factored in.

Table 2.4.10.1: Theophylline Binding Selectivity Factor for the Micro-column at Different Flow Rates.

Flow Rate (mL/min)	Binding Selectivity Factor [1]
1.00	0.49
0.73	0.52
0.49	0.57
0.23	0.83
0.05	4.24

[1]calculated from the ratio of PE peak areas, theophylline to acetaminophen

It highlights the trend of increasing theophylline binding selectivity factor with decreased flow rates, thereby implicating the predominance of molecular recognition. On the contrary, non-specific binding was stronger for acetaminophen than theophylline as indicated by binding selectivity factor values of less than 1.00 at the high flow rates. This was merely the consequence of a higher pKa value for acetaminophen than theophylline, which provided a stronger interaction between the basic nitrogen of acetaminophen and the acidic carboxylic moieties in the MIP matrix. Although a reduction in mobile phase flow rate could alleviate the interference problem, it would obviously compromise the analysis time. Even at the lowest flow rate of 0.05 mL/min, which was most favorable to the selective binding of theophylline, non-specific binding of acetaminophen and other

interferences still occurred and their elimination was essential before theophylline could be determined accurately.

2.4.11 Temperature Dependence

An alternative solution would be temperature elevation by submerging the micro-column into a thermostatic water bath. Temperature was an optimization parameter that had often been overlooked in SPE studies, despite its well-known advantages of increased sample solubility, improved column efficiency and reduced column pressure drop.[142] The theophylline MIP had good thermal stability that permitted the use of elevated column temperatures up to 60°C for better theophylline accessibility to the binding sites inside the porous MIP by molecular diffusion. As mentioned above and suggested in a previous report[143], solvent polarity was critical in the MISPE selectivity. The highest selectivity was obtained with solvents of low polarity, where electrostatic forces dominated the binding process. Over the temperature range of 20-60°C, the dielectric constant of chloroform was confirmed by refractive index measurements to decrease with increasing temperature. Hence the solvent polarity was decreased in the chloroform mobile phase for MISPE, providing a reduced elution power and greatly improved molecular recognition of theophylline.

DPE experiments were next performed on the micro-column heated to 40°C and 60°C. Better results were accomplished at 60°C, where all tested interferences were

completely removed as summarized in Table 2.4.11.1. In contrast, removal of theophylline from the micro-column *decreased* to a low value of 10%.

Table 2.4.11.1: Percentage of Injected Drug Interference Desorbed from Theophylline MIP Micro-column at 60 °C by one 20-μL Pulse of Acetonitrile.

Analyte	Concentration (μg/mL)	% Removed by Acetonitrile
Acetaminophen	50	100
Dyphylline	50	100
Phosphatidylcholine	10000	100
Theobromine	50	100
Theophylline	50	10

The elevated temperature increased the diffusion rate of theophylline (and interferences) and hence its mass transfer to the strong and selective binding sites inside the porous MIP particles. Due to the high selectivity of these inner binding sites, however, only theophylline was strongly bound. Interferences would be engaged only in non-specific binding, which was easily overcome by the subsequent wash with a 20-μL pulse of acetonitrile. The improved molecular recognition at 60 °C was also essential to the success of quantitative removal of interferences with 90% retention of theophylline in the present DPE technique. It attained maximal detection sensitivity, while maintaining the high flow rate of 0.5 mL/min and the short analysis time of 3 min. To the best of the author's knowledge, this is the first report that has utilized temperature to enhance MIP selectivity based on mass transfer and solvent polarity effects.

2.4.12 Flow Rate Dependence at 60°C

When a temperature of 60 °C was used for MISPE-PE at various chloroform flow rates, much reduced efficacy of PE was observed at 0.05 mL/min. One plausible explanation is that such a low flow rate allowed plenty of time for the methanol to approach 60 °C, which decreased the polarity of methanol and hence its elution strength. At 0.25 and 0.50 mL/min, the efficacy of PE was re-established probably due to insufficient time for the methanol to reach 60°C. The combined effect of theophylline accessibility and PE efficacy are illustrated in Figure 2.4.12.1, where blank-subtracted PE peak areas are plotted against theophylline concentrations for the two flow rates at 60°C.

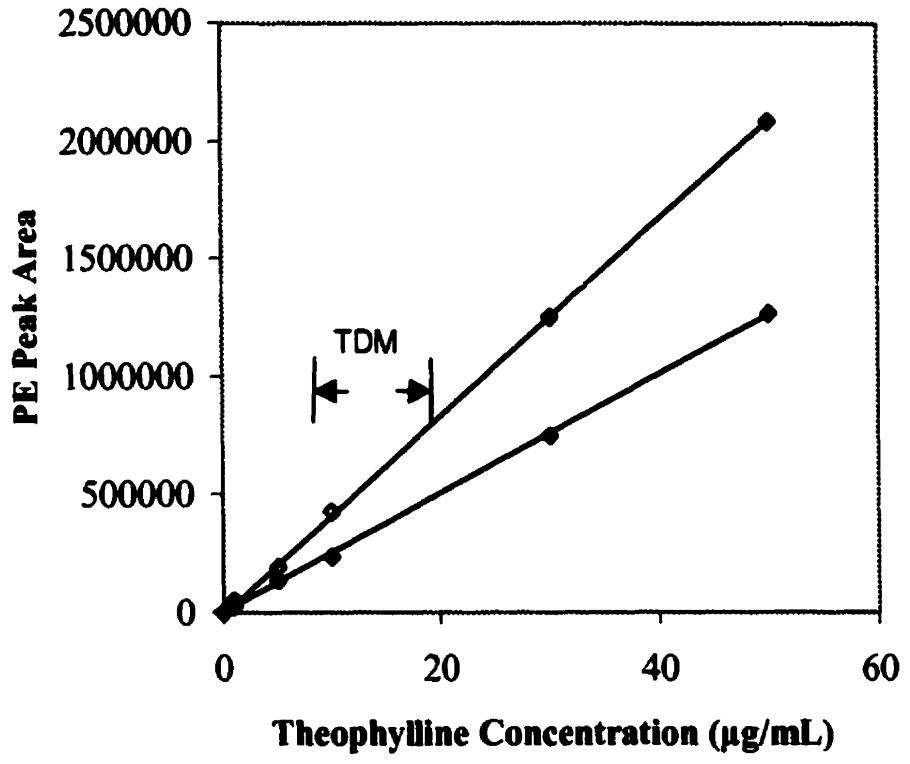

Figure 2.4.12.1: MISPE-PE standard calibration curve for theophylline at 60 °C using mobile phase flow rates of 0.25 (◊) and 0.50 (♦) mL/min.

Table 2.4.12.1 indicates, while a linear response was generated in both cases, a greater analytical sensitivity was attained at 0.25 mL/min. This flow rate also yielded a better detection limit of 0.7 µg/mL, as compared with 1.1 µg/mL for 0.50 mL/min. However, both detection limits would satisfy the therapeutic drug monitoring (TDM) range of 10-20 µg/mL for theophylline.[144, 145]

Table 2.4.12.1: MISPE-PE Standard Curve Statistics for Two Flow Rates.

Flow Rate (mL/min)	Slope (mL/μg)	Correlation Coefficient
0.25	41800	0.9993
0.50	25098	0.9999

2.4.13 Serum Analysis by MISPE-DPE

In the traditional use of HPLC and GC methods for therapeutic drug analysis in such human biological fluids as blood serum, extensive sample cleanup is necessary to remove interferences and extended chromatographic time is required. Conventional SPE for sample cleanup can involve much effort and time, as the sorbent must be pre-conditioned, followed by analyte elution with a large volume of solvent (>0.5 mL) under a vacuum manifold. In addition, there are several chemical limitations (including pH sensitivity in the case of silica-based sorbents) and the awkward requirement of a wetted sorbent that must not dry out.

Rapid determination of theophylline in blood serum was achieved by MISPE-DPE with direct UV detection, utilizing a micro-column temperature of 60°C and a chloroform flow rate of 0.5 mL/min. The use of isocratic chloroform mobile phase provides additional robustness to the technique as it eliminates the requirement for the preparation of more complex mobile phase solutions routinely used in the HPLC analysis of theophylline. Blood serum samples were first extracted with chloroform, which served to isolate theophylline while simultaneously removing interferences such as proteins in the serum. Since theophylline is relatively weakly bound[146] to albumin proteins in serum[147] and the presence of an organic solvent like chloroform has been shown to effectively displace any bound drug [148], the total theophylline concentration is determined with the MISPE-DPE micro-column.

After the chloroform extract was injected onto the micro-column, some interferences would pass through rapidly in approximately 1 minute. DPE of non-specifically bound interferences was next performed, ending with quantitative desorption of theophylline. A MISPE-DPE standard calibration curve for theophylline serum analysis at 60°C was constructed, with excellent linearity ($R^2 = 0.997$) in the concentration range up to 20 μg/mL and a detection limit of 1 μg/mL. Note that this detection limit was better than the 2.5 μg/mL obtained at room temperature, and that the highly selective determination of theophylline was accomplished in less than 3 min as shown in Figure 2.4.13.1.

Multiple analysis (20 injections) of the serum sample resulted in an instrument precision (% RSD) of 2.9 %. Independent preparation and analysis of different serum samples produced a repeatability (intra-assay precision) of < 4.3 %. Several analysts have confirmed these results over a span of many weeks indicating the ruggedness of the technique. Effectively the selective MISPE-DPE technique with UV detection has accomplished all of the sample cleanup, interference removal and analyte determination for serum analysis, with excellent column reusability.

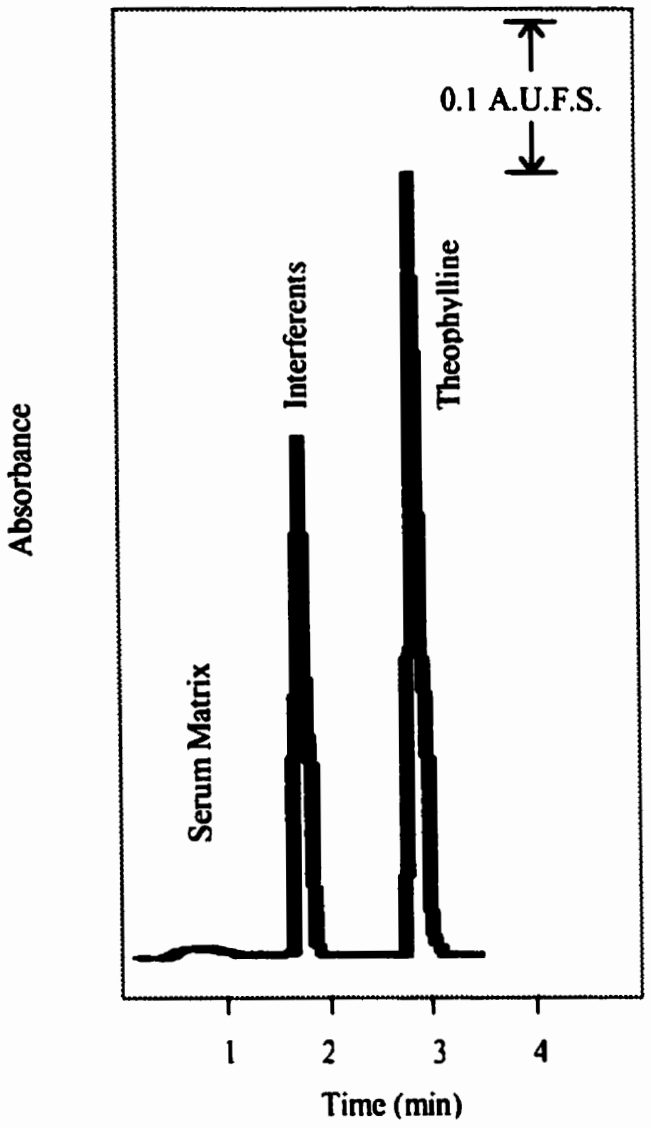

Figure 2.4.13.1: MISPE-DPE of spiked chloroform extract from serum containing 10.0 µg/mL of theophylline using a theophylline MIP micro-column at 60 °C. (8.0 cm X 0.8 mm i..d); mobile phase = 100 % chloroform; flow rate = 0.5 mL/min; sample volume = 20 µL; DPE and PE volume = 20 µL; detection λ = 270 nm.

2.4.14 Nicotine

2.4.14.1 MISPE

The first requirement of MISPE-PE was to determine the conditions under which nicotine could be quantitatively bound by the MISPE micro-column. Nicotine is a basic organic compound ($pKa_1 = 8.02$) that is capable of forming hydrogen bonds. Therefore, its binding interaction with the methacrylic acid (MAA) functionality in the MIP was expected. The binding affinity was however influenced by the mobile phase, as the hydrogen bonding capability of protic solvents would compete with the MAA for nicotine. Likewise, polar solvents would weaken the electrostatic interaction between the MAA recognition sites and nicotine. Chloroform was initially chosen as an aprotic solvent with low polarity, for evaluation in the MISPE-PE determination of nicotine. Solvent polarity was next increased with the use of acetonitrile. The absence of a break-through nicotine peak indicated that both solvents provided quantitative binding of the 2 μg of nicotine (20 μL of 100 μg/mL standard solution prepared in acetonitrile) by the micro-column. However, the binding was irreversible in the case of chloroform when PE with methanol, which is a polar and protic solvent, resulted in no significant desorption of the bound nicotine. In the case of acetonitrile, PE with methanol produced a 19% desorption of the bound nicotine. A binding constant of 2.7×10^5 M^{-1} had previously been reported for a similar nicotine MIP.[149] Together they suggested that a stronger PE solvent would be needed, unless a more polar and aprotic solvent than acetonitrile could be found for the MISPE-PE determination of nicotine.

Water was next tested as a more polar solvent than methanol for PE, and still it was only able to desorb 45 % of the bound nicotine. Therefore, the role of pH in the PE solvent strength was investigated for quantitative desorption of bound nicotine from the MIP micro-column. Several solvents were evaluated, ranging over acidic, neutral and basic pH values. Since the molar absorptivity of nicotine varied with pH, the percentage of nicotine desorbed by the first 20 μL PE aliquot was determined for each solvent as a ratio of the first PE peak area divided by the sum of all four PE peak areas. In terms of analysis speed, accuracy and reproducibility, it was desirable that the first PE could elute the bound nicotine quantitatively. As illustrated in Figure 2.4.14.1.1, the correlation between the nicotine elution efficacy and pH of the PE solvent is obvious ($R^2 = 0.997$), with quantitative elution obtained using 1.0% TFA at pH 0.8.

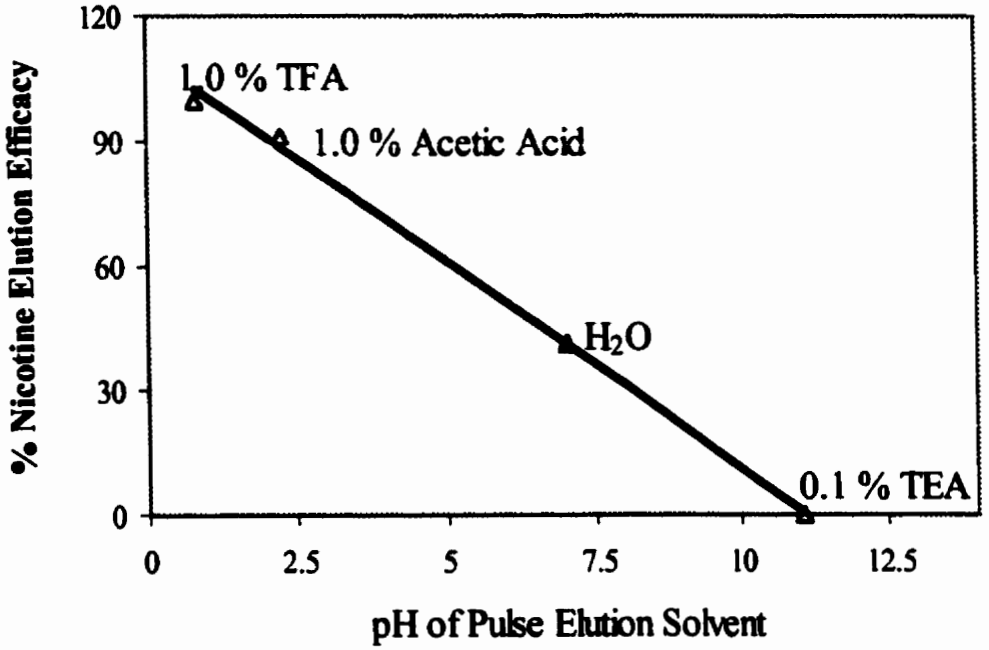

Figure 2.4.14.1.1: Correlation between nicotine elution efficacy and pH of PE solvent on nicotine MIP micro-column. (8.0 cm X 0.8 mm i..d); mobile phase = 100 % acetonitrile; flow rate = 0.5 mL/min; sample volume = 20 µL; PE volume = 20 µL; detection λ = 254 nm.

This acidic PE solvent was able to compete with the MIP's carboxylic acid groups, charging the bound nicotine molecules via protonation and releasing them from the MIP. Removal of nicotine was also assisted by the aqueous property of 1% TFA, which provided adequate polarity to electrostatically disrupt the hydrogen bonding interaction between nicotine and carboxylic acid groups. The result was rapid desorption of nicotine, producing a very sharp PE peak as shown in Figure 2.4.14.1.2.

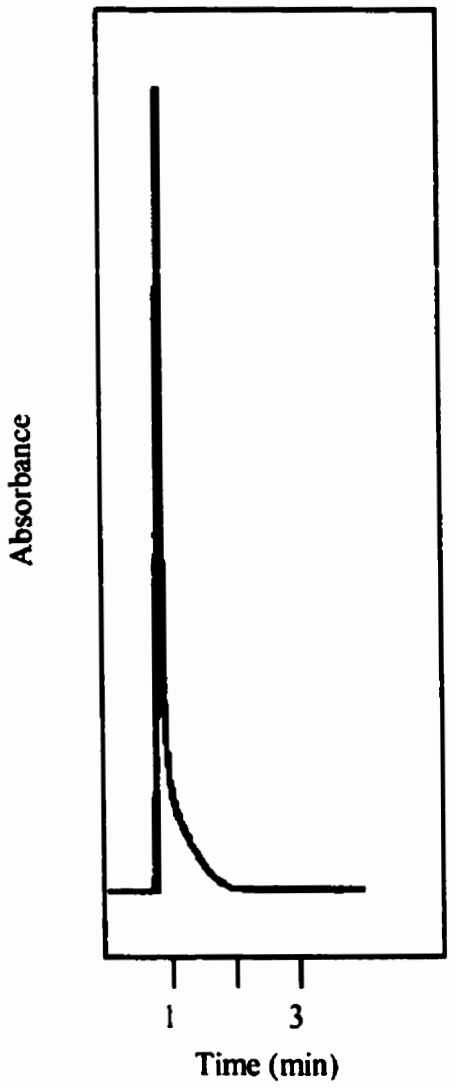

Figure 2.4.14.1.2: 1% TFA PE of nicotine from nicotine MIP micro-column. (8.0 cm X 0.8 mm i..d); mobile phase = 100 % acetonitrile; flow rate = 0.5 mL/min; sample volume = 20 μL; PE volume = 20 μL; detection λ = 254 nm.

The use of a low pH in the PE solvent had the additional advantage of enhanced detection sensitivity, as the diprotonated form of nicotine has a larger molar absorptivity at its λ_{max} of 254 nm.[150] On the contrary, PE under basic conditions with 0.1% TEA would make nicotine exist in its unprotonated form that bound strongly to the carboxylic acid groups. The resulting nicotine elution efficacy was hence very low (< 1%).

Development of the MISPE-PE method for nicotine determination included optional sample preconcentration. This was evaluated with 845 μL injections of 10-100 ng/mL nicotine standard solutions, each followed by a 20 μL PE with 1 % TFA. A linear calibration response was obtained, and a detectable peak signal was observed for 10 ng/mL nicotine.

2.4.14.2 Selectivity of MISPE-DPE

Nicotine extraction from tobacco could yield many organic interferents, including the trace alkaloid myosmine. This molecule is structurally identical to nicotine with the exception of a hydrogen replacing the methyl group on the pyrrolidine ring nitrogen (see Figure 2.4.14.2.1).

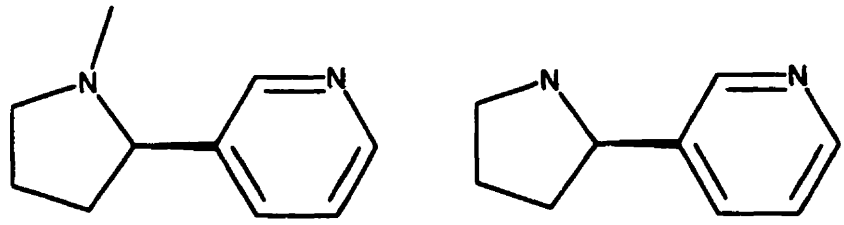

(a) (b)

Figure 2.4.14.2.1: Molecular structures of nicotine (a) and myosmine (b).

Hence, myosmine was chosen to evaluate the selectivity of the MIP micro-column. Selectivity was evidenced as there was almost quantitative (99.5%) binding of nicotine to the micro-column while only 30% of myosmine was bound, as indicated in Table 2.4.14.2.1.

Table 2.4.14.2.1: Evaluation of Nicotine Micro-Column Selectivity by MISPE-DPE.[1]

Test Analyte (in Methanol)	% Break Through	% Bound	% of Bound Analyte Eluted by 20 μL of Methanol	% of Bound Analyte Eluted by 20 μL of 1% TFA
100 μg/mL Nicotine	0.5	99.5	42.8	57.2
100 μg/mL Myosmine	70	30	95.0	5.0

[1] column temperature = 60°C; mobile phase = 100% acetonitrile; flow rate = 0.5 mL/min; sample volume = 20 μL; detection λ = 254 nm.

The non-specifically-bound myosmine had to be removed before accurate determination of nicotine was possible. Fortunately, a protic solvent of high polarity such as methanol could overpower the weak interaction that governed the non-specific binding of

myosmine. A 20-μL pulse of methanol resulted in as much as 95.0% desorption of the bound myosmine. In contrast, the MIP material provided selective cavities for strong binding of nicotine, which was able to partially resist the methanol wash. This was illustrated with only 42.8 % of the bound nicotine being removed by a 20-μL pulse with methanol. Afterwards, complete desorption of the remaining 57.2 % nicotine was made possible with a 20 μL PE with 1% TFA in water. This combination of two pulses (methanol and 1% TFA) provided a differential pulse elution (DPE) technique that allowed the determination of nicotine to be free of myosmine interference, even though the sensitivity of the MISPE-DPE method was somewhat sacrificed.

2.4.14.3 Nicotine Determination in Tobacco

Nicotine standard solutions prepared in methanol produced a MISPE-DPE calibration curve over the concentration range of 1-1000 μg/mL with good linearity (R^2 = 0.984 at n = 5) with a limit of detection of 1.8 μg/mL, using a column temperature of 60°C. An elevated temperature of 60°C increased the rate of analyte (and interferences) diffusion and hence mass transfer to the strong and selective binding sites inside the porous MIP particles. Due to the high selectivity of these binding sites, however, only analyte molecules were strongly bound. Interferences would be engaged only in non-specific binding, which was easily overcome by a subsequent wash with a polar solvent.

A sample of 0.7985 g cigarette tobacco was sonicated with 100 mL of methanol/0.1 N NaOH to extract the nicotine. Dilution of the tobacco extract filtrate with methanol (33

X) provided a nicotine sample suitable for direct MISPE-DPE analysis. When methanol was the sample solvent, only 0.5% of nicotine would be lost in the break-through peak (as well as 70% of myosmine, see Table 2.4.14.2.1. This break-through peak, which also contained other matrix components, was rapidly eluted from the column as illustrated in Figure 2.4.14.3.1. A 20 μL pulse of methanol then washed away any residual bound interferents (including myosmine) and some bound nicotine. Finally, a 20 μL pulse of 1% TFA desorbed the remaining bound nicotine for direct UV detection. The inherent selectivity of the MIP material provided a faster overall analysis time (3 minutes) and a simpler determination of nicotine in the tobacco extract when compared to a typical reverse-phase HPLC result shown in Figure 2.4.14.3.2.

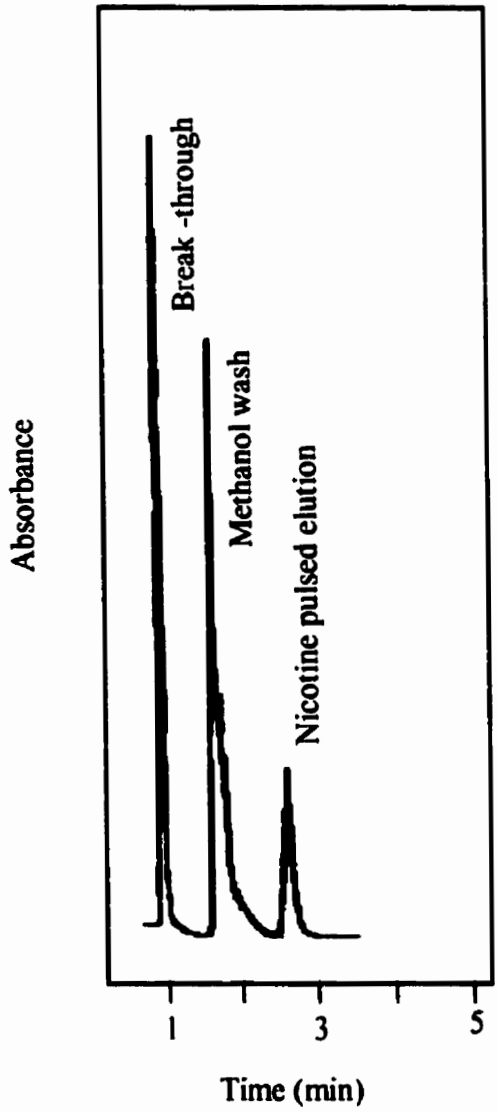

Figure 2.4.14.3.1: MISPE-DPE determination of nicotine in tobacco sample extract with nicotine MIP micro-column. (8.0 cm X 0.8 mm i..d); mobile phase = 100 % acetonitrile; flow rate = 0.5 mL/min; sample volume = 20 μL; DPE and PE volume = 20 μL; detection λ = 254 nm.

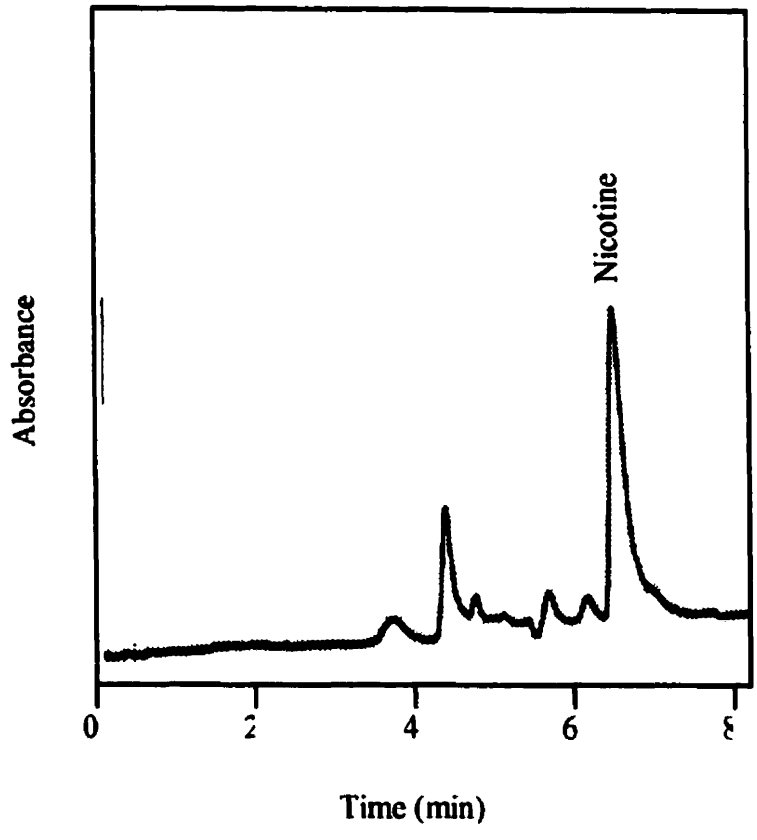

Figure 2.4.14.3.2: Reverse-Phase HPLC chromatogram of nicotine in tobacco extract. Supelcosil LC-18 column (25.0 cm X 4.6 cm, 5 μm particles); mobile phase = methanol-citrate/phosphate buffer (15:85 v/v, pH = 2.4) with 0.1 % TEA; flow rate = 0.7 mL/min; sample volume = 20 μL; detection λ = 255 nm.

Precision was evaluated by 5 injections of the diluted tobacco extract filtrate, which demonstrated a RSD of 5 %. The amount of nicotine in the 0.7985 g tobacco sample was determined to be 15.8 ± 0.8 mg by MISPE-DPE. A relative error of 1.5% was calculated

when the same diluted extract filtrate was analyzed by reverse-phase HPLC (15.6 ± 0.2 mg nicotine in the tobacco sample). These values also correspond well with values reported previously in the literature.[151]

The role of TEA in the mobile phase for the determination of nicotine by reverse-phase HPLC is noteworthy. In the absence of this modifier, nicotine exhibited a very broad elution profile due to ionic interaction of basic nicotine molecules with the residual acidic silanol groups of the stationary material. The addition of TEA to the mobile phase covered these silanol groups, thus reducing their availability for interaction with nicotine.

2.4.15 2-Aminopyridine

2.4.15.1 MISPE-PE

The working principle of MISPE-PE has been also extended to a 2-aminopyridine MIP material. In this work, quantitative SPE of 2-aminopyridine by the MIP micro-column was possible with a non-polar aprotic solvent such as chloroform. PE of the bound 2-aminopyridine was then achieved through a 20-μL injection of 1% TFA in methanol, which is a polar protic solvent. A typical MISPE-PE profile for 2-aminopyridine is illustrated in Figure 2.4.15.1.1. The narrow elution peak of 2-aminopyridine yields a better detection limit and rapid analysis time.

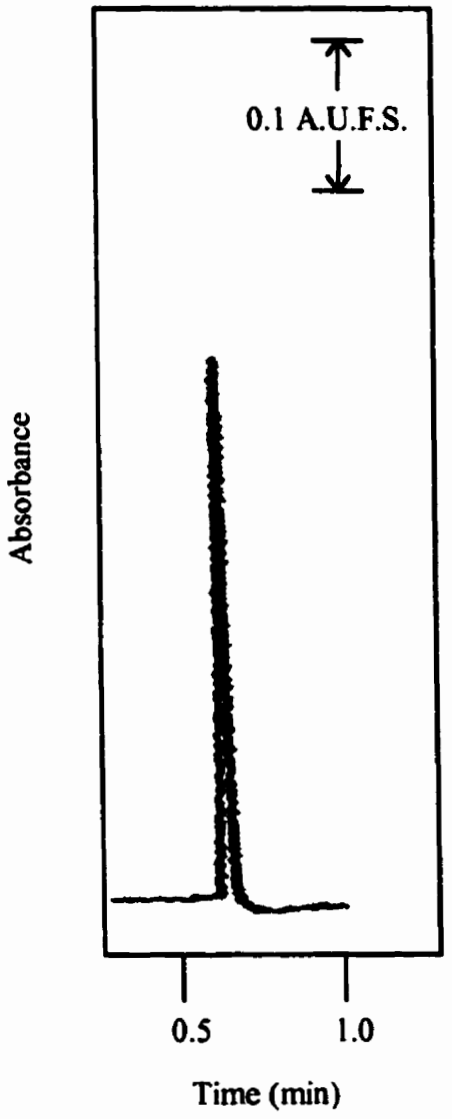

Figure 2.4.15.1.1: MISPE-PE profile for 10 µg/mL 2-aminopyridine (in $CHCl_3$) from a 2-aminopyridine MIP micro-column. (8.0 cm X 0.8 mm i..d); mobile phase = 100 % chloroform; flow rate = 0.5 mL/min; sample volume = 20 µL; PE volume = 20 µL; detection $\lambda = 241$ nm.

2.4.15.2 Selectivity Evaluation

The MIP micro-column was evaluated for its binding selectivity towards several structural analogues of 2-aminopyridine. Table 2.4.15.2.1 summarizes the evaluation results alongside their molecular structures.

Table 2.4.15.2.1: Evaluation of 2-Aminopyridine MIP Micro-column Selectivity by MISPE-PE.

Analyte	Structure	Retention Time (min)	Capacity Factor
2-Aminopyridine	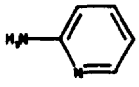	∞	2.9
3-Aminopyridine	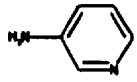	0.53	1.65
4-Aminopyridine	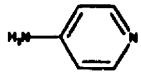	∞	∞
Aniline	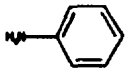	0.22	0.1
2-Methylpyrazine	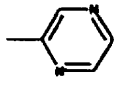	0.22	0.1
2-Picoline	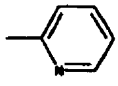	0.22	0.1
4-Picoline	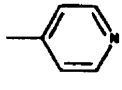	0.24	0.2

The molar volumes of these structures were theoretically calculated by the ACD/ILab Web Database Service (version 3.06) [152], and they differed by a relative standard deviation of 4.4 % only. Such similarity in molecular size and shape between the structural analogues and 2-aminopyridine eliminates any significant effect of steric hindrance to accessing the MIP binding sites. Hence, the observed binding of 2- and 4-aminopyridine with the MIP (in terms of retention time or capacity factor) was mainly the result of strong interactions. One important parameter is the number of interaction functionalities present on the target molecule, complementary to MAA.[83] For example, aniline, 2-picoline and 4-picoline all possess only one hydrogen bonding acceptor functionality at the nitrogen and were therefore unable to strongly interact with the MIP binding sites. Hence, they exhibit low values for the capacity factor. Although 2-aminopyridinde, 3-aminopyridine and 4-aminopyridine all possess two nitrogen functionalities for interaction with the MIP, large differences in binding affinity are evident. Most interestingly, the 2-aminopyridine MIP could retain 2- and 4-aminopyridines strongly but not 3-aminopyridine.

This preferential binding of 4-aminopyridine versus 2-aminopyridine may appear unusual, considering that the MIP was imprinted with 2-aminopyridine. However, a similar result had previously been reported for a 2,4'-bipyridyl MIP, where the nitrogens in the 2 position were less favorable for interaction than those in the 4 position.[153] The authors speculated that the proximity of the pyridyl nitrogens caused a steric hindrance, which adversely affected the monomer – template complex formation. A better understanding of the aminopyridine isomers' interactions with the binding sites in the MIP may be gained

from their resonance structures, a parameter that has been overlooked in all previous studies of monomer-target interactions. As shown in Figure 2.4.15.2.1, the stable resonance structures illustrate the importance of the pyridine nitrogen position in regard to where the negative charge lies on each isomer molecule.

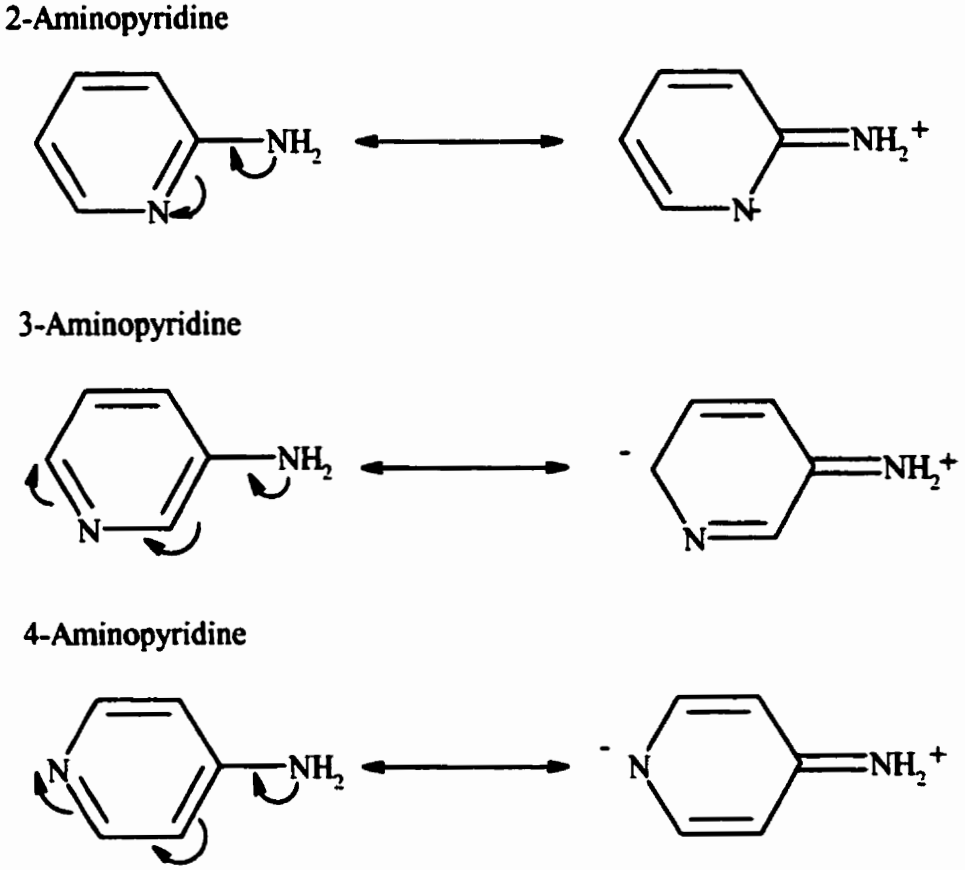

Figure 2.4.15.2.1: Stable resonance structures of 2-aminopyridine, 3-aminopyridine and 4-aminopyridine.

In the case of 2- and 4–aminopyridines, the negative charge present on the pyridine nitrogen provides for strong ionic interaction with the carboxylic acid group of MAA in a binding site. The position of this negative charge may further explain why 4-aminopyridine binds more strongly to the MIP. The para nitrogen in 4-aminopyridine increases the basicity of the molecule. Using the ACD/ILab Web Database Service[152], pKa values were obtained for 4-aminopyridine and 2-aminopyridine to be 9.26 and 6.67 respectively. The interaction between a target molecule and the carboxylic acid group becomes stronger with increasing molecular basicity, as had previously been discussed.[154,155] In addition, it is possible that the large separation of negative and positive charges on 4-aminopyridine, relative to 2-aminopyridine, minimizes steric hindrance for the MAA carboxylic acid group. Therefore, 4-aminopyridne is expected to exhibit a stronger interaction with MAA in the MIP binding sites than 2-aminopyridine.

The above results highlight an interesting possibility that may have important implications in the future preparation of new MIPs. A MIP can be imprinted with a structural analogue (or surrogate) of similar size and shape to the target molecule (or analyte) but with a lower pKa value. The resulting MIP will presumably exhibit a stronger interaction with the analyte than the surrogate. This approach would prove beneficial in instances where the target molecule is either expensive or unavailable, but a cheap structural analogue exists. A similar approach was previously taken by Andersson *et al* to avoid contaminating the sample with leakage of the original target molecule from the MIP in trace analysis.[38] In this thesis work, the surrogate approach has been successfully applied for the selective determination of 4-aminopyridine using a 2-aminopyridine MIP micro-column.

Regardless, 2-aminopyridine (and other interferents) must be differentially removed from the column prior to desorption of the 4-aminopyridine for quantification.

2.4.15.3 Interference Removal by MISPE-DPE

The effect of aprotic solvent polarity, as previously discussed, represented a convenient parameter for controlling the binding of 4-aminopyridine versus 2-aminopyridine on the MIP micro-column. By adjusting the polarity, any bound 2-aminopyridine could be differentially removed from the MIP micro-column by an intermediate wash with 20-μL aliquots of the DPE solvent. Table 2.4.15.3.1 summarizes the efficacy (in terms of % analyte removed) of four solvents for the DPE of 2-aminopyridine and 4-aminopyridine. The dielectric constant is included to represent the role of solvent polarity in the DPE.

Table 2.4.15.3.1: Efficacy of 20-μL DPE Wash for Removal of Bound Analyte on 2-Aminopyridine MIP Micro-column.

Solvent	Dielectric Constant (25 °C)	% Analyte Removed	
		2-Aminopyridine	4-Aminopyridine
Methylene chloride	8.9	0	0
Acetonitrile	37.5 (20 °C)	0	0
DMSO	47	99	0
Methanol	32.6	92	82

As stated earlier, solvents of low polarity (or dielectric constant) are unable to disrupt the interactions responsible for the molecular recognition process in MIPs.

Consequently, methylene chloride and acetonitrile were ineffective for the removal of either 2- or 4-aminopyridine. A solvent of higher polarity, such as DMSO, was required to ensure complete removal (99%) of the 2-aminopyridine from the MIP micro-column without sacrificing any bound 4-aminopyridine. The inability of this aprotic solvent to act as a hydrogen bond donor was essential in ensuring the removal of only 2-aminopyridine but not 4-aminopyridine. For comparison, washing with a protic solvent such as methanol (which has a lower dielectric constant than DMSO) was able to remove a substantial portion of both 2-aminopyridine and 4-aminopyridine. Methanol acted as a hydrogen bond donor to compete with the MIP sites for the two bound analytes, resulting in their rapid elution with little differentiation (92% versus 82%).

A typical MISPE-DPE profile for 10 μg/mL 4-aminopyridine (in $CHCl_3$) from a 2-aminopyridine MIP micro-column is shown in Figure 2.4.15.3.1.

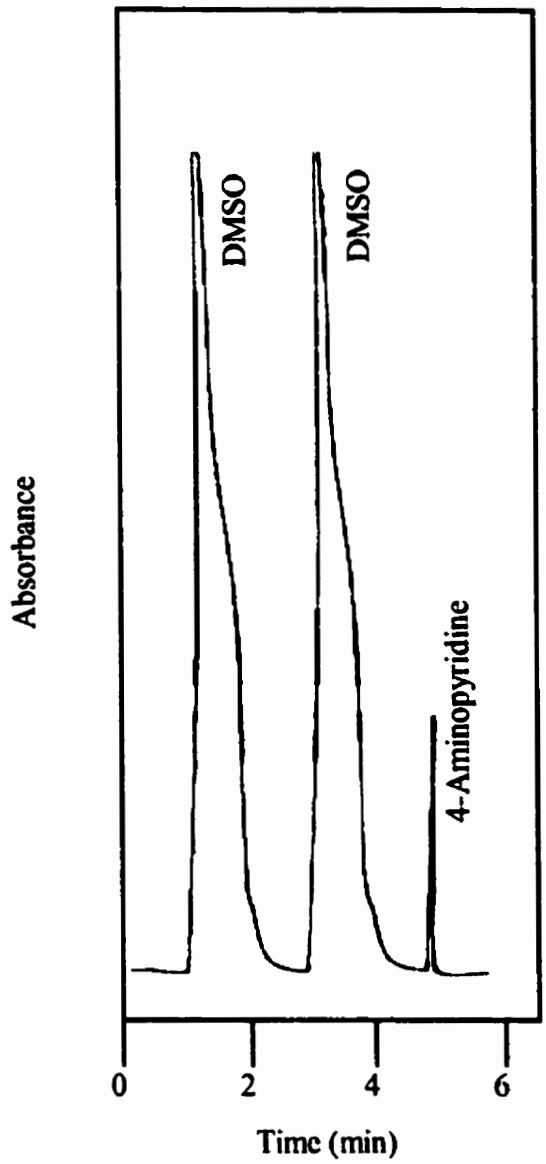

Figure 2.4.15.3.1: MISPE-DPE profile for a 10 µg/mL 4-aminopyridine (in $CHCl_3$) from a 2-aminopyridine MIP micro-column. (8.0 cm X 0.8 mm i..d); mobile phase = 100 % chloroform; flow rate = 0.5 mL/min; sample volume = 20 µL; DPE and PE volume = 20 µL; detection λ = 241 nm.

Although the analysis time was compromised by the broad elution peak of DMSO (due to its significant absorptivity at 241 nm), it was still under 5 minutes. A MISPE-DPE calibration curve was constructed with 4-aminopyridine standard solutions (in $CHCl_3$) over the 2.5 – 100 μg/mL range, by performing two 20-μL DPE washes with DMSO and one 20-μL PE with 1% TFA in methanol. Good linearity (R^2 = 0.9903) and precision (%RSD = 5.1) were observed. A detection limit of 0.5 μg/mL was calculated by dividing the slope of the calibration line by three standard deviations of the blank. This detection limit can be enhanced by analyte preconcentration from a large volume of sample solution, due to the complete adsorption of 4-aminopyridine onto the MIP micro-column. A 845-μL sample loop was employed for sample injection, to construct a new MISPE-DPE calibration curve yielding an improved detection limit of 52 ng/mL.

2.5 Conclusions

The present study has achieved a better understanding of the fundamental molecular recognition process that is responsible for the selective binding of drug molecules with MIPs. The effects of solvent on the molecular recognition process directly implicated the role of hydrogen bonding and electrostatic interactions between the print molecule and the MIP binding site. The use of aprotic and non-polar solvents, such as chloroform, could therefore provide optimal interactions between the MIP particles in the column and the print molecule. Rapid desorption of the print molecule was possible by disrupting these interactions with a 20-μL pulse of polar and protic solvent, while non-specifically bound interferents were eliminated with an intermediate wash. This MISPE-DPE approach had the advantage of compensating for the heterogeneous nature of the binding sites as numerously reported in the MIP literature. The variable binding affinities of MIPs have plagued previous attempts to utilize MIPs as HPLC stationary phase materials. However, the development of the MISPE-DPE approach has now been proven a significant advancement over chromatography. The on/off mechanism of adsorption and desorption in the MISPE-DPE can be considered a form of "digital chromatography". This phrase was first used by Wells and Michael[156] to describe solid phase extraction. However, unlike MISPE-DPE, the poor selectivity of traditional SPE can not completely purify any target compound rendering it useless as an independent analysis technique.

The effects of experiment parameters such as column size, column temperature, sample volume and compositions of the mobile phase and DPE solvents have all been investigated and optimized. Fast analysis time, simple interference removal, high analyte

recovery, low detection limit, minimal consumption of solvents (1.5 mL per analysis), and excellent column reusability (even after drying out) all make this versatile MISPE-DPE technique particularly attractive in comparison to established methods of pharmaceutical analysis. A further merit is that the reproducibility of packing MIP columns for MISPE-DPE analysis is not critical because the analyte peak is always identified by its late appearance due to the selective molecular recognition, not by retention time as in HPLC methods.

CHAPTER 3: SPECTROSCOPIC INVESTIGATION OF THE MOLECULAR IMPRINTING PROCESS

3.1 INTRODUCTION

A range of approaches to molecular imprinting and a vast number of applications of MIPs have been reported. However, a strong understanding of the process underlying the mechanism of molecular recognition has not been realized. To date, chemical intuition has driven the decisions regarding monomer choice, and a judicially chosen cocktail of monomers is often used for MIP synthesis. Unfortunately, this approach often requires the time-consuming synthesis and chromatographic evaluation of several MIPs prior to deciding on an optimized protocol to prepare a successful MIP. Therefore, a more rational design towards MIP synthesis is essential.

The first step towards the preparation of a MIP is the formation of a self-assembled complex between the monomer and chosen template molecule. This binding affinity will form the basis of the MIP recognition sites. Therefore, the ability to determine the appropriate monomer-template interactions will help ensure a successful MIP preparation.

Various types of spectroscopy, such as NMR[157] and UV[158,159], have been employed to confirm non-covalent monomer and template interactions. UV spectroscopy can provide a simple tool for the observation of complex formation. The UV spectrum of a molecule reflects its transitions between electronic energy levels. As a consequence, changes in the surroundings of a molecule that affect the distribution of electrons within its structure will alter the absorption spectrum. Monitoring either the absorbance and/or absorption maximum wavelength during the titration of a monomer into a solution of a template can be used to probe molecular interactions.

The approach here was to study non-covalent complexation in a series of monomer and templates by UV spectroscopy. Scatchard plots were generated for 2-aminopyridine, theophylline and their structural analogues for the simple determination of an association constant, K_{ass}, value in the presence of MAA. The linearity of each Scatchard plot was used to confirm the interactions between a template and MAA providing an overall strength of interaction. These K_{ass} values were correlated with the degree of binding with the 2-aminopyridine MIP. When compared with the functional groups present in the template molecule, the K_{ass} value illustrates that specificity in MISPE originates mainly from additive effects of multiple interactions between the template and monomers. In general, this approach yields a better understanding of the functional groups and forces responsible for the molecular recognition process in MISPE.

3.2 THEORY

3.2.1 Stability of Monomer Template Assemblies

The functional monomers must strongly interact with the template prior to and during polymerization to achieve a high yield of imprinted binding sites. Several factors are responsible for the recognition properties of the site as summarized in Figure 3.2.1.1. An important part of the optimization process is the stabilization of the monomer-template complex. The thermodynamic balance between enthalpic and entropic factors will guide the degree of self-assembly of monomer and template in a given solvent and is the net result of positive interactions such as hydrogen bonding and electrostatic versus negative interactions such as columbic repulsion and steric hindrance.

3.2.1.1 Number and Type of Interaction Sites on Monomer and Template

A large number of complementary interactions will increase the binding strength of the complex. Thus, a template offering multiple functional groups for interaction with several monomers are likely to yield a binding site of high selectivity and affinity for the template. The relative strength and positioning of these interactions are equally important. Therefore, functional monomers are selected based on the maximum number of complementary interactions with the template. This approach can be extended to include a mixture of monomers, yielding imprinted copolymer or terpolymer materials.[160,161]

Number of interactions

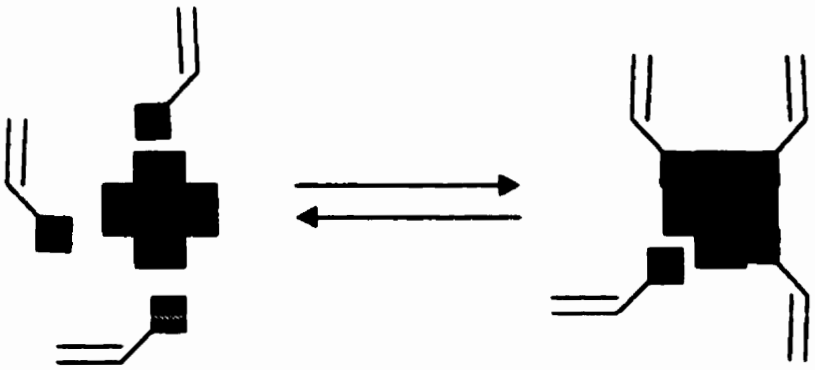

Nature and position of interactions

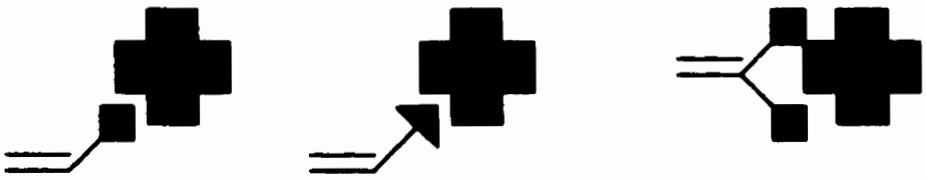

Template shape

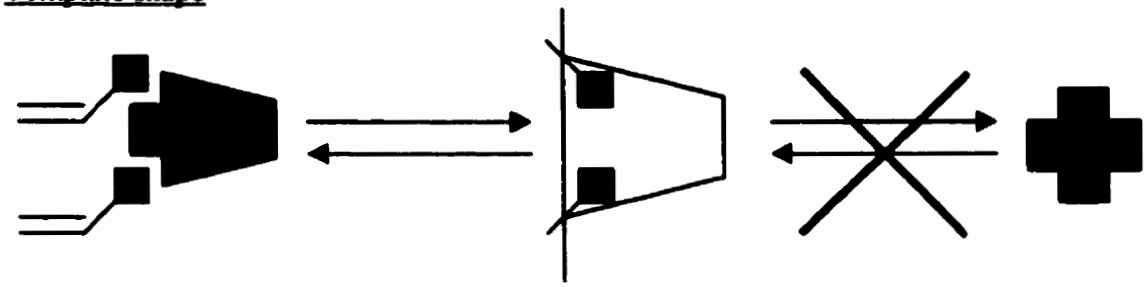

Monomer template rigidity

Figure 3.2.1.1: Factors influencing the formation of template binding sites (as proposed by Sellergren[162]).

3.2.1.2 The Template Shape

The shape of the template molecule can play a critical role to ensure the necessary steric complementarity for efficient discrimination from other molecules. It has become customary to validate a new MIP material by determining its ability to discriminate the template from a group of structural analogues. A plethora of evidence exists in the literature illustrating this effect.

3.2.1.3 Monomer Template Rigidity

The more conformationally defined the monomer and the template, the better defined the recognition sites will be synthesized.[163] This effect has a further advantage of minimizing the loss of rotational entropy upon MISPE binding. In other words, the better the fit between a monomer and template, the less entropy will be lost due to conformational changes in the binding site or the template molecule during binding. Consequentially, the most successful MIP materials have been imprinted with well-defined templates such as nitrogen heterocycles.[162]

3.2.2 Scatchard plots

Scatchard plots can be employed to determine a value of the equilibrium constant, K_{ass}, for the complex formation between the target molecule and different functional monomers of the monomer and template molecule. This value should be maximal for the template molecule but minimal for potential interferents.

The equilibrium between MAA monomer (M) and the test compounds (T) is represented in below:

$$M + T \rightleftharpoons MT$$ **Equation 3.2.2.1**

Neglecting activity coefficients, the equilibrium constant is:

$$K_{ass} = \frac{[MT]}{[M][T]}$$ **Equation 3.2.2.2**

If the amount of template in the solution is held constant while increments of monomer are added, the total concentration of template is given by:

$$T_o = [T] + [MT]$$ **Equation 3.2.2.3**

Rearrangement of equation 3.2.2.2 to:

$$\frac{[MT]}{[M]} = K_{ass}(T_o - [MT])$$ **Equation 3.2.2.4**

A graph of [MT]/[M] versus [MT] yields a slope of $-K_{ass}$. The concentration of the complex [MT] can be measured by UV spectrometry as ΔA, which is the observed absorbance after each addition of MAA minus the initial absorbance of the template solution.

3.3 EXPERIMENTAL

3.3.1 Spectroscopic Analysis

A 2.5 mL solution of each of the 2-amino structural analogues (0.1 mM prepared in $CHCl_3$) was placed in the 10 mm quartz sample and reference cuvettes of a Varian Cary 3 UV-VIS spectrophotometer (Palo Alto, CA). Six additions of a 1-μL aliquot of 1.25 M MAA were placed in the sample cuvette followed by 2 min of mixing and 5 min of equilibration time prior to recording an UV spectrum. A second UV spectrum was recorded at 20 minutes to confirm the change of any spectral shift. Scatchard plots were calculated for 2-aminopyridine and its structural analogues. The UV absorbance spectra of the MAA monomer in solution were also recorded in the absence of any template molecule.

Scatchard plots were prepared in the identical manner for the theophylline and caffeine molecules. A nicotine Scatchard plot was not possible due to the spectral overlap of nicotine with the MAA monomer.

3.4 RESULTS AND DISCUSSIONS

3.4.1 2-Aminopyridine

If ΔA was the measured absorbance after each addition of MAA minus the initial absorbance of a 2-aminopyridine solution (in $CHCl_3$) at 311 nm, a changing ΔA value would confirm the interaction between MAA and 2-aminopyridine as shown in Figure 3.4.1.1. Equilibrium between the monomer and the target molecule was reached, as the measured spectra were constant over the 20-minute period. The observed change in absorbance was due to the complexation of the MAA monomer with the 2-aminopyridine template molecule and not due the increasing concentration of the MAA monomer. As illustrated in Figure 3.4.1.2, the UV absorption profiles of MAA in chloroform over the same concentration range. Although, a rise in absorbance is evident, it occurs at a much lower wavelength (λ= 215nm) than the MAA - 2-aminopyridine complex.

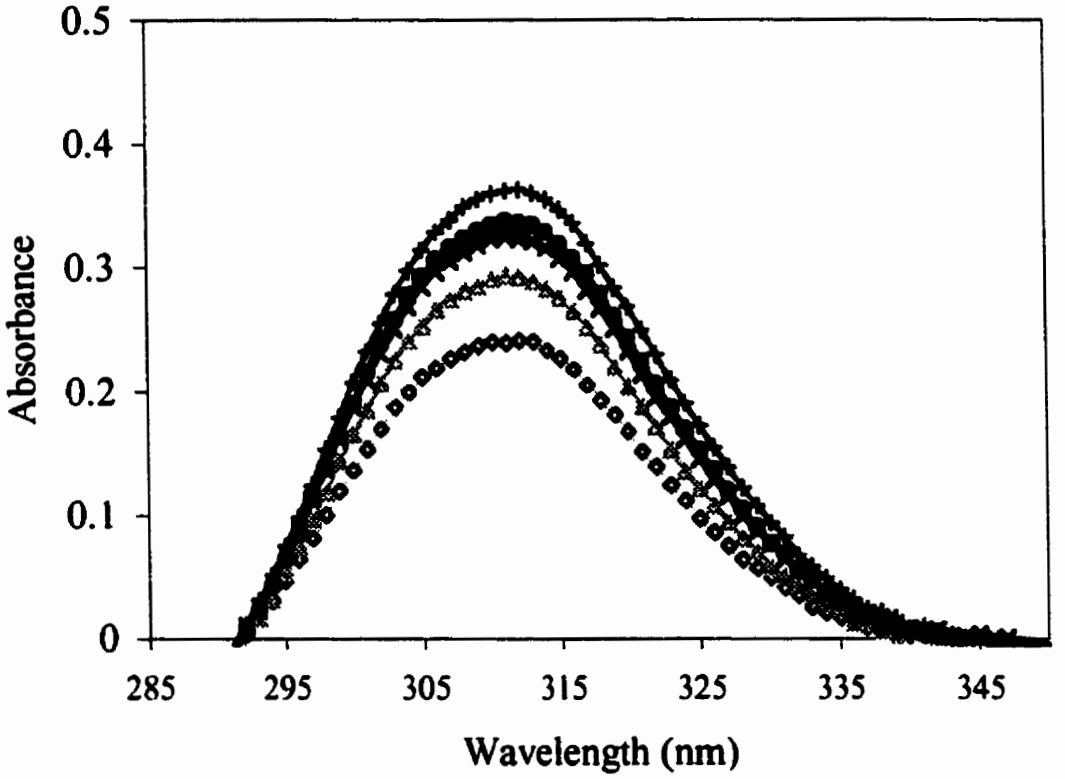

Figure 3.4.1.1: UV spectra for a mixture of 0.1 mM 2-aminopyridine and various concentrations of MAA in chloroform; 0.5 mM (◊), 1.0 mM (Δ), 1.5 mM (x), 2.0 mM (o) and 2.5 mM (+).

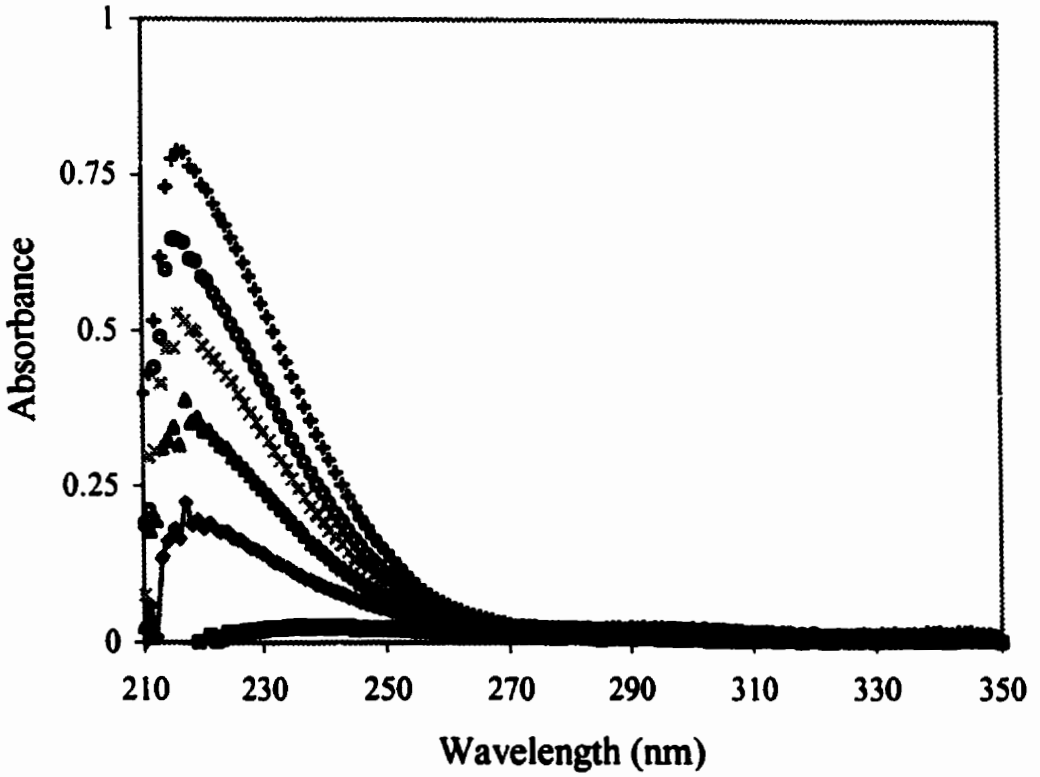

Figure 3.4.1.2: UV spectra for MAA at various concentrations in chloroform; 0.0 mM (□), 0.5 mM (◊), 1.0 mM (Δ), 1.5 mM (x), 2.0 mM (o) and 2.5 mM (+).

The Scatchard plot for the complexation of MAA with 2-aminopyridine is illustrated in Figure 3.4.1.3, where ΔA represents [MT] in Equation 3.2.2.4. The linearity of the plot (R^2 = 0.9899) confirmed the non-covalent complexation of MAA with 2-aminopyridine, yielding a K value of 2941 M^{-1}.

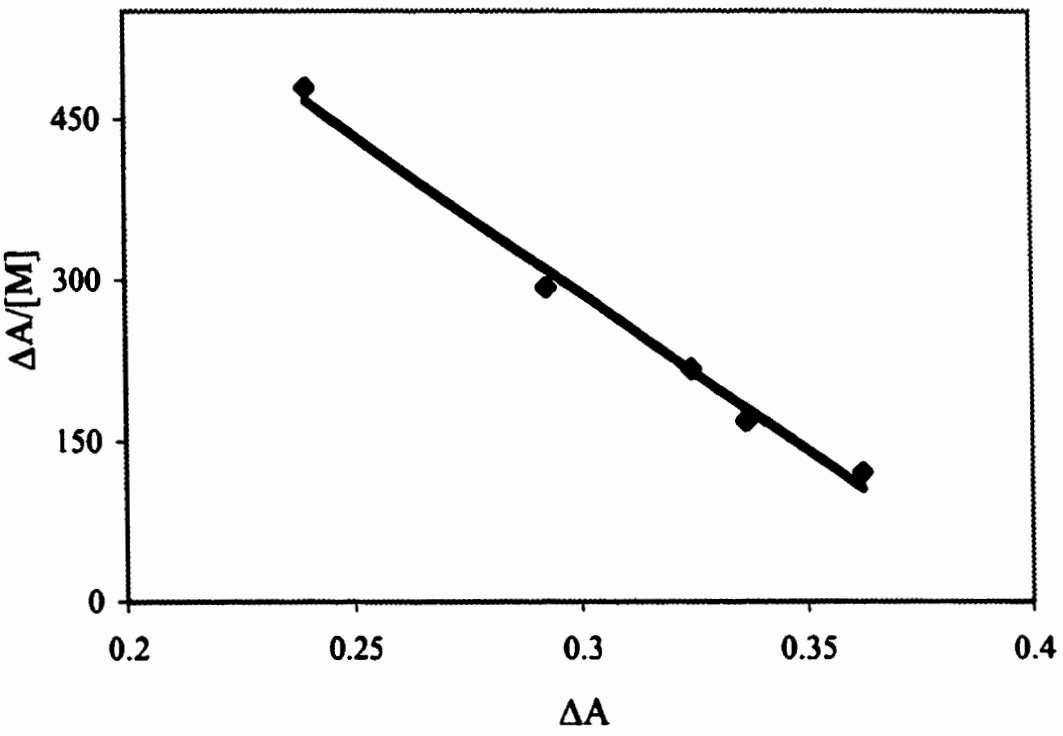

Figure 3.4.1.3: Scatchard plot for the complexation of 2-aminopyridine (0.1 mM) with MAA (0.5 – 3.0 mM).

The magnitude of this value is important as it represents the stability of the complex. Improved complex stability leads to greater adduct populations in solution and in turn yields polymers with greater selectivity and higher capacities on account of the greater number of binding sites. Therefore, Scatchard plots were performed in the present study to yield an empirical value of equilibrium constant, K_{ass}, for the complexation of MAA with 2-aminopyridine or any of its structural analogues. Scatchard plots were also constructed for several structural analogues of 2-aminopyridine, in an attempt to identify the functionalities responsible for strong non-covalent interaction. Unfortunately, some analogues such as 4-aminopyridine could not be evaluated by this UV spectrometric method due to their absorption spectral overlap with MAA. Table 3.4.1.1 summarizes the experimentally determined K_{ass} values and the corresponding binding results for the 2-aminopyridine MIP micro-column. The K_{ass} value correlates well with the MIP column binding.

Table 3.4.1.1: Complexation Constant (K_{ass}) Values for 2-Aminopyridine and its Structural Analogues.

Analyte	Structure	K_{ass} Value (M^{-1})	MIP Column Binding
2-Aminopyridine	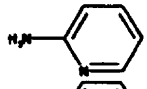	2941	98
3-Aminopyridine	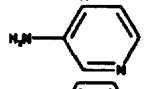	205	0
Aniline	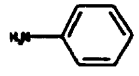	0	0
2-Methylpyrazine	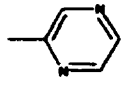	0	0

For instance, the low K_{ass} value for 3-aminopyridine is reflected in the low capacity factor value presented in Table 2.4.15.2.1. It becomes obvious that subtle differences in the structure of a target molecule may jeopardize its complexation with MAA. One important parameter is the number of interaction functionalities present on the target molecule, complementary to MAA. For example, aniline only possesses one hydrogen bonding acceptor functionality at the nitrogen and was therefore unable to strongly interact with the MIP binding sites. Hence, it exhibits a zero value for MIP binding. Although 2-aminopyridinde, 3-aminopyridine and 2-methylpyrazine all possess two nitrogen functionalities for interaction with the MIP, large differences in binding affinity are evident. Therefore, the relative position of each nitrogen group also plays a critical role.

3.4.2 Scatchard Analysis of Theophylline and Caffeine with MAA

The chromatographic data presented in Chapter 2 provided compelling evidence for a strong interaction between theophylline, nicotine and the MAA binding sites in their respective MIPs. These interactions have been confirmed and their magnitude determined using the Scatchard plot approach. Figure 3.4.2.1 represents the change in absorbance for a theophylline solution in response to increasing MAA concentration. The formation of the theophylline – MAA self-assembled complex is evident as indicated by the rise in the UV absorption spectrum at 292 nm. Increasing the amount of MAA monomer present in the pre-polymerization mixture, facilitated the formation of this complex. More importantly, the change in absorbance at this wavelength can be used to construct a Scatchard plot. As

shown in Figure 3.4.2.2, the linearity of the plot ($R^2 = 0.9899$) confirmed the non-covalent complexation of MAA with theophylline, yielding a K_{ass} value of 1832 M^{-1}.

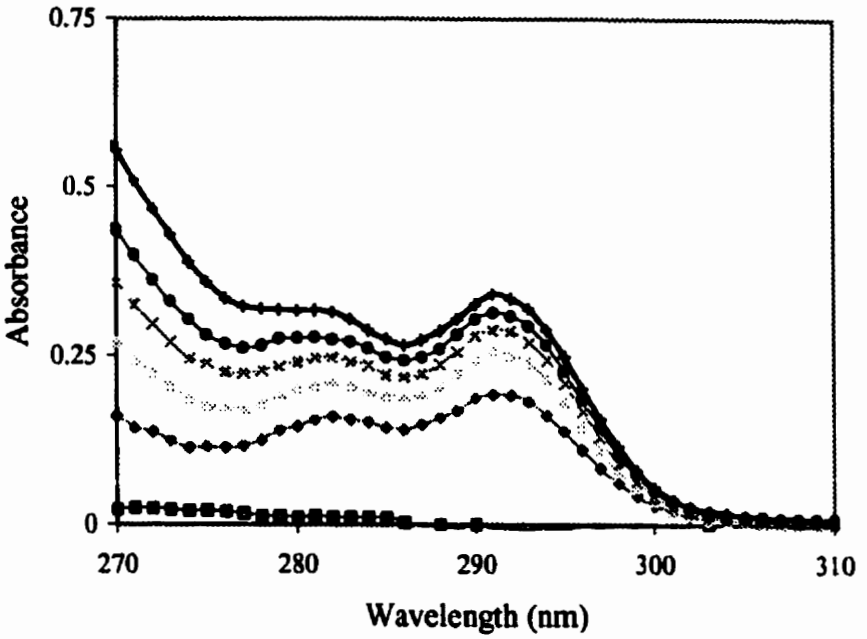

Figure 3.4.2.1: UV spectra for a mixture of 0.1 mM theophylline and MAA at various concentrations in chloroform; 0.0 mM (□), 0.5 mM (◊), 1.0 mM (Δ), 1.5 mM (x), 2.0 mM (o) and 2.5 mM (+).

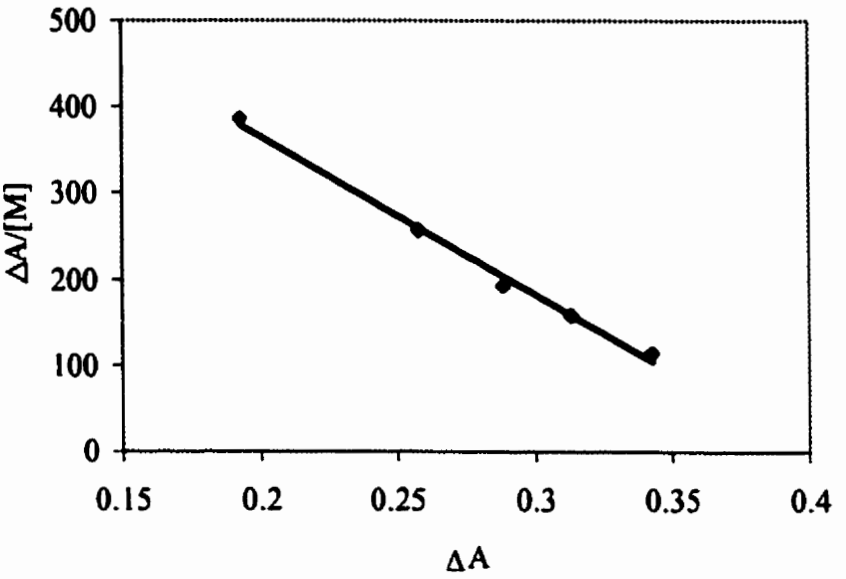

Figure 3.4.2.2: Scatchard plot for the complexation of theophylline (0.1 mM) with MAA (0.5 – 3.0 mM).

Such sensitivity of the complexation can be used to better evaluate new functional monomers, in an effort to increase the selectivity of the resulting MIP. The K_{ass} value will also suggest a better choice of analogue structures for evaluating the MIP selectivity. It may even predict an unsuccessful MISPE-DPE method development for a target molecule due to potentially strong interferences by structural analogues.

3.5 CONCLUSIONS

The UV spectroscopic Scatchard plot method has been applied to study the pre-polymerization stage of the molecular imprinting process. The Scatchard plot results accurately reflected the MIP micro-column's binding strength (in terms of retention time and capacity factor). A systematic evaluation of the 2-aminopyridine MIP's selectivity was performed and the results suggested how the functionalities on a target molecule might be responsible for strong versus weak interactions with the MAA monomer. This method provides a valuable tool for the rapid design of new molecular imprinting systems.

CHAPTER 4: SURFACE PLASMON RESONANCE IMMUNOASSAY

4.1 Introduction

4.1.1 Immunoassay

Immunoassay is an analytical method that employs antibodies for the determination of sample components. Antibodies are remarkable molecules and serve as paradigms of molecular recognition. Their selective binding nature with antigens allows these compounds to be employed in the development of immunoassay methods that are highly specific and that can often be used directly with even complex biological matrices such as blood, plasma or urine.[164] Presently, there are numerous forms of immunoassays each classified according to a range of criteria including sample type, nature of analyte, assay conditions, etc. Most immunoassays require the use of fluorescent, luminescent, light scattering or enzyme labels to quantify the antigen-antibody interaction. However, the labelling processes and the subsequent analysis are time consuming and in some cases, the labelling process itself may alter the structure and activity of the analyte and consequently its binding characteristics.

Consequently, there is an emphasis on non-labeled antibodies and improved formats for performing immunoassays. The development of immunosensors capable of direct detection of the binding event has shown great promise. Immunosensors can detect the specific antigen-antibody binding events by coupling the immunochemical reaction to the surface of the transducer. The transducer device is responsible for converting a binding event into an electronic signal. One of the more recent methods for direct transduction utilizes the optical phenomenon of surface plasmon resonance.

4.1.2 Surface Plasmon Resonance

Utilization of the optical phenomenon, surface plasmon resonance (SPR), has seen extensive growth since its initial observation by Wood in 1902.[165] It was initially exploited for a variety of spectroscopic and physical characterizations including enhanced holography,[166] surface enhanced Raman scattering (SERS) or coherent anti-Stokes Raman scattering (CARS),[167] and surface plasmon microscopy (SPM) for high contrast imaging of thin dielectric films.[168,169]

SPR is a simple and direct sensing technique that can be used to probe refractive index (η) changes that occur in the very close vicinity of a thin metal film surface.[170] This technique utilizes a thin film of metal, typically gold or silver, between two transparent media of different refractive index (i.e., glass prism and sample solution) to function as an optical sensor surface. Above a critical angle, a plane-polarized light beam entering the higher refractive index medium (glass prism) can undergo total internal refraction. Under these conditions, an electromagnetic field component of the light called the evanescent wave will penetrate into the gold film. At a specific angle of incidence, interaction of this wave with free oscillating electrons at the gold film surface will cause the excitation of surface plasmons, resulting subsequently in a decrease in the reflected light intensity. This phenomenon is called surface plasmon resonance and occurs only at a specific angle known as the resonant angle (θ_r). This SPR angle is modified by the addition of the analyte onto the gold film surface, thereby allowing the monitoring of binding events. The phenomenon of SPR is completely non-specific. It cannot distinguish between different chemical changes. While this may appear to be a limitation, it is really a powerful advantage.

Specificity depends upon selection of pairs of molecules that react only with each other. One member of the pair is the detector and the other is the target analyte (i.e. the substance we wish to detect/quantitate). Any pair of molecules that exhibit specific binding can be adapted to SPR measurement. These may be an antigen and antibody, a DNA probe and complementary DNA strand, an enzyme and its substrate, or a chelating agent and metal ion.

4.1.3 Surface Plasmon Resonance Biosensors

The potential of SPR for optical biosensing purposes was soon realized by Liedberg *et al* in 1982-83 who adsorbed an IgG antibody overlayer on the gold sensing film resulting in the subsequent selective binding and detection of IgG.[171,172] A flurry of immunochemical research, based on antibody-antigen association and/or disassociation[173,174,175,176,177,178,179,180,181,182,183,184,185], has since occurred and the principles of SPR as a biosensing technique have been reviewed.[186,187,188,189,190,191,192,193] In general, SPR biosensors can correlate changes in concentration or mass to direct changes in the reflected light intensity. This analytical signal is proportional to the binding of a ligand, from the solution, to the receptor immobilized on the gold film surface.

This format can be used as the basis for a sensor that is capable of sensitive and quantitative measurement of a broad spectrum of chemical and biological entities. For example, the versatility of SPR biosensing has been demonstrated by a wide range of applications and molecules, from virus particles[194] to sex-hormone-binding globulin[195] and syphilis.[196] SPR biosensing offers a number of important practical advantages over current analytical techniques. Most importantly, its inherent advantage over other types of

immunosensors is its versatility and capability to monitor antibody-antigen binding interactions without the need for fluorescence or radioisotope labeling of the biomolecules. The time from sample application to reported result varies with the specific chemistry but can be as short as 5 minutes. In most cases, there is no need to pretreat the sample before its presentation to the sensor. A single sensor format (i.e. size, storage and usage protocol, reader, etc.) may be used for a variety of assay chemistries including immunological, nucleic acid binding, enzymatic, chemical, and gas adsorption. This approach has also shown promise in the real-time determination of concentration, kinetic constant and binding specificity of individual biomolecular interaction steps. Antibody-antigen interactions, peptide/protein-protein interactions, DNA hybridization conditions, biocompatibility studies of polymers, biomolecule-cell receptor interactions, and DNA/receptor-ligand interactions can all be analyzed.[197]

Most recently, the commercial potential of SPR has been harnessed by companies such as Biacore (Uppsala, Sweden),[198] Windsor Scientific (U.K.),[199] Quantech (Minnesota, U.S.A.),[200] and Texas Instruments (Dallas, U.S.A.).[201] for application in areas such as, medical diagnostics, environmental monitoring, agriculture pesticide and antibiotic monitoring, food additive testing, military and civilian airborne biological and chemical agent testing. Biacore has successfully commercialized this technology; however, the complexity and cost of their research-grade instrumentation do not provide a simple and inexpensive SPR system for the fast screening assays of toxins in field settings.

4.1.4 Fumonisin Mycotoxin

Fumonisins are the most recently discovered group of mycotoxins produced by several fungal species,[202,203] including *Fusarium moniliforme* which is a common contaminant of corn in many parts of the world.[204] The production of fumonisins can occur during corn growth, storage or transportation. Of the currently identified fumonisins, FB_1, FB_2 and FB_3 are the most abundant in naturally contaminated food and feedstuff.[205,206,207,208,209] FB_1 has been shown to induce a wide range of adverse biological effects, including fatal leukoencephalomalacia in horses,[210] pulmonary edema in pigs,[211] and nephrotoxictiy and liver cancer in rats.[212] They are also toxic to turkey poults and broiler chickens.[213] FB_2 and FB_3 have also been shown to exhibit cancer-initiating activities similar to those of FB_1.[214] Although the minimal dose of fumonisins required for these conditions has yet to be determined, the Mycotoxin Committee of the American Association of Veterinary Laboratory Diagnosticians recommends that feeds having greater than 5 ppm fumonisins not to be fed to horses.[215] There is also a significant epidemiological association between fumonisin exposure and human esophageal cancer.[216,217] Geographical regions containing levels of fumonisin-contaminated corn, in the 1-2 ppm range, also possess the highest rates of esophageal cancer.[218] Based on toxicological evidence, the International Agency for Research on Cancer and the California Environmental Protection Agency have declared *Fusarium moniliforme* toxins as potentially carcinogenic to humans.[219] Unfortunately, no effective detoxification process in food or feedstuffs has yet been developed.

Accurate monitoring of fumonisin levels is therefore necessary to ensure safe exposure, especially in corn-based baby food. The analytical methods which have been

developed for fumonisins mainly fall into the chromatographic techniques: high performance liquid chromatography,[220,221,222] gas chromatography,[223] and capillary electrophoresis.[224,225] However, all these methods require a lengthy sample cleanup and some forms of chemical derivatization of the fumonisins before detection is possible, with perhaps the exception of mass spectrometry. A simple and cost effective assay of FB_1 is desirable. Recently, several immunoassays for FB_1 have been reported.[226,227,228,229,230,231] These methods are generally selective and sensitive, however, they require an analysis time of several hours and have certain setup costs.

The objective of this work is to develop a sensitive and economical SPR biosensor specifically for the rapid determination of fumonisin FB_1, with matrix-independent accuracy. High-affinity polyclonal antibodies selective for FB_1 are first immobilized on a gold film. Selective binding of FB_1 to the antibody is then allowed, followed by washing. The amount of bound FB_1 can be measured by the generation of a SPR response. The inherent selectivity of the antibody eliminates the requirement for extensive sample cleanup, thus greatly reducing the total analysis time and minimizing procedural errors. More importantly, the high-affinity antibody sets up the biosensor in a cumulative detection mode that can determine trace amounts of FB_1 in dilute samples with great sensitivity.

4.2 Theory

4.2.1 Structure of Antibody

The strong and variable interaction between an antibody and an antigen renders the immune system with the unique power of molecular recognition. Although antigens range in size from small drug molecules such as theophylline (MW = 180) to large proteins such as albumin (MW = 66,000), there is only one portion of the antigen that binds to the antibody. The region is referred to as the epitope of the antigen, which binds to the paratope of the antibody. Antibodies are classified as a family of proteins known as immunoglobulins (Ig). The most common type is the IgG molecule, which contains two identical paratopes located at the surface of the molecule. Each paratope is able to specifically bind to an area of 30 Å X 30 Å on the complementary antigen. As shown in Figure 4.2.1.1 the structure of an IgG molecule consists of a heterodimer with four polypeptide chains linked by disulfide bridges. The four chains are labeled according to their relative sizes, two heavy chains (H) and two smaller or light chains (L). The amino-terminal domain of both H and L chains differs in antibodies of different specificity and are called the variable (V) regions. The remaining domains are invariant and are referred to as the constant (C) regions. More specifically, there are three constant domains called C_H1, C_H2, and C_H3. Between the C_H1 and C_H2 domains, there is an additional segment termed the hinge which contains the inter-heavy chain disulfide bridges and which confers a certain amount of flexibility on the molecule. Lastly, the L chains contain a single constant domain called C_L.

All immunoglobulins can be cleaved at the middle of their H chains by various proteases.[232] For example, papain cleaves chains at the N-terminal side of the disulphide

bridges that keep the H chains together, thereby generating two F_{ab} (fragment antigen binding) fragments and one F_c (fragment crystallizable) fragment.

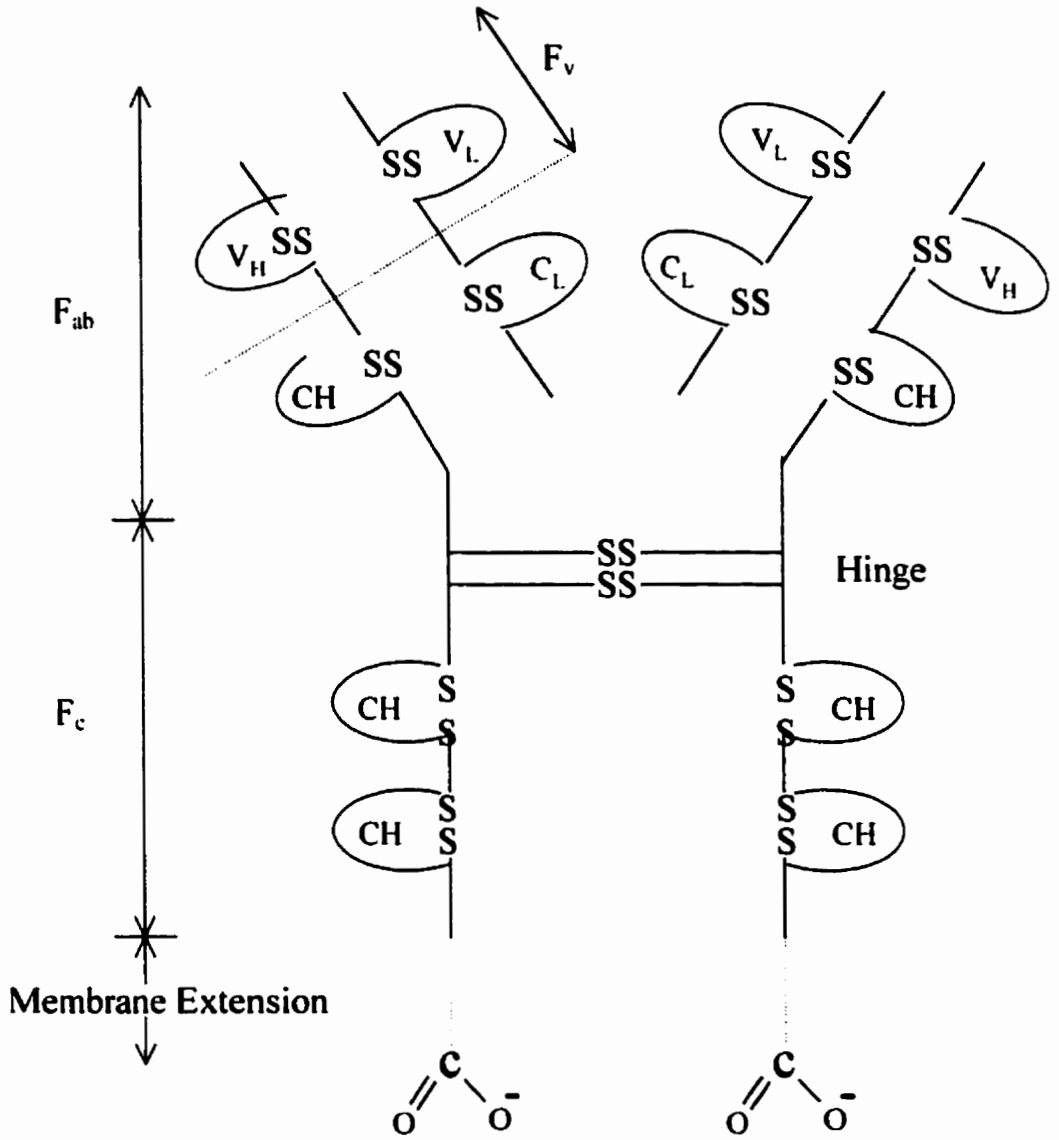

Figure 4.2.1.1: Schematic representation of an IgG antibody molecule.

4.2.2 Chemistry of Antibody Antigen Interactions

Protein molecules naturally repel each other in aqueous environments due to the hydrophilic nature of the surface in response to a layer of water molecules present there. This repulsion effect occurs over a distance of 20-30 Å, therefore the antibody–antigen complex must overcome this barrier.[233] The primary forces of attraction between antibodies and antigens are hydrophobic and electrostatic interactions. Hydrophobic interaction is the propensity of non-polar chains and groups to aggregate when immersed in water. Electrostatic interactions are the result of one or more charged sites on the epitope with oppositely charged sites on the paratope. The magnitude of this interaction is inversely proportional to the distance between the two sites and depends on the ionic strength of the liquid medium, which controls the shielding effect of the diffuse ionic double layers surrounding the charged sites. Therefore, in dilute salt solutions, electrostatic interactions can exert their influence at a greater distance than they can in a solution of high ionic strength. In general, these primary interactions can be felt over distances of 30–100 Å.

Only after the primary binding has occurred through these interactions will the antibody and antigen surfaces approach each other sufficiently to allow van der Waals and hydrogen bonding to become effective. Van der Waals interactions are caused by the transient asymmetry of the electron distribution around one atom. As two atoms approach each other, the attractive forces are countered by repulsion between the electron clouds of the atoms until separation between the atoms has reached a minimum value defined as the sum of their van der Waal radii. Consequentially, these secondary forces are effective over very short distances, between 2-10 Å. Beyond the influence of chemical interactions, the

high degree of steric or physical complementarity between epitope and paratope regions also plays a critical role in the molecular recognition process between an antibody and antigen.

The interaction between antibody (Ab) and antigen (Ag) is represented by the expression:

$$Ab + Ag \underset{k_d}{\overset{k_a}{\rightleftharpoons}} AbAg \qquad \textbf{Equation 4.2.2.1}$$

where k_a and k_d are the association and dissociation rate constants, respectively. It is important to realize that all antigen-antibody interactions are reversible. At equilibrium, the affinity constant can be expressed as an association constant:

$$K_a = \frac{k_a}{k_d} = \frac{[AbAg]}{[Ab][Ag]} \qquad \textbf{Equation 4.2.2.2}$$

The association constant, K_a, is thermodynamically linked to the free energy (ΔG) of antibody-antigen interactions by the equation:

$$\Delta G = -RT \ln K_a \qquad \textbf{Equation 4.2.2.3}$$

4.2.3 Surface Plasmon Resonance

The quantum optical-electronic basis of SPR is the fact that the energy carried by photons of light can be "coupled" or transferred to electrons in a metal. The angle of light at which coupling (i.e. energy transfer) occurs is characteristic of the particular metal and the environment of the metal surface. When there is a match or resonance between the energy of the light photons and the electrons at the metal surface, a transfer of energy occurs. The transfer can be observed by measuring the amount of light reflected by the bottom surface of

the metal film. All the light at most angles is reflected, except at the resonant angle where a majority of the light is absorbed.

From a practical standpoint, the Kretschmann prism arrangement is the most frequently employed geometry in SPR. As illustrated in Figure 4.2.3.1, this configuration uses an evanescent wave created by total internal reflection at a waveguide interface that excites charge density oscillation at the surface of the film. These electron oscillations are more commonly referred to as surface plasmons. The penetration depth of the evanescent field will depend on the wavelength of the light, the refractive index ratio of the waveguide to the surroundings and the photon intensity in the mode. The field energy will decay exponentially with distance from the surface, and thus penetration depth falls off rapidly as shown schematically in Figure 4.2.3.1.

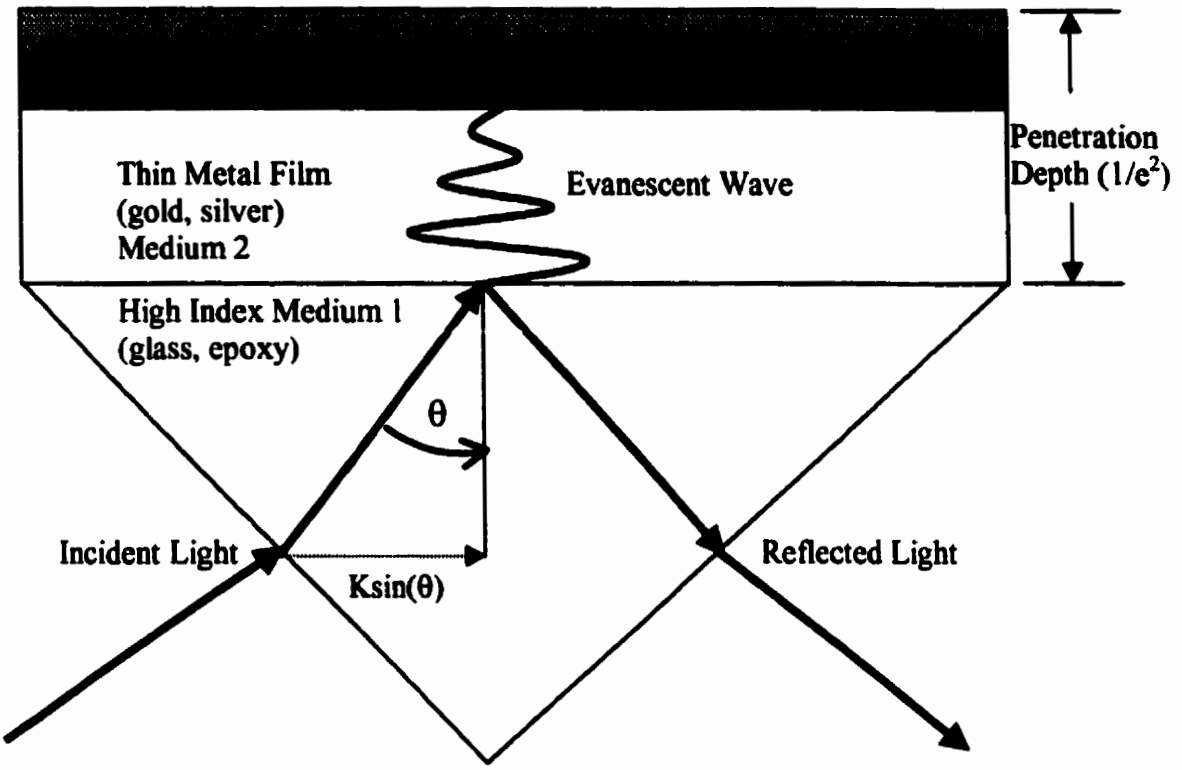

Figure 4.2.3.1: Total internal reflection at a dielectric boundary.

An estimation of the penetration depth is given by the following expression[234]

$$d_p = \frac{\lambda}{4\pi\sqrt{\eta_1^2 \sin^2\theta - \eta_2^2}} \qquad \textbf{Equation 4.2.3.1}$$

where η_1 and η_2 are the refractive index of medium 1 and medium 2 respectively. Typically, this will be approximately equal to one-fourth of the incident light wavelength. Light that is p-polarized with respect to the metal surface is launched into the prism for coupling to the metal film. Only p-polarized light can be utilized for plasmon generation

because this particular polarization has the electric field vector oscillations normal to the metal film. This is referred to as the transverse magnetic (TM) wave of the electron plasma along the flat metal surface.[235,236] In contrast, the s-polarized, transverse electric (TE) polarization cannot generate surface plasmons since its electric field vector is orientated parallel to the metal film. The wave vector of the oscillations, K_{sp}, is given by the expression:

$$K_{sp} = \frac{\omega}{c}\sqrt{\frac{\varepsilon_m \varepsilon_s}{\varepsilon_m + \varepsilon_s}} \qquad \textbf{Equation 4.2.3.2}$$

where ω is the frequency of the oscillations, c is the speed of light, ε_s the dielectric function of the sample medium adjacent to the metal surface, and ε_m is the dielectric function of the metal. The wave vector for a component of incident light can be described by the equation:

$$K_x = \frac{\omega}{c}\eta_p \sin\theta \qquad \textbf{Equation 4.2.3.3}$$

where θ is the angle of incidence of the light onto the metal film and η_p the refractive index of the prism. Surface plasmons, which oscillate and propagate along the upper surface of the metal film, absorb some of the p-polarized light energy from the evanescent field to change the total-internal-reflection light intensity I_r. Therefore, a plot of I_r versus incidence (or reflection) angle (θ_r) produces an angular intensity profile that exhibits a sharp dip at the resonance angle.

The presence of the prism (and its high refractive index value) is essential since it is not possible to generate surface plasmons directly with incident light radiation in air. The wave vector for both the incident light and the surface plasmon field must be equal during

SPR. However as shown in Figure 4.2.3.2, the dispersion curve of light in air ($K_a = \omega/c$) and that of plasmons in the metal do not intersect. Hence, there is no possibility of matching simultaneously both the wave vector and the frequency. In contrast, the intersection of the dispersion curves K_{sp} and K_g, also shown in Figure 4.2.3.2, indicates the ability of glass to increase the light vector enabling the necessary matching for plasmon generation.

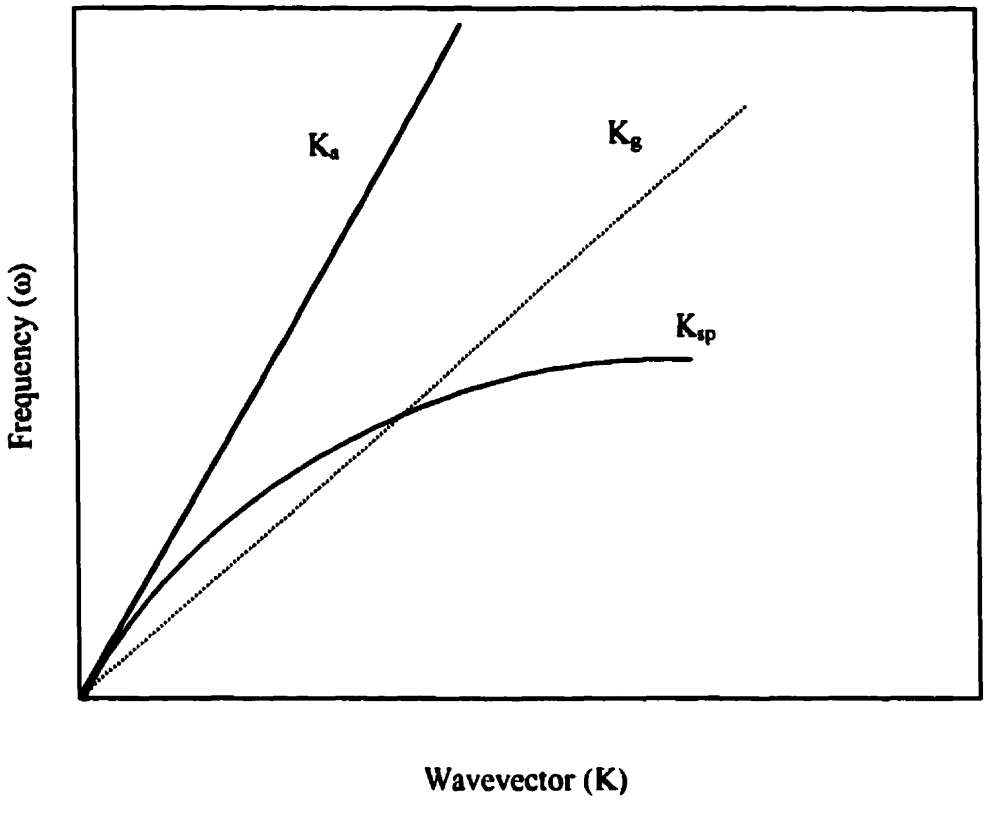

Figure 4.2.3.2: Dispersion curves for air, glass and surface plasmons.

The surface plasmon wave vector can be related to the refractive index of the medium on the near vicinity of the metal film by simplification of Equation 4.2.3.2. Disregarding the imaginary portion of ε, K_{sp} can be rewritten as

$$K_{sp} = \frac{\omega}{c}\sqrt{\frac{\eta_m^2\eta_s^2}{\eta_m^2+\eta_s^2}} \qquad \textbf{Equation 4.2.3.4}$$

where η_m is the refractive index of the metal and η_s is the refractive index of the sample. The imaginary component of the complex refractive index term can be related to absorbance.

The SPR profile is affected by the choice of metal due to its inherent optical properties, such as dielectric permittivity. Figure 4.2.3.3 compares the SPR curve, a plot of reflected light intensity vs the incident angle, for gold and silver films in air. The sharper resonance peak of silver is obvious and can be attributed to the intrinsic dampening of the surface plasmon oscillations on the metal film. All surface plasmon metals will tend to dampen these oscillations due to scattering of the electric field of the excitation light. A variety of metals will produce SPR. To sustain SPR a metal must have conduction band electrons capable of resonating with light of the appropriate angle and chemical compatibility with the chemistries needed to perform assays. Gold is the preferred metal as other metals are not as practical. For example, some are too expensive (In), violently reactive (sodium), too broad in their SPR response (copper, aluminum), or too susceptible to oxidation (silver).[237]

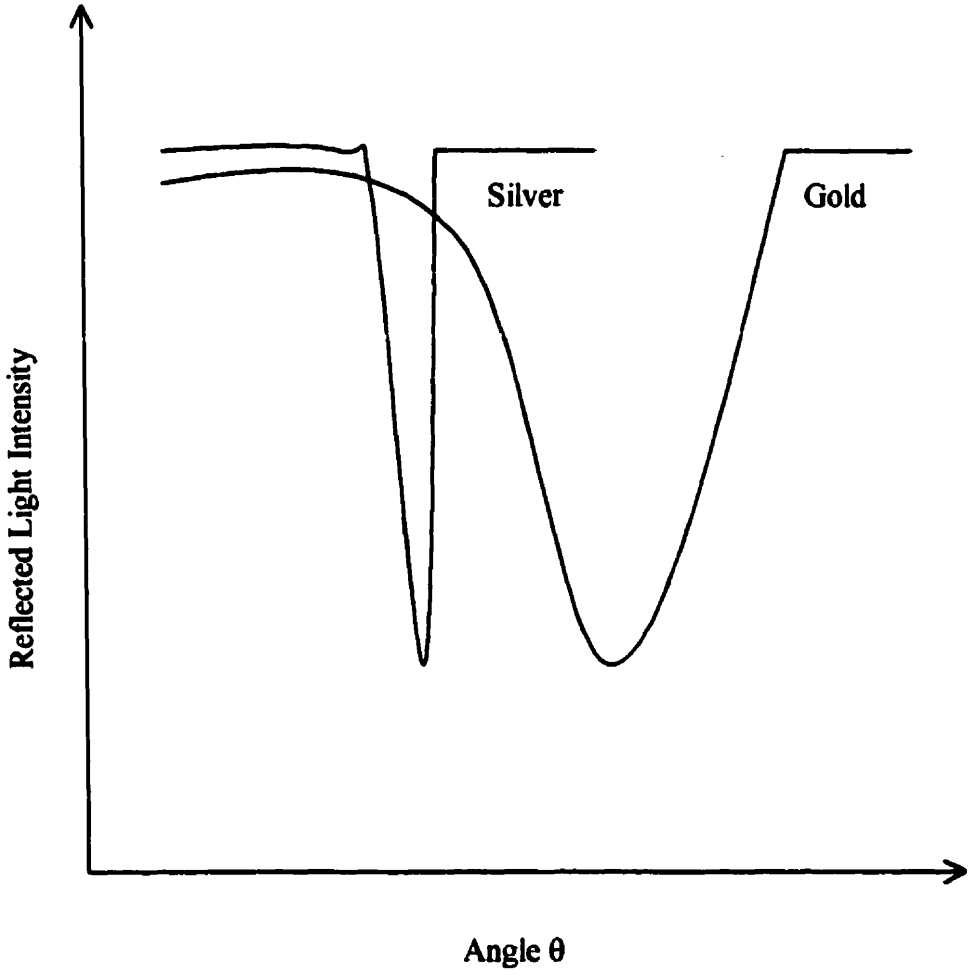

Figure 4.2.3.3: SPR curves for silver and gold.[237]

The characteristic of this phenomenon which makes SPR an analytical tool is that any change in the chemical composition of the environment within the range of the plasmon field causes a change in the angle of light that resonates with the plasmons. That is, a chemical composition change results in a shift in the angle of incidence at which light is absorbed and the magnitude of the shift is quantitatively related to the magnitude of the

chemical change. In an immunoassay, a thin film of metal is applied to a prism that has been deposited onto a substrate (typically glass or plastic). Then antibodies specific to a particular analyte (e.g. hormone, drug, tumor marker, etc.) are non-specifically adsorbed to the metal film. When the sensor is exposed to a sample containing that analyte, the binding of the antibody and the analyte causes a chemical composition change at the metal surface, within the plasmon field, and the shift in the resonant angle of the incident light is measured. The size of the shift is proportional to the quantity of the analyte in the sample. Because of the very specific relationship between the antibody and analyte, no other molecules in the sample can be mistakenly measured by the sensor.

4.3 Experimental

4.3.1 Chemicals and Antibodies

FB_1, bovine serum albumin (BSA) and Tween 20 were purchased from Sigma (St. Louis, MO). Standard solutions of FB_1 were prepared in phosphate-buffered saline (PBS), pH = 7.4, containing 20 mM of NaH_2PO_4 and 140 mM of NaCl. Safety note: fumonisins are suspected carcinogens and should be handled with care. The FB_1 antiserum (2000 μg/mL) was supplied by Health Canada (Ottawa, ON); its preparation and characterization has previously been described by Yeung *et al.*[238] Antibodies should always be stored at a concentration of 1 mg/mL or greater; a diluted antiserum loses activity much more rapidly than the corresponding antiserum.[239] All solvents were of HPLC grade and from Caledon (Georgetown, ON). 40-nm-thick gold film substrates, prepared by vapor-deposition on glass slides coated with a thin layer of chromium, were commercially available from Lumonics Optics Group (Nepean, ON). Gold films deposited directly onto glass substrates can delaminate when exposed to aqueous solutions[240] however, the chromium layer minimizes such delamination.[241] These gold films were stored under vacuum; they would change from being hydrophilic to hydrophobic if kept in air[242] and most proteins adsorb more extensively at hydrophilic than hydrophobic surfaces.[243,244,245]

4.3.2 Instrumentation

The home-made SPR apparatus is schematically shown in Figure 4.3.2.1.

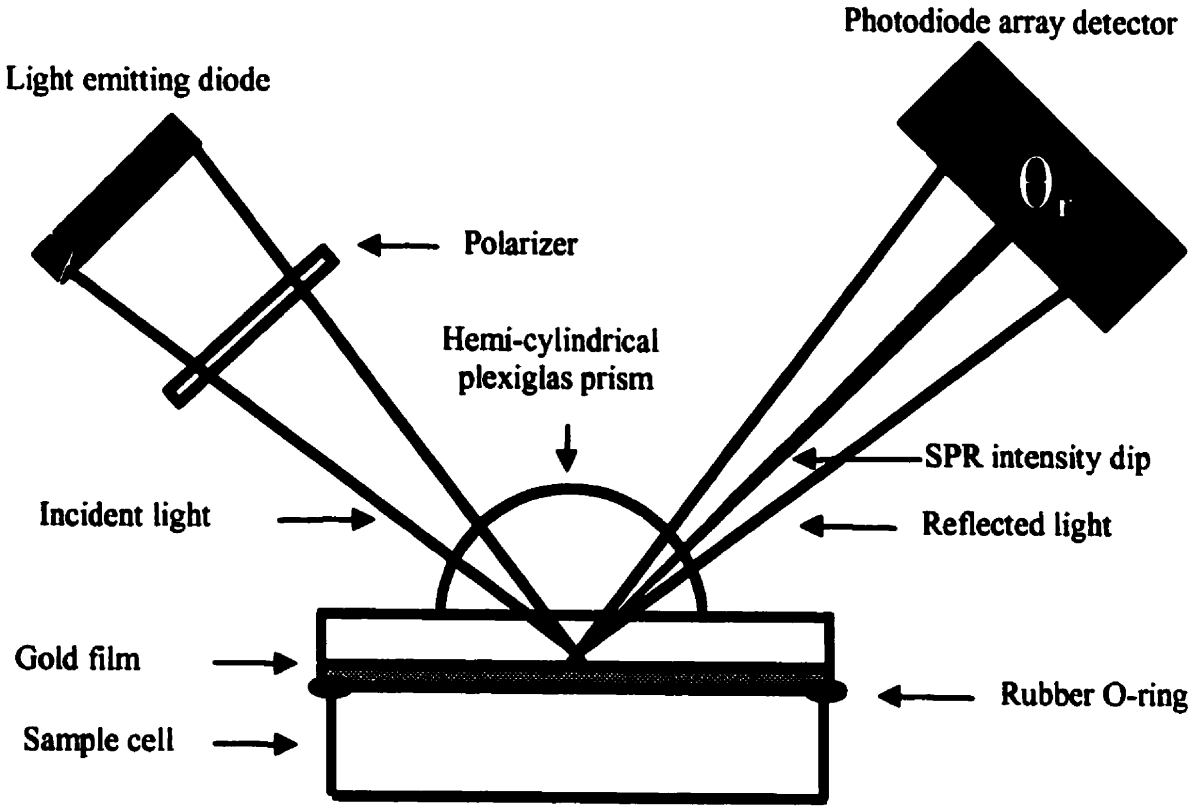

Figure 4.3.2.1: SPR apparatus.

A planar light emitting diode (15 mm X 10 mm; $\lambda = 635$ nm) was used as the light source. Its spatially large output beam was p-polarized and focused into a rotatable Plexiglas hemi-cylindrical prism (12 mm radius) which allowed the use of a large range of incident angles. A gold deposited slide was optically coupled to the prism with a refractive-index-matching oil (dibutyl phthalate) to minimize reflection losses. The reflected light intensity as a function of incident angle was measured using a photodiode array (PDA) detector model RY-1024 (Princeton Instruments, NJ) to generate a SPR angular profile. Its output signals were acquired by an ST120 controller and processed by an ST1000 OSMA computer program for display on a monitor or printing on a plotter.

4.3.3 Immunoassay of FB_1

For comparison purposes, an initial SPR angular profile for deionized water was first recorded and the SPR angle corresponding to minimum reflection intensity was determined. An antibody overlayer was produced on the gold film by placing the antiserum (2000 µg/mL diluted 1:5000 to 1:20000 with 10 µg/mL BSA in PBS) in the sample cell and allowing adsorption to occur at room temperature (21±1°C) over a period of 1 hour. A new SPR angular profile was then recorded as the reference, and a change in SPR angle relative to the water profile could be observed. The cell was rinsed with deionized water and next filled with an FB_1 standard solution (in PBS). After an incubation period of ten minutes to allow for mass transfer effects due to a depletion of the analyte concentration at the biosensor surface, the sample cell was washed with PBS containing 0.1% Tween 20 and 10 µg/mL BSA. This washing step removed all unbound FB_1 molecules from the antibody layer, thus preventing any interference with SPR angle measurement by these free analyte

molecules in solution. After filling up the cell with PBS, the amount of FB_1 binding to the antibody overlayer was determined by a further shift in SPR angle. Afterwards, the reversibility of the binding between FB_1 and the antibody was investigated. The bound FB_1 and antibody overlayer was exposed to 90% methanol for a period of ten minutes, after which the cell was rinsed and filled with the PBS and the new SPR angle was recorded.

Klotz's equation was used to transform the experimental data into a linear plot. The analytical limit of detection was determined based on the slope of this linear relationship and three standard deviations of the average blank value. This blank value was obtained with replicate additions of PBS to the cell.

Dry immunoassay measurements were performed by allowing the FB_1 molecules in a sample to bind with the antibody overlayer (1:20,000 dilution) for 10 min, emptying the sample cell and washing with deionized water to remove any non-specific proteins weakly bound to the antibodies. The gold film was allowed to dry (with an antibody overlayer and bound FB_1 molecules) in air for 30 min, before a SPR angular profile was recorded.

4.4 Results and Discussions

4.4.1 Refractive Index Measurements

In the SPR biosensor constructed according to Figure 4.3.2.1, p-polarized light was directed through the hemi-cylindrical prism onto the gold film substrate containing the sample cell, and the SPR angular profile was monitored by the PDA detector. The SPR angle was dependent on the refractive index of the sample solution in the close vicinity of the gold film surface. The functionality of the device was tested with various solvents of known refractive index. As shown in Figure 4.4.1.1, the instrument was very responsive to changes in refractive index as indicated by the linearity of the line ($R^2 = 0.9901$). The chart provides useful information for calibrating the angular scale of the SPR device for refractive index measurements.

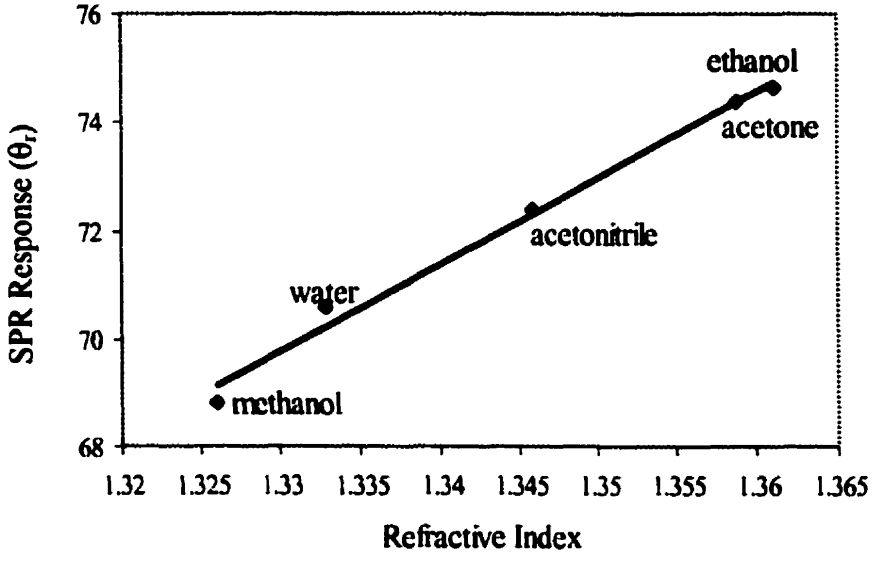

Figure 4.4.1.1: SPR angular response to refractive index.

4.4.2 SPR Immunoassay of FB_1

An addition of FB_1 in PBS to the sample cell produced no measurable shifts in the SPR angle, indicating that non-specific binding of FB_1 to the gold sensing film was insignificant.

However, immobilization of a non-optically absorbing antibody overlayer (specific for FB_1) onto the gold film, using 1:5000 dilution of the antiserum, caused a change in refractive index and a corresponding shift in the SPR angle. When equilibrium for the adsorption of antibodies to the gold film was reached, the SPR angle stopped shifting. A new angular profile was then measured, using PBS in the sample cell, to serve as a blank reference. Subsequent binding of FB_1 from a standard solution to the antibody overlayer would produce a further shift in the SPR angle as illustrated in Figure 4.4.2.1.

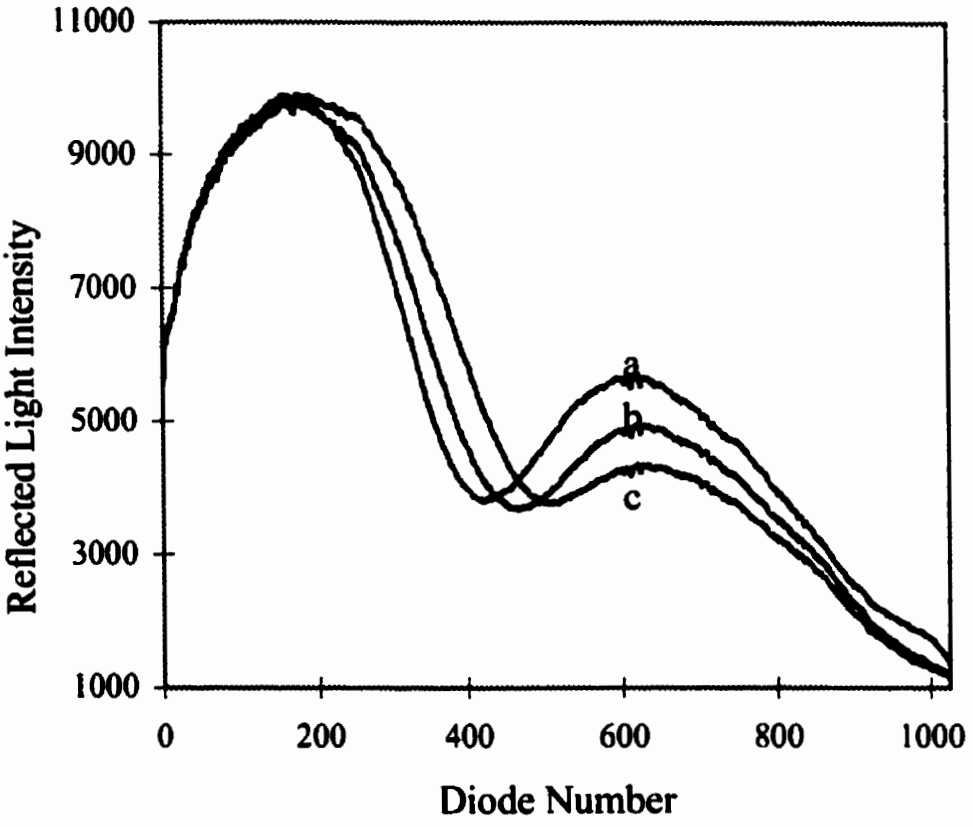

Figure 4.4.2.1: SPR angular profiles for (a) water, (b) immobilization of an antibody overlayer onto the gold film and (c) after binding of FB_1 from a 100 µg/mL solution to the antibody overlayer.

Inertness against non-specific binding of FB_1 to open sites left on the gold surface was achieved by sorption of a non-active protein, BSA, onto the gold surface to serve as a blocking agent prior to FB_1 assay.[189,246] The surface-bound BSA also acts as a steric blocker against denaturation of the antibodies caused by the hydrophobic gold surface. A nonspecific control surface consisting of the BSA overlayer in the absence of antibodies was tested, but it did not produce any significant shifts in the SPR angle in response to FB_1 additions. Preparation of another nonspecific control surface, composed of an overlayer of BSA and an irrelevant antiserum, was not performed as the specificity of the antibodies was previously characterized by an independent method.[238]

The antibody surface was treated with Tween 20 detergent to ensure a more stable antibody-antigen overlayer. The common usage of detergent in the immobilization of antibodies has been previously investigated by atomic force microscopy (AFM).[247] The experiments showed it removes loosely adsorbed IgG molecules from the surfaces, reduced surface roughness and the adhesive force.

After the bound FB_1 and antibody overlayer was exposed to 90% methanol for a period of 10 min and the cell was rinsed and filled with PBS, the SPR angle returned to its initial value for the blank. The interaction between FB_1 and the antibody has a stronger hydrophobic than hydrophilic component, which explains why their binding was sensitive to methanol. After washing with methanol to remove the bound FB_1, the antibodies were restored to their original state and the same biosensor could be reused to perform new measurements of various FB_1 standard solutions.

Curve fitting software from GraphPad was used to perform nonlinear regression on the experimental data (Δ SPR angle vs FB_1 concentration) in order to evaluate the binding of

FB_1 to the antibody overlayer for its fit as a single site binding isotherm. The resultant high correlation ($R^2 = 0.9904$) indicates that the binding of FB_1 ligand to the antibody receptor follows the law of mass action. In order the better describe the experimental results, the Klotz's equation: $1/v = 1/n + 1/nK(L)$, was used to transform the experimental data into a linear relationship, where v is the number of moles of ligand bound per antibody (as indicated by a change in SPR angle), n is the number of binding sites on the antibody, K is the association constant and L is the FB_1 (ligand) concentration. The binding isotherm presented in Figure 4.4.2.2 verifies that the reciprocal shift ($1/\Delta$) in SPR angle was directly proportional the reciprocal FB_1 concentration up to 100 μg/mL ($R^2 = 0.9987$). Such a relationship could be used for the determination of FB_1 down to a detection limit of 300 ng/mL (for a S/N ratio of 3).

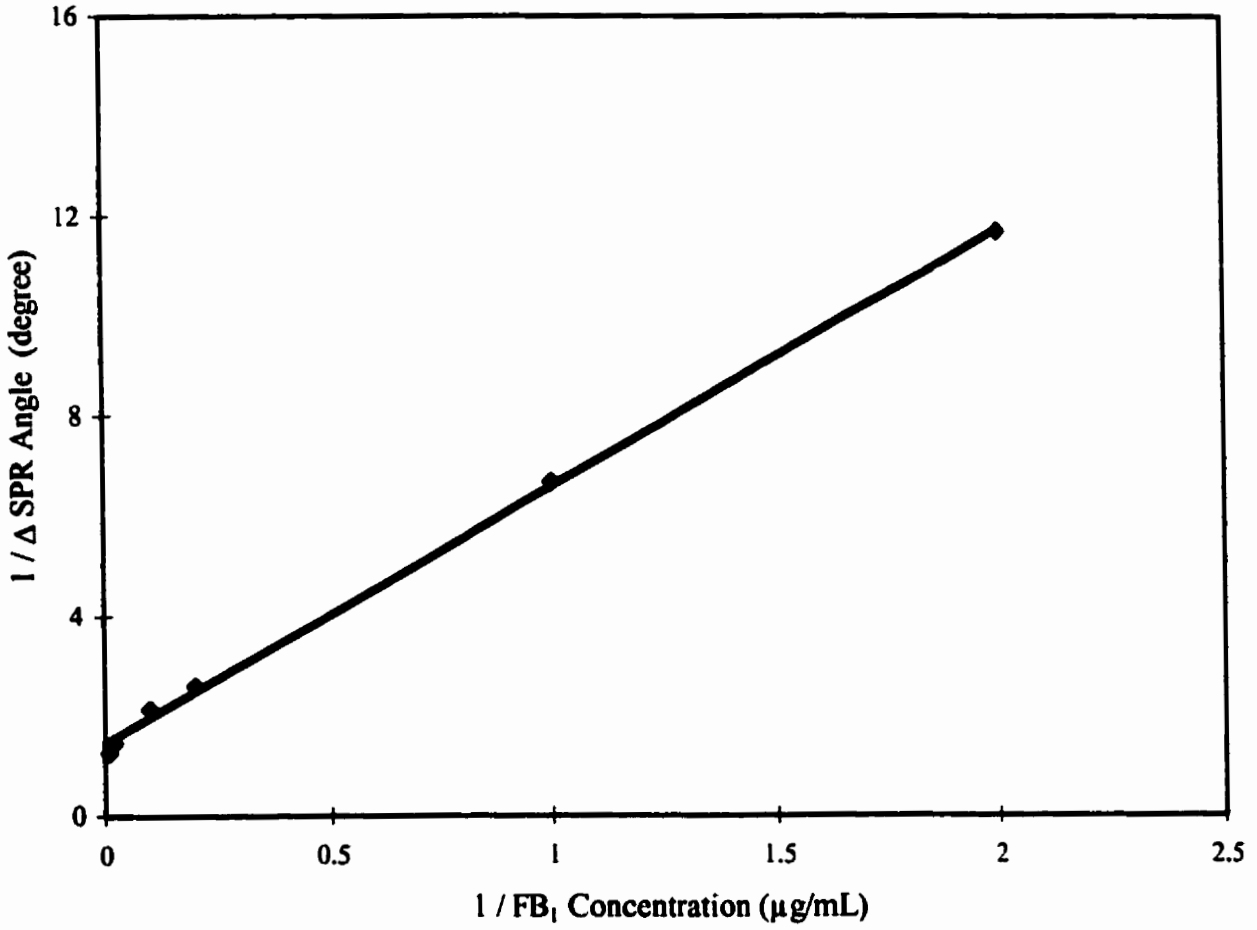

Figure 4.4.2.2: Binding isotherm of 1/ΔSPR angle versus 1/FB_1 concentration.

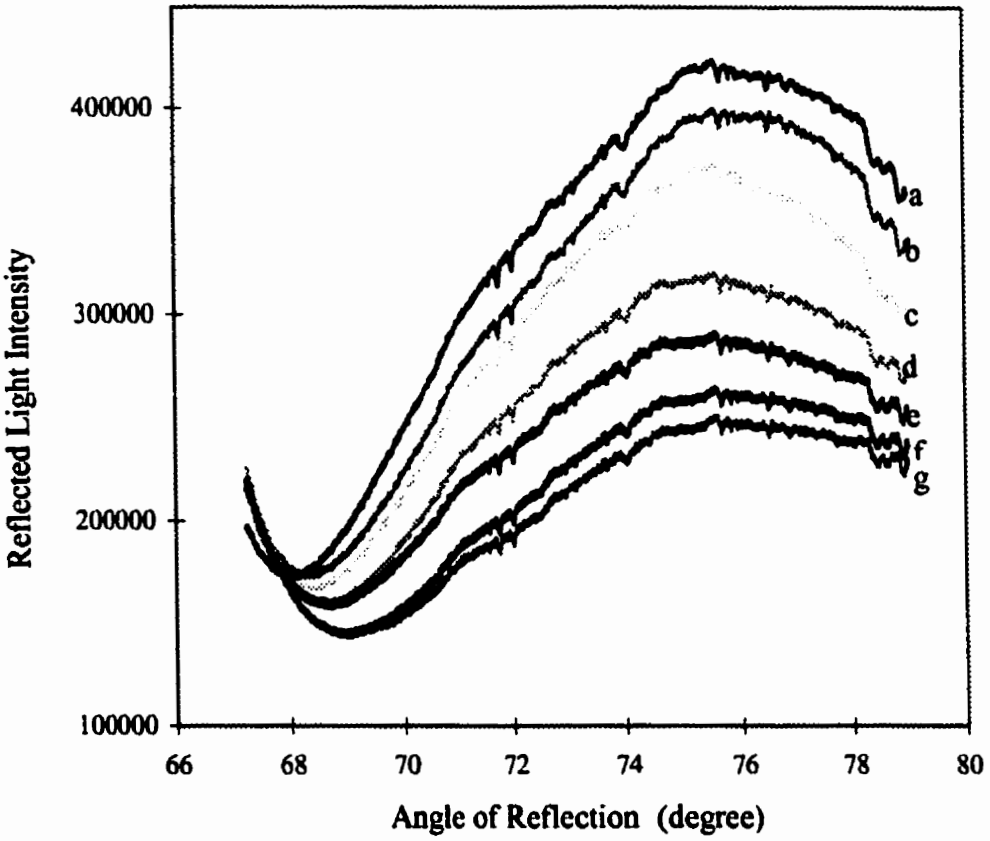

Figure 4.4.2.3: SPR angular profiles for different FB_1 concentrations: (a) 0.0 µg/mL; (b) 0.5 µg/mL; (c) 1.0 µg/mL; (d) 5.0 µg/mL; (e) 10 µg/mL; (f) 50 µg/mL; (g) 100 µg/mL.

Upon closer examination of the SPR angular profiles in Figure 4.4.2.3, obtained for the different FB_1 samples, the binding of FB_1 and antibodies on the gold film surface caused the SPR angle to increase and the angular profile to broaden. On the upper angle side of the resonance minimum, a decrease in reflected light intensity was also observed. This resulted in the evaluation of a different data analysis protocol for better FB_1 determination. Instead of measuring the shift in the SPR angle with FB_1 concentration, the intensity of the reflected light could be monitored at a fixed angle.[248] As the FB_1 concentration was increased from 0.0 µg/mL for the top profile to 100 µg/mL for the bottom profile, the intensities (in

arbitrary units) monitored by selected diodes at fixed angles of 72.03°, 73.64° and 77.92° decreased. Such decreases in intensity are inversely plotted versus the inverse of FB_1 concentration from 1.0 μg/mL to 100 μg/mL in Figure 4.4.2.4. These results indicate a high degree of linearity (average $R^2 = 0.9950$) and an decreased detection limit of 100 ng/mL.

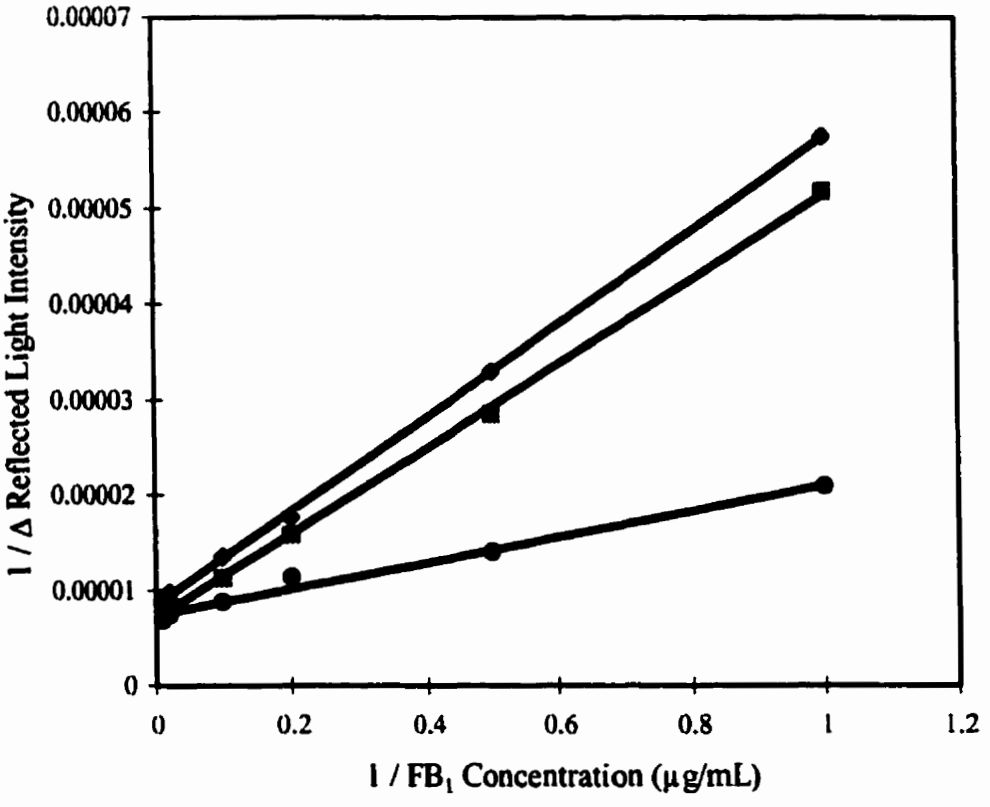

Figure 4.4.2.4: Binding Isotherm of 1/Δ reflected light intensity verus $1/FB_1$ concentration, as measured at three different angles of incident: (♦) 72.03, (■) 73.64, (●) 77.92.

Immobilization of an antibody overlayer onto new gold films, using 1:5000, 1:10000, 1:15000 and 1:20000 dilutions of the antiserum with the addition of 10 μg/mL BSA in PBS, was evaluated for immunosensing sensitivity. A logarithmic plot of detection

limit vs. dilution factor, as shown in Figure 4.4.2.5, illustrates a linear relationship representing progressively enhanced detection sensitivity (in terms of shifts in the SPR angle) for the immunoassay.

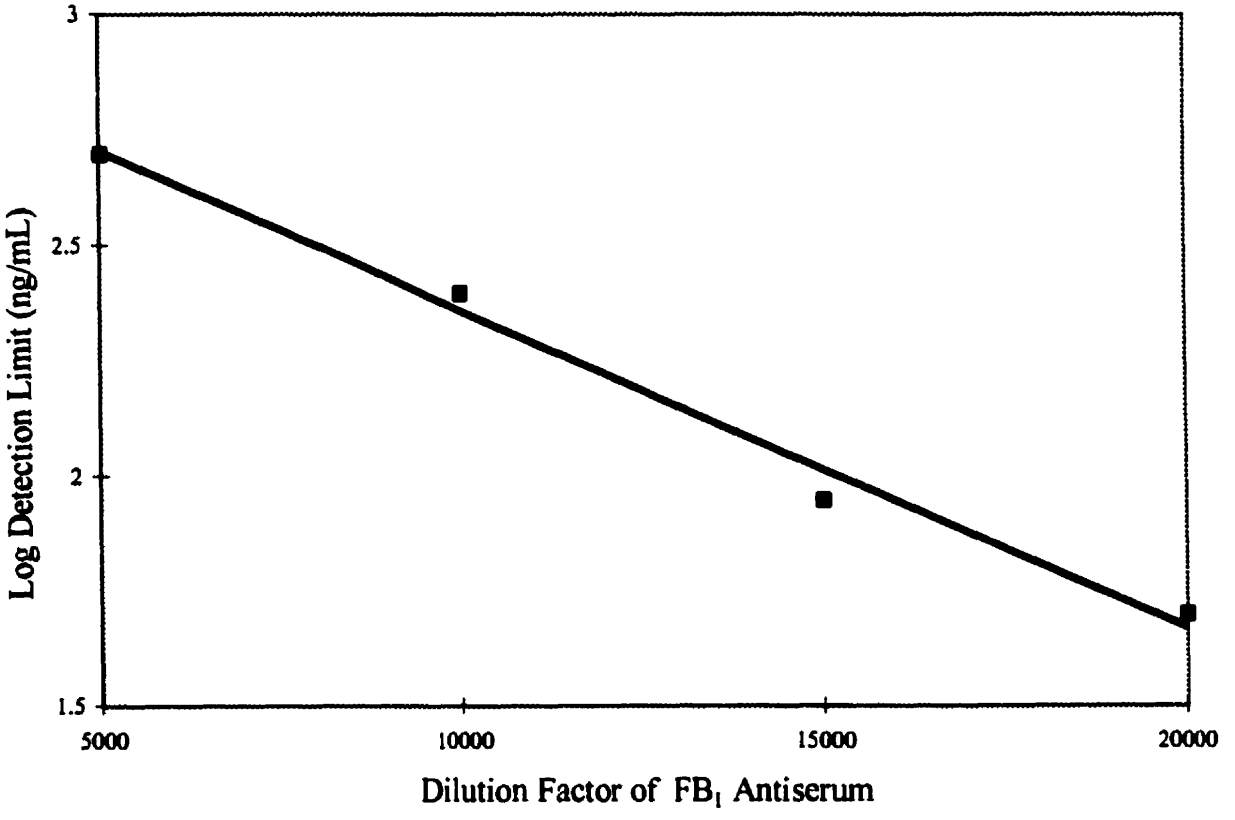

Figure 4.4.2.5: Effect of antiserum dilution on detection limit of SPR immunoassay for FB_1.

This trend is optimized at a dilution factor of 20000, which corresponds to a detection limit of 50 ng/mL. These improvements can be understood from the fact that globular IgG antibodies adsorb to a gold film surface with random orientation.[249] This surface orientation of gold-adsorbed antibodies controls the subsequent binding of FB_1, which occurs if the F_{ab} receptor sites on the antibodies are accessible to the FB_1 analyte

molecules. Since a more dilute antiserum puts fewer antibodies on the gold film during the equilibrium adsorption time, the adsorbed antibodies would be less crowded, leaving more space around the binding sites to facilitate easy access of FB_1 molecules. There should be an optimum surface density of antibodies which provides the best immunosensing efficiency. Further dilution of the antiserum will eventually yield a decreased sensitivity.

As high-affinity antibodies were used in this immunosensor development, step isotherm results were observed when several aliquots of a standard FB_1 solution (0.75 μg/mL) were added to the sample cell one after another without any washing or desorption steps in between. As shown by the data points (■) in Figure 4.4.2.6 (a), the SPR angle changes progressively with every consecutive standard added (which represents the total amount of FB_1 bound to the antibodies) resulting in a proportionally increasing signal until saturation is reached.

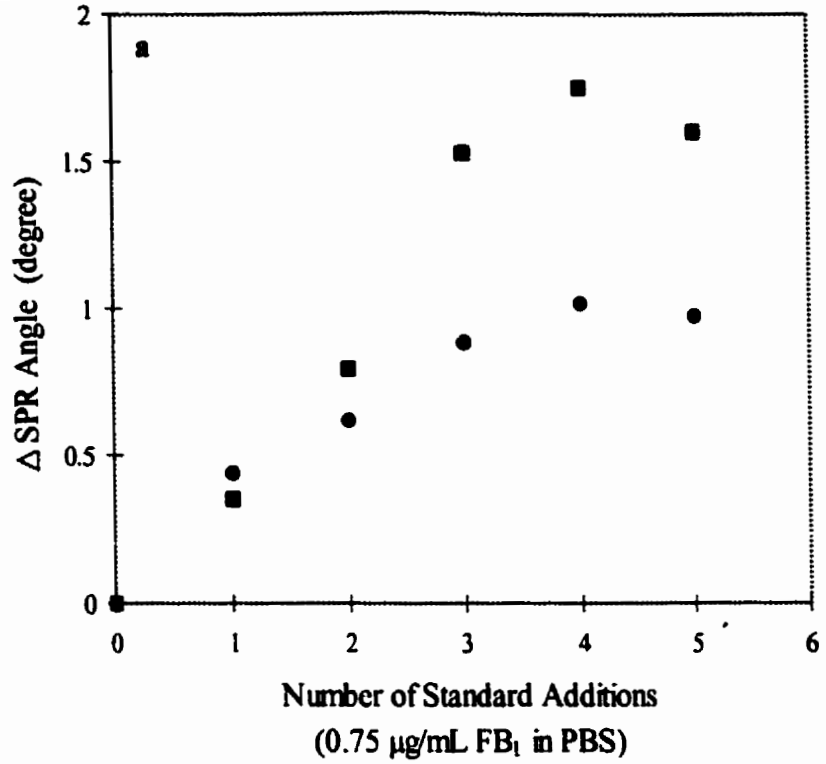

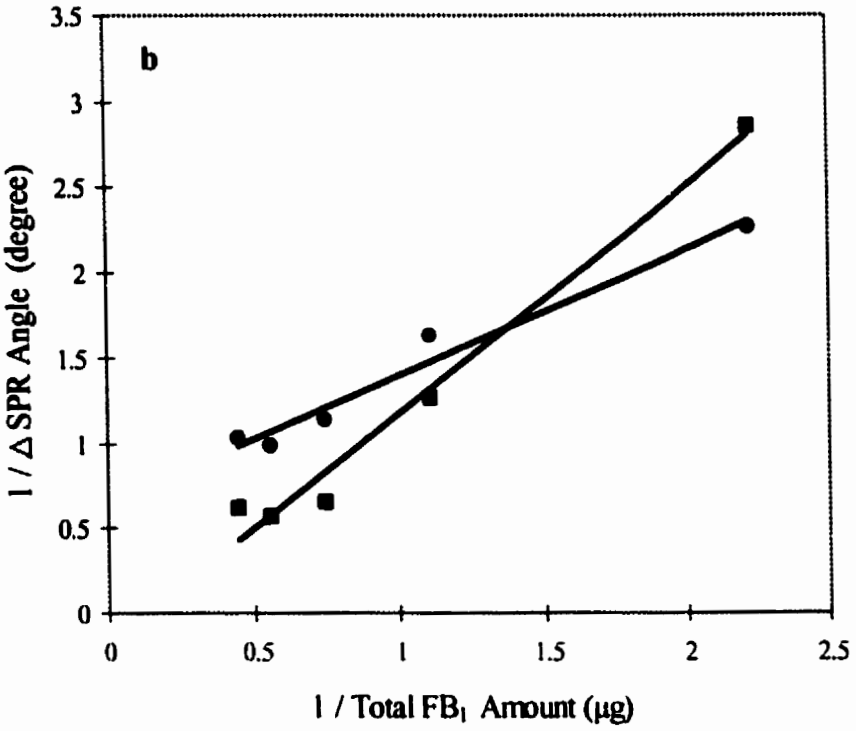

Figure 4.4.2.6: (a) Shift in SPR angle with multiple additions of 0.75 μg/mL FB_1 standard to the immunosensor: (•) solution measurements, (■) air dry measurements. (b) Binding isotherm of 1/ΔSPR angle versus 1/total FB_1 concentration: (•) solution measurements, (■) air dry measurements.

These results strongly suggest that the immunosensor effectively accumulates the FB_1 molecules from all standard additions, until the antibody binding sites are completely saturated (i.e., fully occupied). Hence, the upper portion of this curve begins to level off. Since no washing is required between the standard additions or different samples for several assays, the overall analysis time is substantially reduced. At the end of each experiment, a mixture of 20% 0.1 M H_3PO_4 and 80% methanol can be used to desorb and wash out the FB_1 molecules. These observations imply that the SPR immunosensor operates in a similar principle to titration. As the immunosensor measures the total quantity of FB_1 added in the sample cell, its detection limit should improve with the use of a larger cell volume. This was indeed proven true when the sample cell volume was changed from 0.60 mL to 1.20 mL by increasing its thickness. Unfortunately, the sensitivity increased only by a factor of 1.35 probably due to diffusion limitations.

Nonetheless, the operating principle can be utilized to its full advantage if a large volume of dilute sample solution is circulated through the sample cell. This potential can be realized with the use of a flow cell that is interfaced to the SPR immunosensor surface. The cell should have such micro-dimensions that direct the flow pattern of all FB_1 molecules towards the immobilized antibodies. Under recirculation conditions, the FB_1 in a large volume of dilute sample solution can eventually be taken up by the high-affinity antibodies to preconcentrate the analyte. This on-line sample enrichment technique will provide a significant enhancement of FB_1 detection sensitivity.

4.4.2.1 Texas Instruments SPREETA™ Sensor Kit with Flow Cell

A miniature integrated SPR liquid sensor equipped with a flow cell accessory is commercially available from Texas Instruments, at a modest cost for such sample enrichment applications.[250] As illustrated in Figure 4.4.2.1.1, the liquid SPREETA™ sensor fully integrates a light source, optical components, photodiode array detector and signal processing into a miniaturized SPR device. The near-infrared LED light beam is reflected off the gold sensing surface (surface plasmon layer) and is subsequently directed onto a linear array of silicon photodiodes by a reflecting mirror. This entire assembly is encapsulated in clear epoxy through a molding process, with the side walls covered with a black coating to prevent entry of external light. A flow cell, shown in Figure 4.4.2.1.2, can be added to the sensing surface.

Noteworthy features of the SPREETA™ device include two thermistors (in the sensor and flow cell) to compensate for SPR's sensitivity to temperature fluctuations. The sensor performance is quantified by a measurable refractive index change of 10^{-5}.[251] Replacement gold films are easily fitted to the device after removal of the original gold sensing surface. This provides the user with versatility and flexibility as the disposable films may be chemically modified for specific applications. This adaptability is especially welcome, considering the large number of antibodies that are commercially available. The device has recently proven its SPR immunosensor capability.[252] The approach utilized a gold-binding peptide (GBP)[253] for antigen attachment to the sensor surface. Under optimized conditions, fluorescyl groups bound to the GBP were able to selectively detect the binding of an anti-fluorescyl monoclonal antibody with a detection limit of 0.67 nM. This

response remained constant over a period of one month with daily use, including many regenerations of the recognition element.[252]

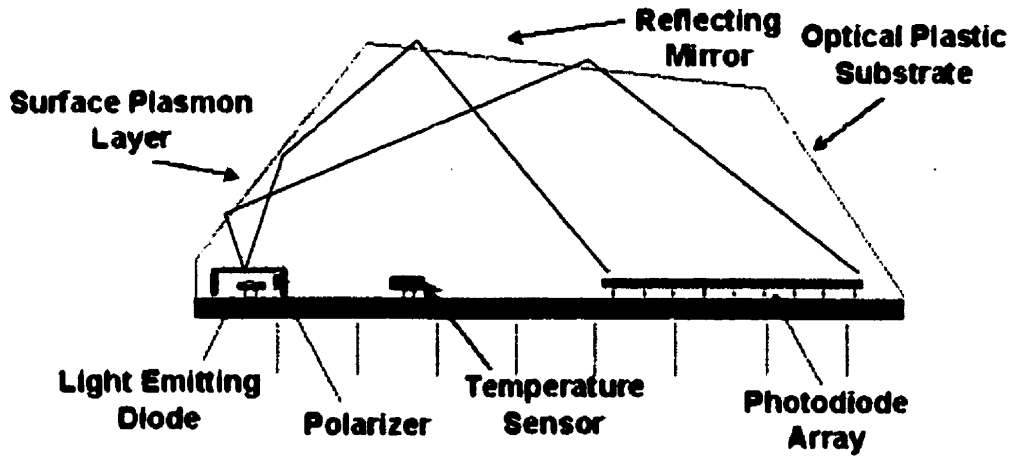

Figure 4.4.2.2.1: Schematic representation of Texas Instruments SPREETA™ sensor.

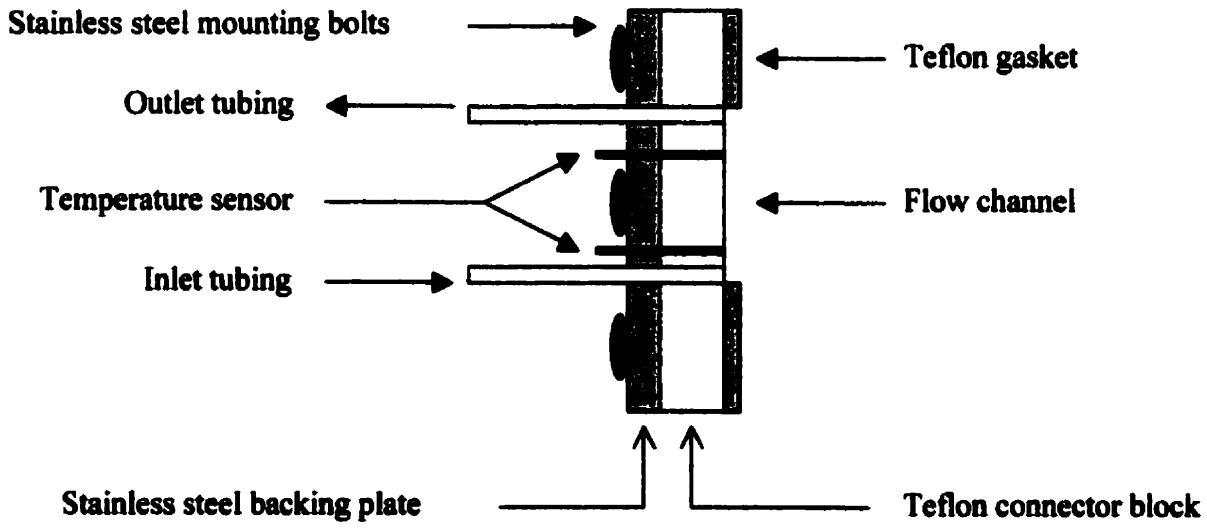

Figure 4.4.2.1.2: Schematic representation of SPREETA™ flow cell.

The data analysis capability of the SPREETA™ device is similar to the home-built SPR apparatus represented in Figure 4.3.2.1. The shift in the SPR angle or the intensity of the reflected light at a fixed angle can be monitored over time. However, the accompanying SPREETA™ software can utilize other algorithms for both smoothing and differentiating the data. For example, analysis of the SPR curves is possible by the 1st moment below a baseline method or the zero-crossing of the first derivative method. A third method, dot product of the SPR curve with its derivative, is in the developmental stage and is yet to be implemented. The first method calculates the first moment of the SPR curve below a baseline, i.e., only parts of the SPR curve that are below the baseline are included in the calculation. This fast, simple, and less noisy analysis method is therefore the most commonly used. The second method is based on the simple fact that at the minimum of the SPR curve, the first derivative will change sign. The zero-crossing algorithm initially finds the approximate minimum point of the SPR curve, performs a linear least-squares fit of the first derivative using a few points about the approximate minimum, and interpolates the zero-crossing point.

The data can be displayed in several formats after the analysis has been completed. Although plots of pixel number, SPR angle, reflectance and temperature vs time are all possible, the most common data display is refractive index vs time. An example of the SPREETA™ display, referred to as a sensogram, is shown in Figure 4.4.2.1.3.

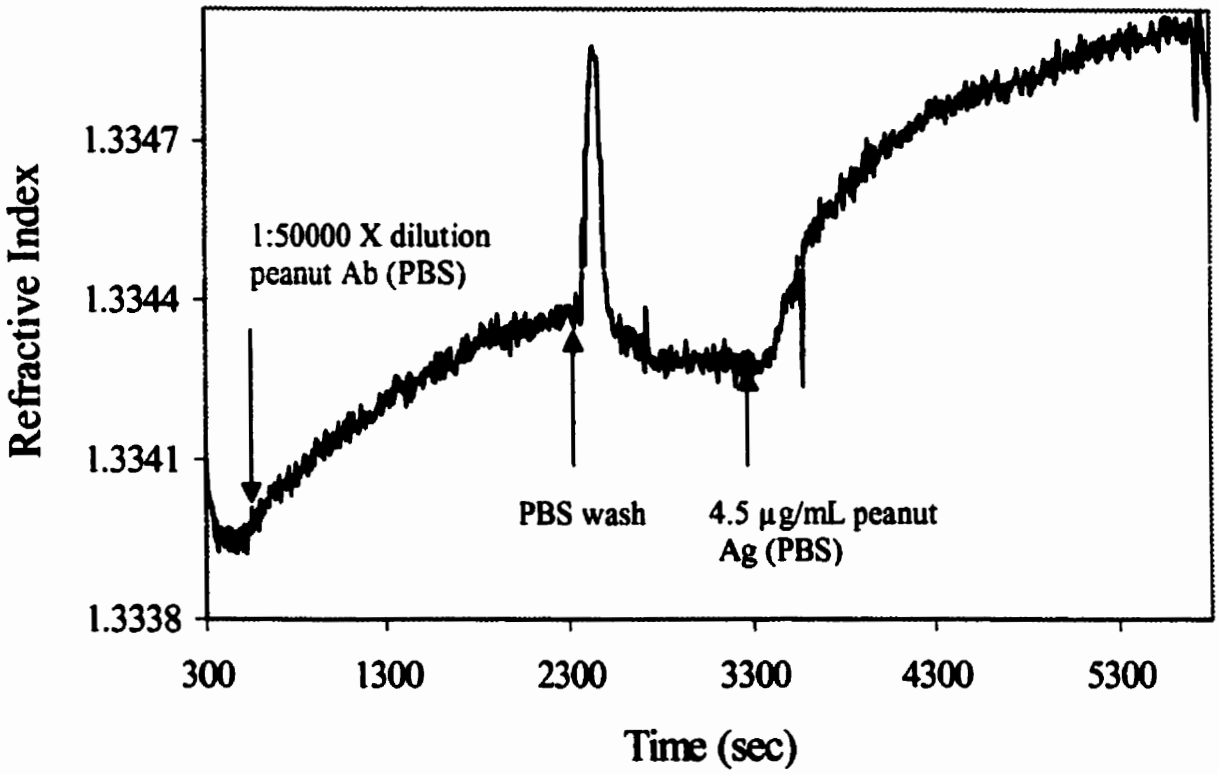

Figure 4.4.2.1.3: SPREETA™ sensogram for SPR immunoassay of peanut antigen. Flow rate = 6.0 ml/hr.

The adsorption of the IgG peanut antibody to the bare gold surface of the SPREETA™ device can be observed in real time as indicated by the rising refractive index. After flushing the flow cell with PBS, only a slight amount of antibody desorption was observed, indicating a stable antibody overlayer. The biosensor capability of the SPREETA™ device was evaluated with a volume of a 4.5 μg/ml peanut antigen standard. The binding of the peanut antigen to the adsorbed antibody overlayer again caused a proportional increase in the refractive index value. The software can also convert the change in refractive index to a thickness value for the protein layer being adsorbed on the film. The conversion is based on a model protein with a molecular weight of 68,000.

In addition to the software capability of the SPREETA™ device, its low cost, durability and portability will likely make a significant impact in SPR immunosensing research and development applications.

4.4.3 Dry Immunoassay Measurements

The analytical sensitivity of the biosensor was next investigated in the dry measurement mode. Immunoassay binding was performed as above, but followed by drying of the gold film (with an antibody overlayer and bound FB_1 molecules) in air. A SPR angular profile was then measured to exhibit a new resonance angle at 45.8 ° (as opposed to 68.5 ° for the solution measurement mode). After the above measurement was repeated six times using a 0.75 μg/mL FB_1 standard solution, a standard addition curve of resonance angle shifts could be obtained. As shown by the data points (■) in Figure 4.4.2.6 (a), the SPR response is proportional to the surface concentration of the analyte. The detection limit of this dry immunoassay was determined to be 63 ng/mL although the sensitivity (or slope

of the standard addition curve) appears to be greater than that for solution measurements. The higher sensitivity of the dry mode is thought to arise from the larger change in dielectric constant when air is replaced by FB_1, as compared to the change when PBS solution is replaced by FB_1 in the solution mode.

For both the solution and dry measurements, a linear regression analysis of the data again shows good agreement with the Klotz's equation. until the onset of saturation at 1/total FB_1 amount = 0.55 μg^{-1}, as illustrated in Figure 4.4.2.6 (b). Despite the slight deterioration of detection limit, immunoassay measurements under dry conditions provide an alternative method of FB_1 determination. One advantage of this method is that the SPR response truly reflects a binding event, rather than a bulk effect due to changes in buffer composition which might occur in unknown solution measurements.[254] In addition, the dry gold films can be potentially analyzed by laser desorption ionization[255] or MALDI[256] time-of-flight mass spectrometry for better detection sensitivity and identification of the bound analyte. Furthermore, the dry films can potentially be stored away in refrigeration as archives for future re-analysis.

4.5 Conclusions

The SPR biosensor has been applied to the determination of fumonisin FB_1 in standard solutions, with a detection limit of 50 ng/mL, using specific antibodies. The analysis time is as short as 10 min, which includes analyte binding, buffer washing and signal recording. No labeling of reagents is required. The highly selective antibodies provide simplicity (no need for extensive sample preparation). Low equipment cost (relative to fluorometers and chromatographs) and ready archiving of dried samples are additional advantages. The analytical sensitivity of this technique is moderate in comparison to alternate enzyme-linked or fluorescent methods. However, considering the present required levels of fumonisin monitoring and the above advantages, this method is potentially useful for screening large numbers of FB_1 contaminated food and feedstuff sample solutions.

CHAPTER 5: FINAL CONCLUSIONS

The focus of this thesis was to provide a better understanding of the forces responsible for molecular recognition for the purpose of improved chemical analysis. Selectivity (molecular recognition) in chemical analysis is at the research frontier in analytical chemistry. The quest for molecular recognition is directed at highly selective and reversible binding interactions. Understanding the basic forces that determine molecular recognition helps to elucidate mechanisms of chemical and biological processes and facilitates discovery of innovative biotechnological methods and materials for therapeutics, diagnostics, and separation science.

The thesis research was broken down into two main approaches towards the application of the molecular recognition processes. The first theme was based on creating molecular cavities (MIP binding sites) in which molecules (template) fit and bind selectively and reversibly. This cavity is similar in size and shape and contains a complementary spatial distribution of interaction points (based on electrostatic and hydrogen bonding to the target molecule). These MIP materials, often referred to as plastic antibodies, have several advantages over natural antibodies as summarized in Table 5.1.

Table 5.1: Imprinted Polymers Versus Antibodies: Advantages and Disadvantages.

Antibodies		Imprinted Polymers	
Advantages	Disadvantages	Advantages	Disadvantages
Aqueous solution assay possible	Immobilization may effect function	High affinity (K_{ass} = 10^8-10^{12}) and selectivity	Heterogeneous binding site distribution
High affinity for a large number of compound classes	Time consuming preparation and purification	Simple, low cost, and little time requirement for preparation	Slow mass transfer
Class specific possible	Instability, difficult to regenerate and reuse	Stable under harsh conditions	Requires preparative amount of template in pure form
Monoclonal antibodies available	Batch to batch variations	Reusable	Affinity is strongly medium dependent
		High sample load capacity	Only few compound classes successfully imprinted

Antibody preparation against low-molecular-weight compounds, also known as haptens, requires the conjugation of the hapten to a carrier protein before injecting to the animal. This conjugation can change the structural properties of the antigen exposed to the immune system and therefore the generated antibodies may be directed against a structure subtly different from the intended one. MIP preparation eliminates the need to derivatize the hapten, in addition to eliminating the use of animals.

For all the above advantages, the area of most extensive growth in molecular recognition is the field of molecular imprinting and its future is extremely bright. The technique of molecular imprinting is gaining acceptance as a means of producing specialty separation media. Researchers have begun to take a vigorous interest in this blossoming

field as indicated by the increasing number of publications (more than 50 last year). The physical and chemical phenomena responsible for recognition in MIPs are becoming better understood.

Molecular imprinting is at the stage where industrial interest in the technology is rapidly increasing and commercial applications are imminent. The most promising format for commercialization is the use of the MIP material as a selective SPE adsorbent. The remaining challenges in molecular imprinting include an improved recognition capability in aqueous samples. Imprinting of larger templates is another significant barrier at present. Lastly, it would be advantageous to prepare MIPs with homogeneous binding sites for improved chromatographic separations. Regardless, biomimetic sensors with their stringent demand for selectivity will welcome further MIP development. These materials will play an ever more significant role in chemical analysis as the range MIPs and their applications continues to widen.

The natural antibody–antigen system was investigated in the second scheme via SPR for real time monitoring of the binding process. It combined the high selectivity of natural antibodies with the optical transduction advantages of SPR. Interaction of analytes and ligands could be analyzed on a microscale without the need to label either interactant. Such optical biosensors will provide an increasing impact on technology for the measurement of biomolecular interaction analyses and provide the bioanalytical chemist with a very powerful tool.

REFERENCES

1. Rollag, J.G.; Liu, T; Hage, D.S. *J. Chromatogr. A.* **1997**, 765, 145-155.

2. Sellergren, B. *Trends Anal. Chem.* **1997**, 16, 310-319.

3. Burton, D.R. *Acc. Chem. Res.* **1993**, 26, 405-411.

4. Pauling, L. *J. Am. Chem. Soc.* **1940**, 62, 2643-2649.

5. Haurowitz, F. *Physiol. Rev.* **1965**, 45, 1-5.

6. Mekler, L.B. *Nature* **1967**, 215, 481-487.

7. Price, C.P.; Newman, D.J. In *Principles and Practice of Immunoassay*, 2nd ed.; Price, C.P., Newman, D.J., Eds.; Stockton: New York, 1997; 1.

8. Adrain, T.E. *Methods. Mol. Bio.* **1997**, 73, 251-267.

9. Edwards, R. In *Principles and Practice of Immunoassay*, 2nd ed.; Price, C.P., Newman, D.J., Eds.; Stockton: New York, 1997; 325-348.

10. Gosling, J.P. In *Principles and Practice of Immunoassay*, 2nd ed.; Price, C.P., Newman, D.J., Eds.; Stockton: New York, 1997; 349-388.

11. Hemmila, I.A. *Immunochemistry I*; Johnstone, A.P., Turner, M.W., Eds. IRL Press: Oxford, 1997; pp 193-214.

12. C.J. Pedersen. *J. Am. Chem. Soc.* **1967**, 89, 2495-2496.

13. C.J. Pedersen. *J. Am. Chem. Soc.* **1967**, 89, 7017-7036.

14. Lehn, J-M. *Angew. Chem. Int. Ed. Engl.* **1988**, 27, 89-112.

15. Karlsson, P.K.; Lutz, E.S.M.; Andersson, L.I. *Trends Anal. Chem.* 1999, 18, 146-153.

16. Wulff, G. *Angew. Chem. Int. Ed. Engl.* **1995**, 34, 1812-1832.

17. Wullf, G; Sarhan, A. *Ange. Chem.* **1972**, 84, 364.

18. Takagishi, T.; Klotz, I.M. *BIPMA.* **1972**, 11, 483-491.

19. Lai, E.P.C.; Fafara, A.; VanderNoot, V.A.; Kono, M.; Polsky, B. *Can. J. Chem.* **1998**, 76, 265-273.

20. McNiven, S.; Kato, M.; Levi, R.; Yano, K.; Karube, I. *Anal. Chim. Acta.* **1998**, 365, 69-74.

21. Tanabe, K.; Takeuchi, T.; Matsui, J.; Ikebukuro, K.; Yano, K.; Karube, I. *Chem. Commun.* **1995**, 2303-2304.

22. Vlatakis, G.; Andersson, L.I.; Müller, R.; Mosbach, K. *Nature.* **1993**, 361, 645-647.

23. Ye, L.; Ramstrom, O.; Mansson, M.O.; Mosbach, K. *J. Mol. Recogn.* **1998**, 11, 75-78.

24. Ramstrom, O.; Yu, C.; Mosbach, K. *J. Mol. Recogn.* **1996**, 9, 691-696.

25. Walshe, M.; Howarth, J.; Kelly, M.T.; O'Kennedy, R.; Smyth, M.R. *J. Pharmaceut. Biomed. Anal.* **1997**, 16, 319-325.

26. Shea, K.J.; Spivak, D.A.; Sellergren, B. *J. Am. Chem. Soc.* **1993**, 115, 3368-3369.

27. Schweitz, L.; Andersson, L.I.; Nilsson, S. *Anal. Chem.* **1997**, 69, 1179-1173.

28. Kriz, D.; Mosbach, K. *Anal. Chim. Acta.* **1995**, 300, 71-76.

29. Kempe, M.; Mosbach, K. *J. Chromatogr. A.* **1994**, 664, 276-279.

30. Spivak, DA.; Shea, K.J. *Macromolec.* **1998**, 31, 2160-2165.

31. Matsui, J.; Takeuchi, T. *Anal. Comm.* **1997**, 34, 199-200.

32. Siemann, S.; Andersson, L.I.; Mosbach, K. *J. Antibiot.* **1997**, 50, 89-91.

33. Lele, B.S.; Kulkarni, M.G.; Mashelkar, R.A. *React. Funct. Polym.* **1999**, 40, 215-229.

34. Sellergren, B. *Anal. Chem.* **1994**, 66, 1578-1582.

35. Kempe, M.; Glad, M.; Mosbach, K. *J. Mol. Recogn.* **1995**, 8, 35-39.

36. Haginaka, J.; Sakai, Y.; Narimatsu, S. *Anal. Sci.* **1998**, 14, 823-826.

37. Schweitz, L.; Andersson, L.I.; Nilsson, S. *J. Chromatogr. A.* **1997**, 792, 401-409.

38. Andersson, L.I.; Paprica, A.; Arvidsson, T. *Chromatogr.* **1997**, 46, 57-62.

39. Matsui, J.; Nicolls, I.A.; Takeuchi. T. *Anal. Chim. Acta.* **1998**, 365, 89-93.

40. Ficher, L.; Muller, R.; Ekberg, B.; Mosbach, K. *J. Am. Chem. Soc.* **1991**, 113, 9358-9360.

41. Suedee, R.; Songkram, C.; Petmoreekul, A.; Sangkunakup, S.; Sankasa, S.; Kongyarit, N. *J. Plan. Chromatogr.* **1998**, 11, 272-276.

42. Kim, J.M.; Chong, B.O.; Ahn, K.D. *Bull. Korean Chem. Soc.* **1998**, 19, 143-145.

43. Kugimiya, A.; Matsui, J.; Abe, H.; Aburatani, M.; Takeuchi, T. *Anal. Chim. Acta.* **1998**, 365, 75-80.

44. Zhou, J.; He, X.W. *Anal. Chim. Acta.* **1999**, 381, 85-91.

45. Sellergren, B; Wieschemeyer, J.; Boos, K.; Seidel, D. *Chem. Mater.* **1998**, 10, 4037-4046.

46. Berglund, J.; Nicholls, C.; Lindbladh, K. Mosbach, K. *Biomed. Chem. Lett.* **1996**, 6, 2237-2242.

47. Ramstrom, O.; Ye, L.; Mosbach, K. *Chem. Biol.* **1996**, 3,471-477.

48. Sreenivasan, K.; Sivakumar, R. *J. Appl. Polym. Sci.* **1997**, 66, 2539-2542.

49. Ye, L.; Cormack, P.A.G.; Mosbach, K. *Anal. Commun.* **1999**, 36, 35-38.

50. DelaCruz, E.O.; Muguruma, H.; Jose, W.I.; Pedersen, H. *Anal. Lett.* **1999**, 32, 841-854.

51. Ramstrom, O.; Ye, L.; Krook, M.; Mosbach, K. *Anal. Commun.* **1998**, 35, 9-12.

52. Tarbin, J.A.; Sharman, M. *Anal. Commun.* **1999**, 36, 105-107.

53. Dauwe, C; Sellergren, B. *J. Chromatogr. A.* **1996**, 753, 191-200.

54. Matsui, J.; Kubo, H.; Takeuchi, T. *Anal. Sci.* **1998**, 14, 699-702.

55. Rashid, B.A.; Briggs, R.J.; Hay, J.N.; Stevenson, D. *Anal. Comm.* **1997**, 34, 303-305.

56. Baggiani, C.; Trotta, F.; Giraudi, G.; Giovannoli, C.; Vanni, A. *Anal. Commun.* **1999**, 36, 263-266.

57. Cheong, S.H.; Rachkov, A.E.; Park, J.K.; Yano, K.; Karube, I. *J. Polym. Sci. A. Polym. Chem.* **1998**, 36, 1725-1732.

58. Haupt, K.; Dzgoev, A.; Mosbach, K. *Anal. Chem.* **1998**, 70, 628-631.

59. Bjarnason, B.; Chimuka, L.; Ramström, O. *Anal. Chem.* **1999**, 71, 2152-2156.

60. Lin, J.M.; Nakagama, T.; Uchiyama, K.; Hobo, T. *Biomed. Chromatogr.* **1997**, 11, 298-232.

61. Hosoya, K.; Tanaka, N. *ACS Symp. Ser.* **1998**, 703,143-158.

62. Hosoya, K.; Iwakoshi, Y.; Yoshikazo, K.; Kimata, K.; Tanaka, N.; Takehira, H.; Haginaka, J. *J. High Res. Chromatogr.* **1999**, 22, 256-260.

63. Haginaka, J.; Sanbe, H. *Chem. Lett.* **1999**, 8, 757-758.

64. Haginaka, J.; Takekira, H.; Hosoya, K.; Tanaka, N. *J. Chromatogr. A* **1999**, 849, 331-339.

65. Piletsky, S.A. *J. Membr. Sci.* **1999**, 157, 263- 278.

66. Dzgoev, A; Haupt, K. *Chirality*. **1999**, 11, 465 - 469.

67. Suedee, R. *J. Planar Chromaotgr. Mod. TLC.* **1998**, 11, 272-276.

68. Suedee, R.; Songkram, C.; Petmoreekul, A.; Sangkunakup, S.; Sankasa, S.; Kongyarit, N. *J. of Planar Chromatogr. Mod. TLC.* **1998**, 11, 272-276.

69. Suedee, R.; Srichana, T.; Saelim, J.; Thavornpibulbut, T. *Anal.* **1999**, 124, 1003-1009.

70. Remcho, V.T.; Tan, Z.J. *Anal. Chem.* **1999**, 71, 248A-255A.

71. Lanza, F.; Sellergren, B. *Anal. Chem.* **1999**, 71, 2092-2096.

72. Lin, J.M.; Nakagama,T.; Uchiyama, K.; Hobo, T. *Biomed. Chromatogr.* **1997**, 11, 298-302.

73. Nilsson, K.; Lindell, J.; Norrlow, O.; Sellergren, B. *J. Chromatogr. A* **1994**, 680, 57-61.

74. Svenson, J.; Andersson, H.S.; Piletsky S.A.; Nicolls, I.A. *J. Mol. Recognit.* **1998**, 11, 83-88.

75. Sergeyeva, T.A.; Piletsky, S.A.; Brovko, A.A.; Slinchenko, E.A.; Sergeeva, L.M.; El'skaya, A.V. *Anal. Chim. Acta.* **1999**, 392, 105-111.

76. Hedborg, E.; Winquist, F.; Lundstrom, I.; Andersson, L.I., Mosbach, K. *Sens. Actuators A Phys.* **1993**, 37, 796 - 799.

77. Kroger, S.; Turner, A.P.F.; Mosbach, K.; Haupt, K. *Anal. Chem.* **1999**, 71, 3698-3702.

78. Piletsky, S A; Piletskaya, E.V.; El'skaya, A.V.; Levi, R.; Yano, K.; Karube, I. *Anal. Lett.* **1997**, 30, 445-455.

79. Kriz, D.; Ramstrom, O.; Svensson, A.; Msbach, K. *Anal. Chem.* **1995**, 67, 2142-2144.

80. Levi, R.; McNiven, S.; Piletsky, S.A.; Cheong, S.; Yano, K.; Karube, I. *Anal. Chem.* **1997**, 69, 2017-2021.

81. Ferrer, I.; Barcelo, D. *Trends Anal. Chem.* **1999**, 18, 180-192.

82. Mullett, W.M.; Lai, E.P.C.; Sellergren, B. *Anal. Commun.* **1999**, 36, 217-220.

83. Sellergren, B. *Trends Anal. Chem.* **1999**, 18, 164-174.

84. Olsen, J.; Martin, P.; Wilson, I.D.; Jones, G.R. *Anal.* **1999**, 124, 467-471.

85. Lord, H.; Pawliszyn, J. *LC-GC.* **1999**, 17, S25-S30.

86. McMahon, G.P.; Kelly, M.T. *Anal. Chem.* **1998**, 70, 409-414.

87. Schreiber-Deturmeny, E; Bruguerolle, B. *J. Chromatogr. B.* **1996**, 677 305-312.

88. Dockendorff, B.; Holman, D.A.; Christian G.D.; Ruzicka, J. *Anal. Commun.* **1998**, 35, 357-359.

89. Howard, C.E.; Capers, C.C.; Bess, D.T.; Anderson, R.J. *Amer. J. Hosp. Pharm.* **1994**, 51, 1672-1675.

90. Slamenova, D.; Gabelova, A.; Ondrejkova, A.; Ruzekova, L.; Farkasova T.; Collins, A. *Mutat. Res. DNA Repair.* **1998**, 408, 11-17.

91. Fattore, C.; Cipolla, G.; Gatti, G.; Bartoli, A.; Orticelli, G.; Picollo, R.; Millerioux, L.; Ciottoli, G.B.; Perucca, E. *Clin. Drug Invest.* **1998**, 16, 387-392.

92. Delbeke, F.T.; Debacker, P.J. *J. Chromatogr. B.* **1996**, 687, 247-252.

93. Li, Z.; Chen, G. *Act. Phar. Si.* **1994**, 15, 267-270.

94. Eldesoky, E.; Meinshausen, J.; Buhl, K.; Engel, G.; Haringskaim, A.; Drewelow, B.; Klotz, U. *Ther. Drug Monit.* **1993**, 15, 281-288.

95. Rodvold, K.A.; Piscitelli, S.C. *Clin. Infect. Dis.* **1993**, 25, 506-515.

96. Schulz, H.U.; Hartmann, M.; Steinijans, V.W; Huber, R.; Luhrmann, B.; Bliesath, H.; Wurst, W. *Int. J. Clin. Pharmacol. Ther.* **1996**, 34, S51-S57.

97. Nagai, N.; Furuhata, M.; Ogata, H. *Biol. Pharm. Bull.* **1995**,18, 1610-1613.

98. Korrapati, M.R.; Vestal, R.E.; Loi, C.M. *Clin. Pharmacol. Therap.* **1995**, 57, 413-418.

99. Delahunty, T.; Schoendorfer, D. *J. Anal. Toxicol.* **1998**, 22, 596-600.

100. Tsanaclis, L.M.; Wilson, J.F. *Ther. Drug Monit.* **1997**, 19, 420-426.

101. Wicks, J.F.C.; Myring, A.; Wilson, J.F. *Ann. Clin. Biochem.* **1994**, 31, 291-292.

102. Yang, S.S.; Smetena,I.; Goldsmith, A.I. *J. Chromatogr.* **1996**, 746, 131-136.

103. Rocecrans, J.A. *Chem. Ind.* **1998**, 13, 525-529.

104. Nakajima, M.; Iwata, K.; Yamamoto, T.; Funae, Y.; Yoshida, T.; Kuroiwa, Y. *Drug Metab. Dispos.* **1998**, 26, 36-41.

105. Troje, Z.S.; Frobe, Z.; Perovic, D. *J. Chromatogr.* **1997**, 775, 101-107.

106. Dash, A.K.; Wong, S. *J. Chromatogr.* **1996**, 749, 81-85.

107. Lu, G.H.; Ralapati, S. *Electrophoresis* **1998**, 19, 19-26.

108. Ayers, G.P.; Selleck, P.W.; Gillett, R.W.; Keywood, M.D. *J. Chromatogr.* **1998**, 824, 241-242.

109. Liu, J.; Feng, Y. *Talanta*, **1999**, 47, 833-840.

110. Lundh, H.; Nilsson, O.; Rosen, I. *J. Neurol. Neurosurg. Psychiat.* **1979**, 42, 171-177.

111. Lundh, H.; Nilsson, O.; Rosen, I. *Prof. Brain Res.* **1990**, 84, 163-166.

112. Capacio, B.R.; Byers, C.E.; Matthews, R.L.; Chang, F.C.T. *Biomed. Chromatogr.* **1996**, 10, 111-120.

113. Williams, D.H. *Aldrichim. Acta.* **1991**, 24, 71-80.

114. Orr, A.A. *J. Paint. Technol.* **1975**, 47, 45-49.

115. WWW URL for Society of Molecular Imprinting Homepage, http://www.ng.hik.se/~SMI/story/Poro.htm

116. Kaliszan, R. *Structure and Retention in Chromatography: A Chemometric Approach*; Harwood Academic: Amsterdam, 1997; Chapter 3.

117. Thruman, E.M.; Mills, M.S. *Solid Phase Extraction. Principles and Practice*, Vol. 147; John Wiley and Sons: New York, 1998; Chapter 4.

118. Armarego, W. L. F.; Perrin, D. D. *Purification of Laboratory Chemicals*, 4th ed.; Butterworth-Heinemann: Oxford, 1996; Chapter 3.

119. Zander, A.; Findlay, P.; Renner, T.; Sellergren, B. *Anal. Chem.* **1998**, 70, 3304-3311.

120. Muldoon, M.T.; Stanker, L.H. *Anal. Chem.* **1997**, 69, 803-808.

121. O'Shannessey, D.J.; Ekberg, B.; Andersson, L.I.; Mosbach, K. *J. Chromatogr.* **1989**, 470, 391-399.

122. Mathew, J.; Buchardt, O. *Bioconjug. Chem.* **1995**, 6, 524-528.

123. Baggiani, C.; Trotta, F.; Giraudi, G.; Moraglio, G.; Vanni, A. *J. Chromatogr. A* **1997**, 786, 23-29.

124. Hosoya, K. *J. Chromatogr. A.* **1996**, 728, 139-147.

125. Ramstrom, O.; Le, Y.; Mosbach, K. *Chem. Biol.* 1996, 3, 471-475.

126. Matsui, J.; Miyoshi, Y.; Matsui, R.; Takeuchi, T. *Anal. Sciences.* **1995**, 11, 1017-1018.

127. Sellergren, B.; Lepisto, M.; Mosbach, K. *J. Amer. Chem. Soc.* **1988**, 110, 5853-5860.

128. Kempe, M.; Mosbach, K. *Tetrahedron Lett.* **1995**, 36, 3563-3566.

129. Kempe, M. *Anal. Chem.* **1996**, 68, 1948-1953.

130. Schweitz, L.; Andersson, L.I.; Nilsson, S. *Anal. Chem.* **1997**, 69, 1179-1183.

131. Petro, M.; Svec, F.; Frechet, J.M.J. *Anal. Chem.* **1997**, 69, 3131-3139.

132. Chang, J.; Gotcher, S.; Gushaw, J.B. *Clin. Chem.* **1982**, 28, 361-367.

133. Eisert, R.; Pawliszyn, J. *Anal. Chem.* **1997**, 69, 3140-3147.

134. Mullett, W.M.; Lai, E.P.C. *Anal Chem.* **1998**, 17, 384-394.

135. Hong, J.M.; Anderson, P.E.; Qian, J.; Martin, C.R. *Chem. Mater.* **1998**, 10, 1029-1033.

136. Kobayashi, T.; Wang, H.Y.; Fujii, N. *Chem. Lett.* **1995**, 10 , 927-928.

137. Matsui, J.; Miyoshi, Y.; Matsui, R.; Takeuchi, T. *Anal. Sciences.* **1995**, 11, 1017-1018.

138. Sellergren, B. *Tr. Anal. Chem.* **1997**, 16, 310-320.

139. Steinke, J.; Sherrington, D.C.; Dunkin, I.R. *Advances in Polymer Sciences. Imprinting of Synthetic Polymers using Molecular Templates*, Vol. 123, Springer: Berlin, 1995; pp. 81-125.

140. Sajonz, P.; Kele, M.; Zhong, P.; Sellergren, B.; Guichon, G.J. *J. Chromatogr.*, in press.

141. Joshi, V.P.; Karode, S.K.; Kulkarni, M.G.; Mashelhkar, R.A. *Chem. Eng. Sci.* **1998**, 53, 2271-2284.

142. Bolliet, D.; Poole, C.F. *Anal.* **1998**, 123, 295-299.

143. Zander, A.; Findlay, P.; Renner, T.; Sellergren, B.; Swietlow, A. *Anal. Chem.* **1998**, 70, 3304-3314.

144. Maguire, T. *Eur. J. Drug Metab. Pharmacokinet.* **1994**, 19, 279-283.

145. Eldesoky, E.; Meinshausen, J.; Buhl, K.; Engel, G.; Haringskaim, A.; Drewelow. B.; Klotz, U. *Ther. Drug Monit.* **1993**, 15, 281-288.

146. Buss, D.; Leopold, D.; Smith, A.P.; Routledge, P.A. *J. Clin. Pharmacol.* **1983**, 15, 399-405.

147. Korrapati, M.R.; Vestal, R.E.; Loi, C.M. *Clin. Pharmacol. Therap.* 1995, 57, 413-418.

148. Herraez-Hernandez, R.; Vandemerbel, N.C.; Brinkman, U.A.T. *J. Chromatogr. B.* **1995**, 666, 127-137.

149. Sellergren, B.; Shea, K.J. *J. Chromatogr.* **1993**, 635, 31-49.

150. Lu, G.H.; Ralapati, S. *Electrophoresis* **1998**, 19, 19-26.

151. Fukumoto, M.; Kubo, H.; Ogamo, A. *Vet. Human. Toxicol.* **1997**, 39, 225-227.

152. WWW URL for ACDLabs, http://www.acdlabs.com/ilab/.

153. Andersson, H.S.; Koch-Schmidt, A.; Ohlson, S. *J. Mol. Recognit.* **1996**, 9, 675-681.

154. Mullett, W.M.; Lai, E.P.C. *Microchemical J.* **1999**, 61,143-155.

155. Dauwe, C.; Sellergren, B. *J. Chromatogr. A.* **1996**, 753, 191-196.

156. Wells, M.J.M.; Michael, J.L. *J. Chromatogr. Sci.* **1987**, 25, 345-350.

157. Shea, K.J.; Saski, D.Y. *J. Am. Chem. Soc.* **1991**, 113, 4109-4120.

158. Svenson, J.; Andersson, H.S.; Piletsky S.A.; Nicolls, I.A. *J. Mol. Recognit.* 1998, 11, 83-89.

159. Andersson, H.S.; Nicholls, I.A. *Bioorgan. Chem.* **1997**, 25, 203-211.

160. Hosoya, K.; Shirasu, Y.; Kimata, K.; Tanaka, N. *Anal. Chem.* **1998**, 70, 943-945.

161. Turkewitsch, B. Wandelt, B.; Darling, G.D.; Powell, W.S. *Anal. Chem.* **1998**, 70, 2789-2781.

162. Sellergren, B. *Trends in Analytical Chemistry.* **1999**, 18, 164-174.

163. Nicholls, I.A. Chem. Lett. **1995**, 1035.

164. Hage, D.S. *Anal. Chem.* **1999**, 71, 294R-304R.

165. Wood, R.W. *Phil. Mag.* **1902**, 4, 396-402.

166. Cowan, J. *Opt. Commun.* **1972**, 5, 69-72.

167. Schneider, F.W. *Non-linear Raman Spectroscopy and its Applications*; D. Reidel, Dordrecht, 1982; 461-470.

168. Rothenhausler, B.; Knoll, W. *Nature.* **1988**, 332, 615-617.

169. Hickel, W.; Knoll, W. *Acta Metallica.* **1989**, 37, 2141-2142.

170. Otto, A. *Zeitschrift für Physik.* **1968**,16, 398.

171. Nylander, C.; Liedberg, B.; Lind, T. *Sens. and Actuators.* **1982**, 3, 79-84.

172. Liedberg, B.; Nylander, C.; Lundstrom, I. *Sens. and Actuators.* **1983**, 4, 229-304.

173. Adamczyk, M.; Johnson, D.D.; Mattingly, P.G.; Moore, J.A.; Pan, Y. *Bioconjugate Chem.*, **1998**, 9, 23-32.

174. Stoecklein, W.F.M.; Warsinke, A.; Michel, B.; Hoehne, W.; Woller, H.; Kempter, G.; Scheller, F. W. *NATO ASI Ser., Ser.2* **1997**, 38, 155-162.

175. Median, M.B. *J. Agric. Food Chem.* **1997**, 45, 389-94.

176. Ohlson, S.; Strandh, M.; Nilshans, H. *J. Mol. Recognit.* **1997**, 10, 135-138.

177. Loomans, E.E.M.G.; Beumer, T.A.M.; Damen, K.C. S.; Bakker, M.A.; Schielen, W.J.G. *J. Colloid Interface Sci.* **1997**, 192, 238-249.

178. Adamczyk, M.; Gebler, J.C.; Gunasekera, A.H.; Mattingly, P.G.; Pan, Y. *Bioconjug. Chem.* **1997**, 8, 133-145.

179. Rauffer-Bruyere, N.; Chatellier, J.; Weiss, E.; Regenmortel, M.H.V.; Altschuh, D. *Mol. Immunol.* **1997**, 34, 165-174.

180. Myszka, D.G.; Morton, T. A.; Doyle, M. L.; Chaiken, I. M. *Biophys. Chem.* **1997**, 64, 127-137.

181. Median, M.B.; Vanhouten, L.; Cooke, P.H.; Tu. S.I. *Biotechnol. Tech.* **1997**, 11,173-176.

182. Fägerstam, L.G.; Frostell-Karlsson, Å.; Karlsson, R.; Persson, B.; Rönnberg, I. *J. Chromatogr.* **1992**, 597, 397-404.

183. Löfas, S.; Johnsson, B.; Tegendal, K.; Rönnberg, I. *Collioids Surf. B: Biointerfaces* **1993**, 1, 83-89.

184. Karlsson, R.; Stählberg, R. *Anal. Biochem.* **1995**, 228, 274-280.

185. Tu, S.I.; Medina, M.B.; Van Houten, L.; Cooke, P.H. *IFT Annual Meeting Book of Abstracts*, **1997**, p. 129.

186. Mullett, W.M.; Lai, E.P.C. *Methods Compan. Methods in Enzymol.*, in press.

187. Sasaki, S.; Nagata, R.; Hock, B.; Karube, I. *Anal. Chim. Acta.* **1998**, 368, 71.

188. Lundström, I. *Biosens. Bioelectron.* **1994**, 9, 725-736.

189. Liedberg, B.; Nylander, C.; Lundstrom, I. *Biosens. Bioelectron.* **1995**, 10, i-ix.

190. Morgan, C.L.; Newman, D.J.; Price, C.P. *Clin. Chem.* **1996**, 42, 193-209.

191. Tapuchi, E.; Venter, E.A.; Kfir, R. *S. Afr. J. Chem.* **1996**, 49, 8-25.

192. VanderNoot, V.A.; Lai, E.P.C. *Spectr.* **1991**, 6, 28-33.

193. Daniels, P.; Deacon, J.; Eddowes, M.; Pedley, D. *Sens. and Actuators.* **1988**, 15, 11-18.

194. Dubs, M-C.; Altschuh, D.; Van Regenmortel, M.H.V. *Immunol. Lett.* **1991**, 31, 59-64.

195. Morgan, H.; Taylor, D. *Biosens. Bioelectron.* **1992**, 7, 405-410.

196. Severs, A.H.; Schasfoort, R.B.M.; Salden, M.H.L. *Biosens. Bioelectron.* **1993**, 8, 185-189.

197. Pathak, S.S.; Savelkoul, H.F.J. *Immunol. Today.* **1997**, 18, 464-467.

198. Jönsson, U.; Fägerstam, L.; Löfas, S.; Stenberg, E.; Karlsson, R.; Frostell, A.; Markey, F.; Schindler, F. *Ann. Biol. Clin.* **1993**, 51, 19-26.

199. WWW URL for Windsor Scientific IBIS Biosensor, http://www.windsor-ltd.co.uk/ibis.htm

200. WWW URL for Quantech, http://www. biosensor.com/quantech/index.htm

201. WWW URL for Texas Instruments, http://www.ti.com

202. Nelson, P.E.; Plattner, R.D.; Shackelford, D.D.; Desjardins, A.E. *Appl. Environ. Microbiol.* **1992**, 58, 984-989.

203. Chen, J.; Mirocha, C.; Xie, W.; Hogge, L.; Olsen, D. *Appl. Environ. Microbiol.* **1992**, 58, 3928-3931.

204. Gelderblom, W.C.A.; Jaskiewicz, K.; Marasas, W.F.O.; Thiel, P.G.; Horak, R.M.; Vleggaar, R.; Kriek, N.P.J. *Appl. Environ. Microbiol.* **1988**, 54, 1806-1811.

205. Chu, F.S.; Li, G.Y. *Appl. Environ. Microbiol.* **1994**, 60, 847-852.

206. Murphy, P.A.; Rice, L.G.; Ross, P.F. *J. Agric. Food Chem.* **1993**, 41, 263-266.

207. Rheeder, J.P.; Marasas, W.F.O.; Theil, P.G.; Sydenham, E.W.; Shepard, G.S. *Phytopathol.* **1992**, 82, 352-357.

208. Ross, P.F.; Rice, L.G.; Osweiler, G.D.; Nelson, P.E.; Richard, J.L.; Wilson, T.M. *Mycopatholo.* **1992**, 117, 109-114.

209. Theil, P.G.; Shepard, G.S.; Sydenham, E.W.; Marasas, W.F.O.; Nelson, P.E.; Wilson, T.M. *J. Agric. Food Chem.* **1991**, 39, 109-111.

210. Kellerman, T.S.; Marasa, W.F.O.; Theil, P.G.; Gelderblom, W.C.A.; Cawood, M.E.; Cootezer, J.A. *J. Vet. Res.* **1990**, 57, 269-275.

211. Harrison, L.R.; Colvin, B.M.; Greene, J.T.; Newman, L.E.; Cole, J.R. *J. Vet. Diagn. Invest.* **1990**, 2, 217-221.

212. Gelderblom, W.C.A.; Kriek, N.P.J.; Marasas, W.F.O.; Thiel, P.G. *Carcinogenesis.* **1991**,12, 1247-1251.

213. Brown, T.P.; Rottinghaus, G.E.; Williams, M.E. *Avian Dis.* **1992**, 36, 450-454.

214. Gelderblom, W.C.A.; Cawood, M.E.; Snyman, S.D.; Vleggaar, R.; Marasas, W.F.O. *Food Chem. Toxicol.* **1993**, 31, 407-414.

215. Norred, W.P.; Voss, K.A. *J. Food Prot.* **1994**, 57, 522-527.

216. ApSimon, J.W.; Miller, J.D. *Na Toxins.* **1996**, 4, 1-2.

217. Gelderblom, W.C.A., Kriek, N.P.J., Marasas, W.F.O., and Thiel, P.G. *Carcinogenesis.* **1991**, 12, 1247-1251.

218. Norred, W.P. *J. Toxicol. Enviro. Health.* **1993**, 38, 309-328.

219. Shepard, G.S.; Theil, P.G.; Stockenstrom, S.; Sydenham, E.W. *J. AOAC Int.* **1996**, 79, 671-686.

220. Sheppard, G.S.; Sydenham, E.W.; Theil, P.G.; Gelderblom, W.C.A. *J. Liq. Chromatogr.* **1990**, 13, 2077-2087.

221. Scott, P.M.; Lawerence, G.A. *J. AOAC Int.* **1992**, 75, 829-834.

222. Bennett, G.A.; Richard, J.L. *J. AOAC Int.* **1994**, 77, 501-506.

223. Holcomb, M.; Sutherland, J.B.; Chiarelli, M.P.; Korfmacher, W.A.; Thompson, H.C. Jr.; Lay, J.O.; Hankins, L.J.; Cerniglia, C.E. *J. Agric. Food Chem.* **1993**, 42, 2064-2067.

224. Maragos, C.M. *J. Agric. Food Chem.* **1995**, 43, 390-394.

225. Hines, H.B.; Brueggemann, E.E.; Holcomb, M.; Holder, C.L. *Rapid Commun. Mass Spectrom.* **1995**, 9, 519-524.

226. Maragos, C.M. *J. Clinical Ligand Assay.* **1997**, 1, 136-140.

227. Scott, P.M. *Food Addit. Contam.* **1997**, 14, 445-450.

228. Yeung, J.M.; Prelusky, D.B.; Savard, M.E.; Dang, B.D.M.; Robinson, L.A. *J. Agric. Food Chem.* **1996**, 44, 3582-3586.

229. Yu, F.Y. *J. Food Prot.* **1996**, 59, 992-997.

230. Sutikno, Abouzied, M.N.; Azconaolivera, J.I.; Hart, L.P. *J. Food Prot.* **1996**, 59, 645-651.

231. Maragos, C.M.; Plattner, R.D.; Miklasz, S.D. *Food Addit. Contam.* **1996**, 13, 105-113.

232. Nezlin, R. *Immunochemistry*; Marcel Dekker: New York, 1994 ; pg. 3-45.

233. Price, C.P. *Clin. Chem. Lab. Med.* **1998**, 36, 341-347.

234. Buck, R.P.; Hatfield, W.E.; Umaana, M.L. Bowden. *Biosensor Technology*; Marcel Dekker: New York, 1990, Chapter 2.

235. Szentirmay, Z. *Spectrochim. Acta.* **1992**, 48A, 9-17.

236. Welford, K. *Opt. Quantum Electron.* **1991**, 23, 1-27.

237. Earp, R.L.; Dessy, R.E. *Commercial Biosensors: Applications to Clinical. Bioprocess. and Enviromental Samples.* John Wiley and Sons: New York, 1996; Chapter 4.

238. Yeung, J.M.; Prelusky, D.B.; Savard, M.E.; Dang, B.D.M.; Robinson, L.A. *J. Agric. Food Chem.* **1996**, 44, 3582-3586.

239. Chard, T. *Laboratory Techniques in Biochemistry and Molecular Biology*, Volume 6; Elsevier: New York, 1995; pg.45.

240. Fontana, E.; Pantell, R.H.; Strober, S. *Appl. Opt.* **1990**, 29, 4694-4701.

241. Cambell, D.S. *Mechanical Properties of Thin Films. Handbook of Thin Films Technology*; McGraw-Hill: New York, 1970; pg. 129.

242. Leidberg, B.; Ivarsson, B.; Hegg, P.O.; Lundström, I. *J. Colloid Interface Sci.* **1986**, 114, 386-392.

243. Malmsten, M. *Biopolymers at Interfaces*, Marcel Dekker: New York, 1998; Chapter 2.

244. Haynes, C.A.; Norde, W. *Collids Surf. B.* **1994**, 2, 517-523.

245. Nordes, W. *Adv. Colloid Interface Sci.* **1986**, 25, 267-271.

246. Oroszian, P.; Thommen, C.; Wehrli, M.; Duveneck, G.; Ehrat, M. *Anal. Meth. Instrum.* **1993**,1, 43-51.

247. You, H.X.; Lowe, C.R. *J. Colloid Interface Sci.* **1996**, 182, 586-591.

248. Geddes, N.J.; Martin, A.S.; Caruso, F.; Urquhart, R.S.; Furlong, D.N.; Sambles, J.R.; Than, K.A.; Edgar, J.A. *J. Immunol. Meth.* **1994**, 175, 149-155.

249. Caruso, F.; Vukusic, P.S.; Matsuura, K.; Urquhart, R.S.; Furlong, D.N.; Okahata, Y. *Colloids Surf. A.* **1995**, 103, 147-157.

250. Texas Instruments TISPR - 1 Experimenters Kit, http://www.ti.com/research/docs/spr/surface.htm.

251. Melendez, J.; Carr, R.; Bartholomew, D.; Taneja, H.; Yee, S.; Jung, C.; Furlong, C. *Sens. and Actuators.* **1997**, 38, 375-379.

252. Woodbury, R.G.; Wendin, C.; Clendenning, J.; Furlong, C.; Melendez, J.; Elkind, J.; Bartholomew, D.; Brown, S. *Biosens. Bioelectron.* **1998**, 13, 1117-1127.

253. Brown, S. *Nat. Biotechnol.* **1997**, 15, 269-272.

254. Fagerstam, L.G. ; Frostell-Karlsson, A.; Karlsson, R.; Persson, B.; Ronnberg, I. *J. Chromatogr.* **1992**, 597, 397-404.

255. Owega, S.; Lai, E.P.C.; Mullett, W. M. *J. Photochem. Photobiol.* **1998**, 119, 123-136.

256. Rudiger, A.H. *Anal. Biochem.* **1999**, 275, 162-170.

APPENDIXES

A.1 Appendix A

All UV absorption spectra were obtained using a Cary 3 UV-spectrophotometer from Varian (Palo Alto, CA). The instrumental parameters included a scan rate of 360 nm/min, signal averaging time of 0.167 second and 10 mm quartz cuvettes.

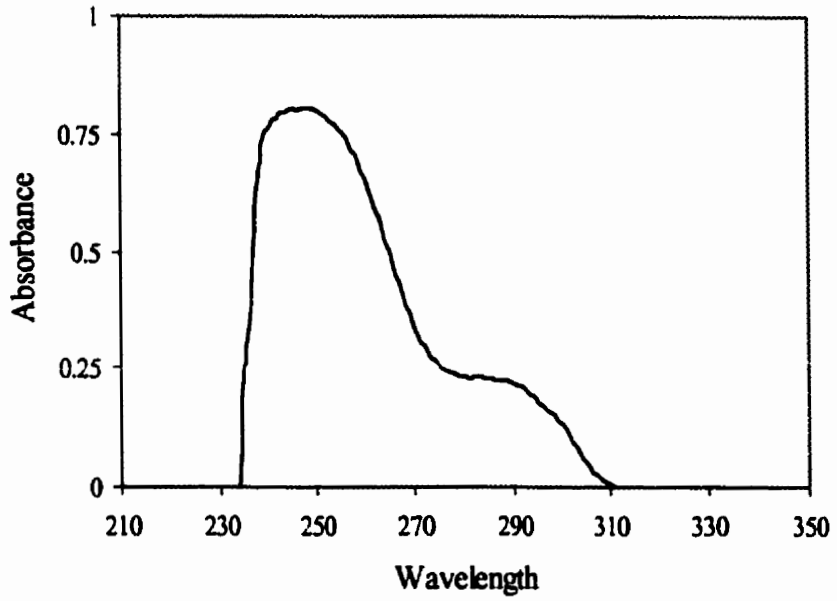

Figure A.1: UV Spectrum of 10 µg/mL acetaminophen in chloroform.

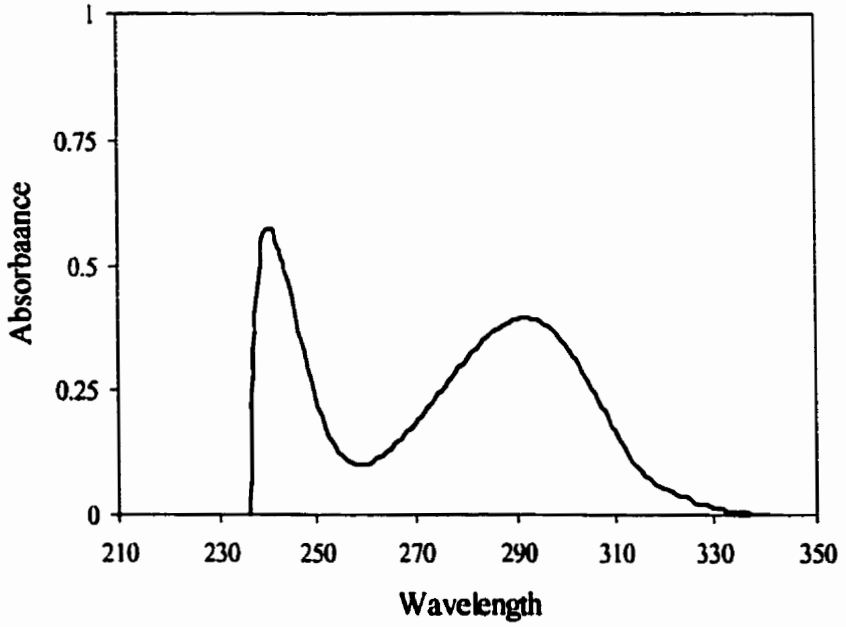

Figure A.2: UV spectrum of 10 µg/mL 2-aminopyridine in chloroform.

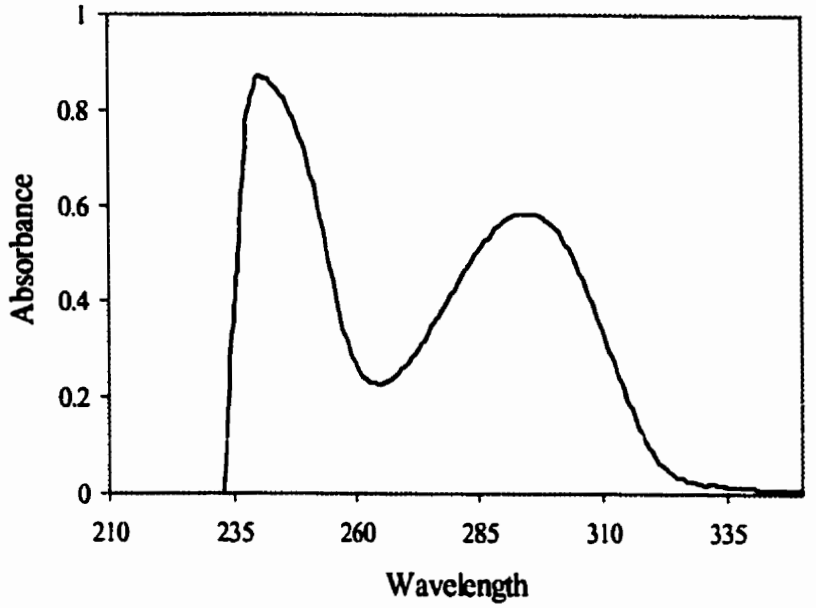

Figure A.3: UV spectrum of 10 µg/mL 3-aminopyridine in chloroform.

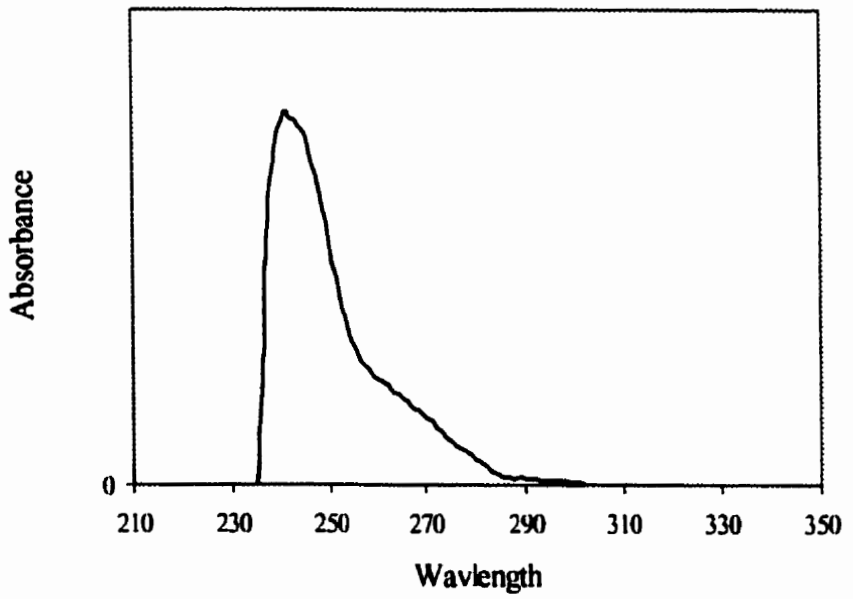

Figure A.4: UV spectrum of 10 µg/mL 4-aminopyridine in chloroform

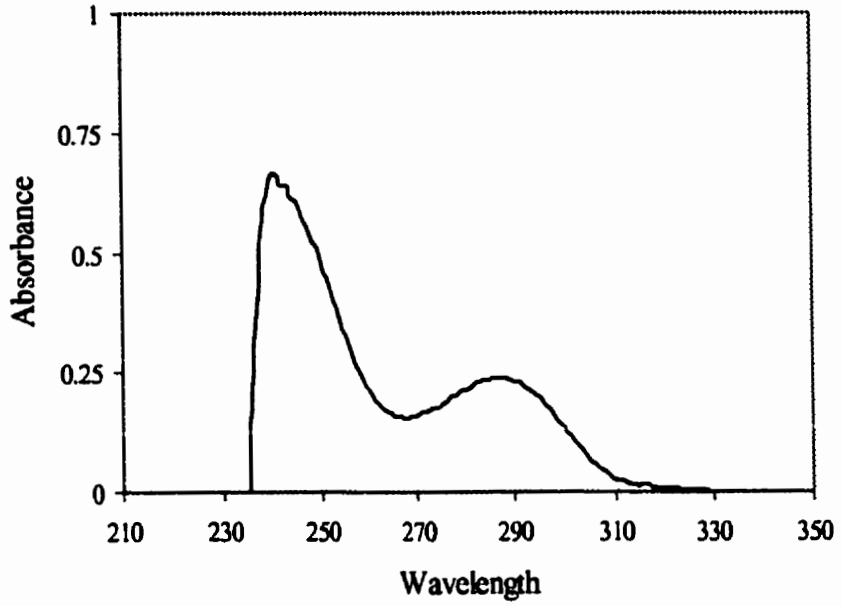

Figure A.5: UV spectrum of 10 µg/mL aniline in chloroform.

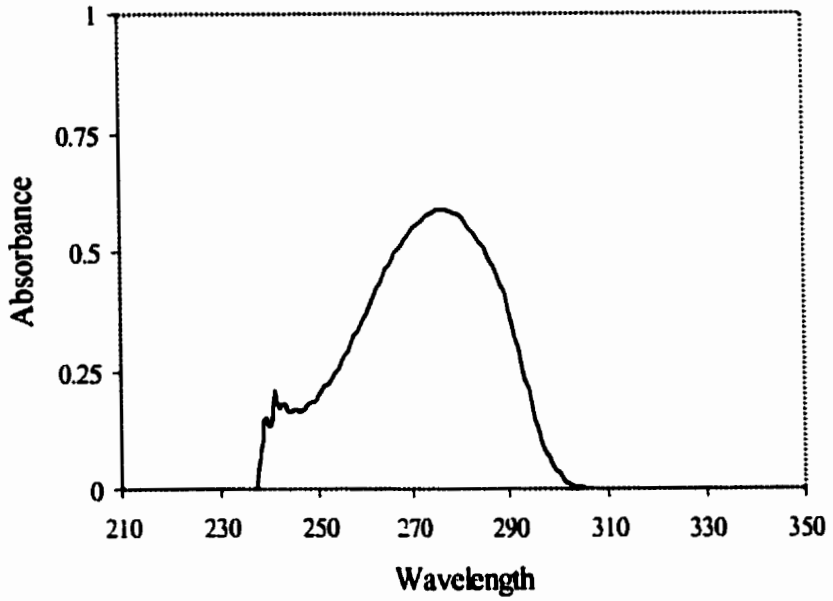

Figure A.6: UV spectrum of 10 µg/mL β-hydroxyethyltheophylline in chloroform.

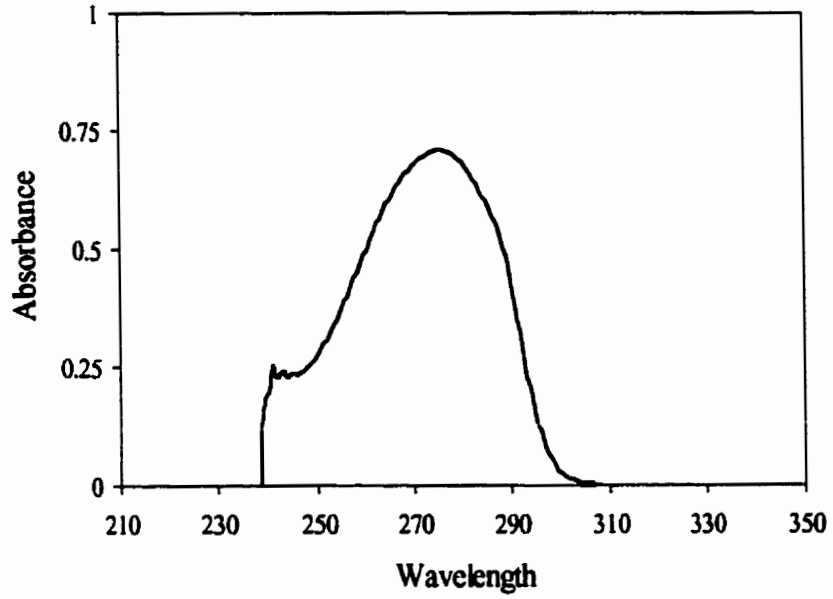

Figure A.7: UV spectrum of 10 µg/mL caffeine in chloroform.

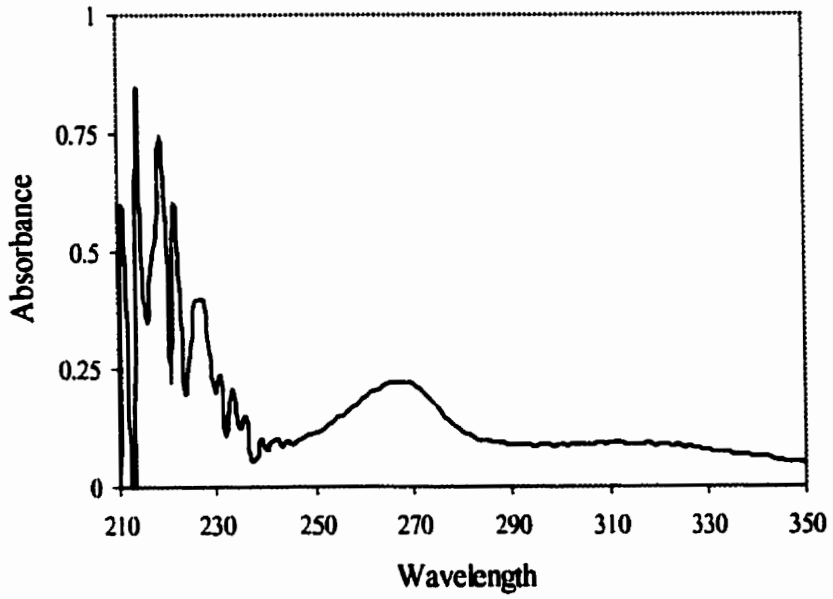

Figure A.8: UV spectrum of 100 µg/mL hydrochlorothiazide in chloroform.

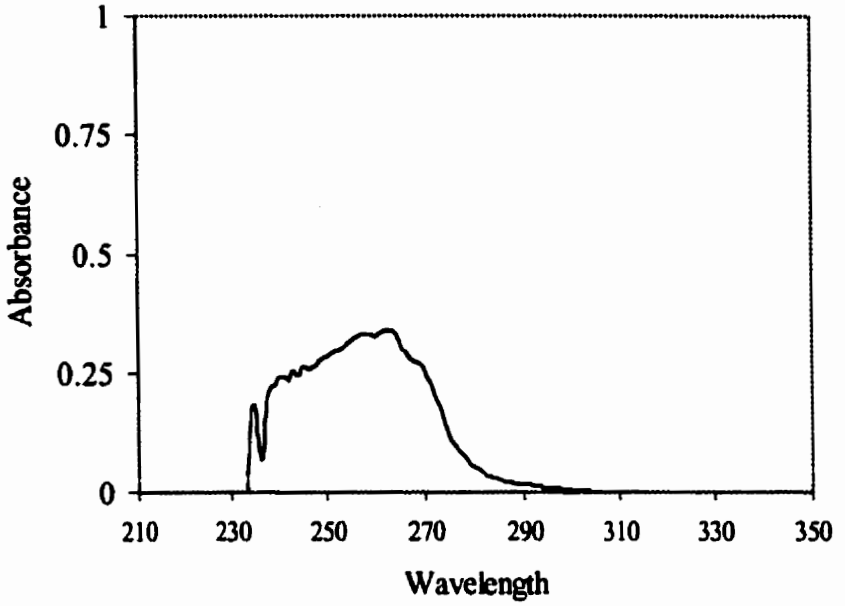

Figure A.9: UV spectrum of 1 µg/mL 2-methylpyrazine in chloroform.

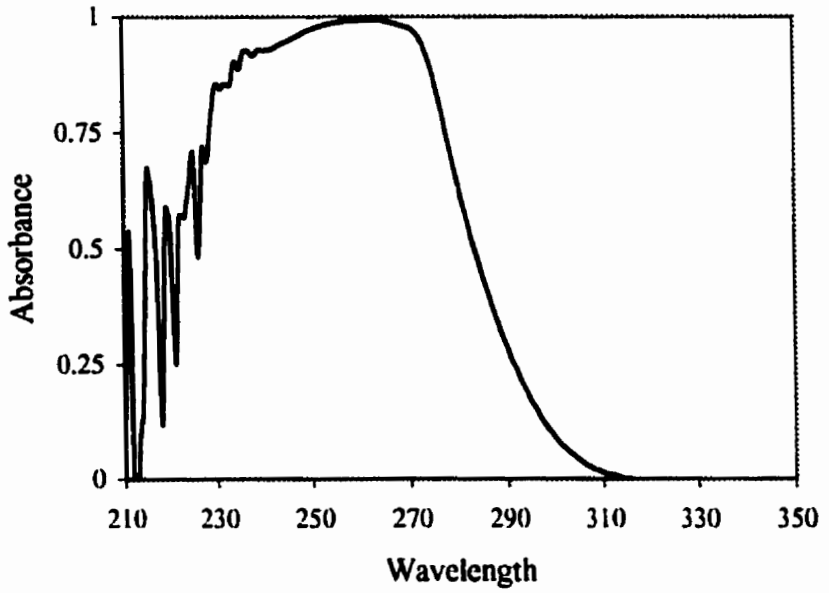

Figure A.10: UV spectrum of 100 µg/mL nicotinic acid in chloroform.

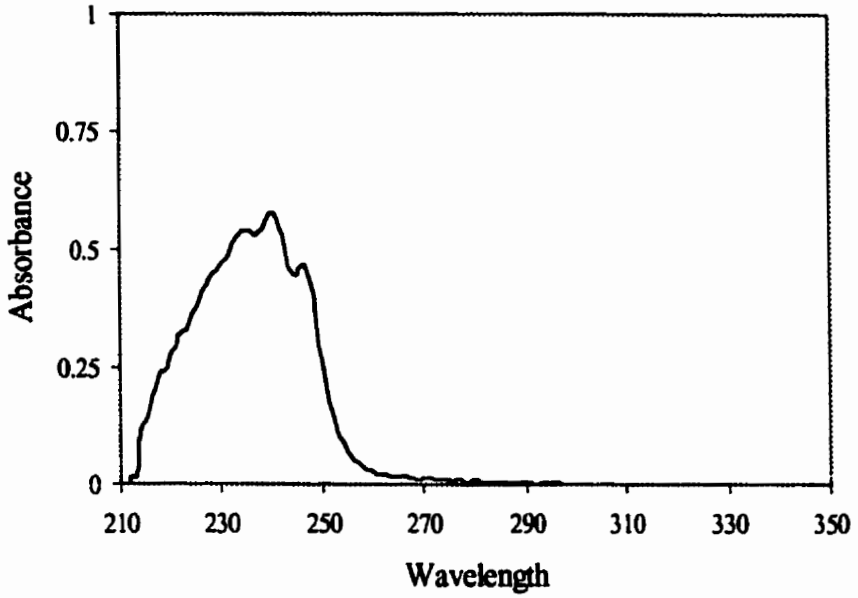

Figure A.11: UV spectrum of 10 µg/mL 2-picoline in chloroform.

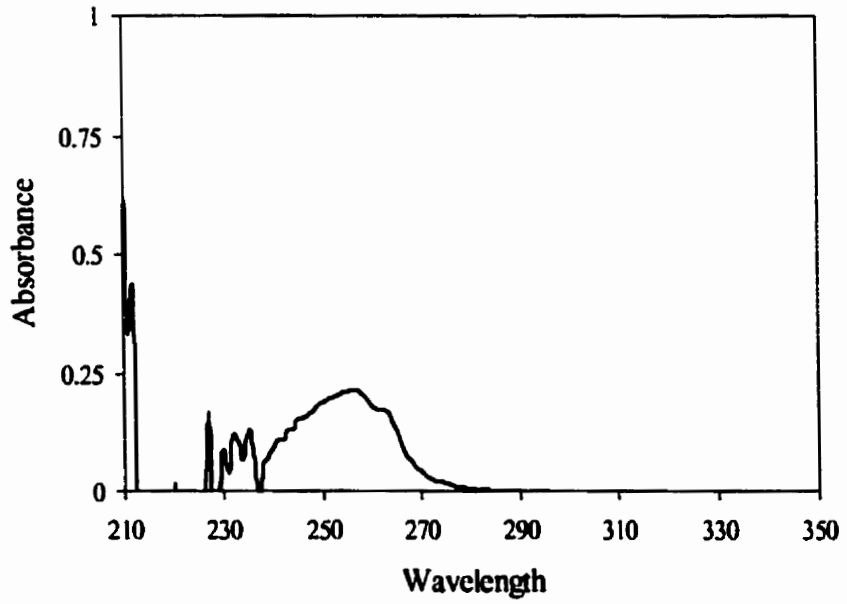

Figure A.12 UV spectrum of 10 µg/mL 4-picoline in chloroform.

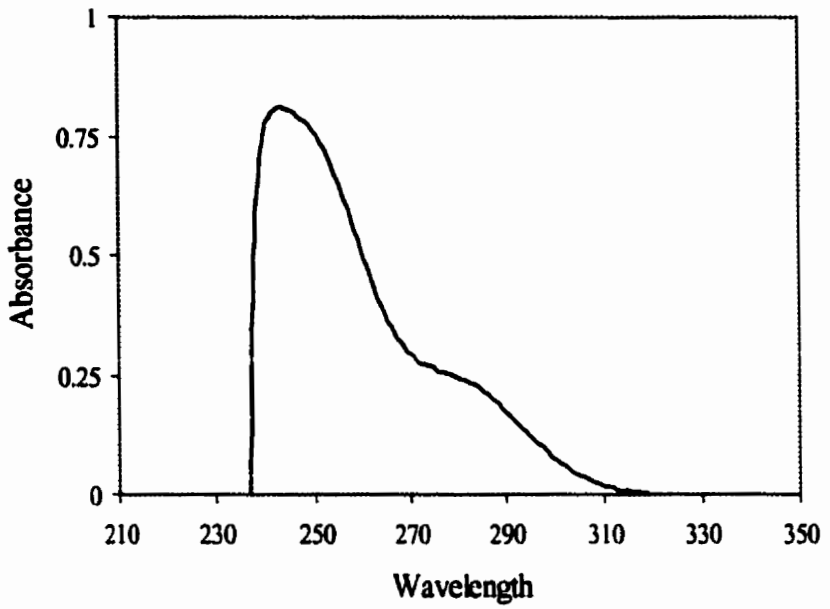

Figure A.13: UV spectrum of 10 µg/mL phenylbutazone in chloroform.

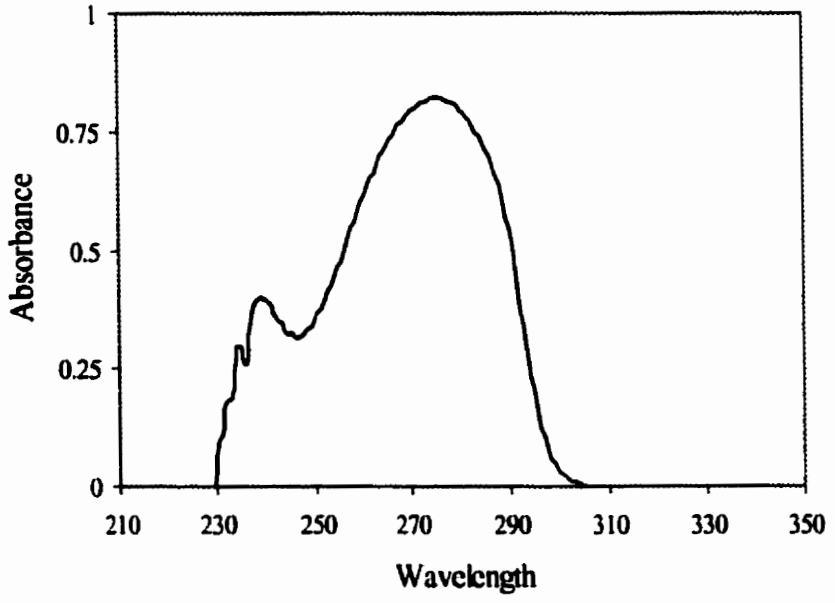

Figure A.14: UV spectrum of 10 µg/mL theobromine in chloroform.

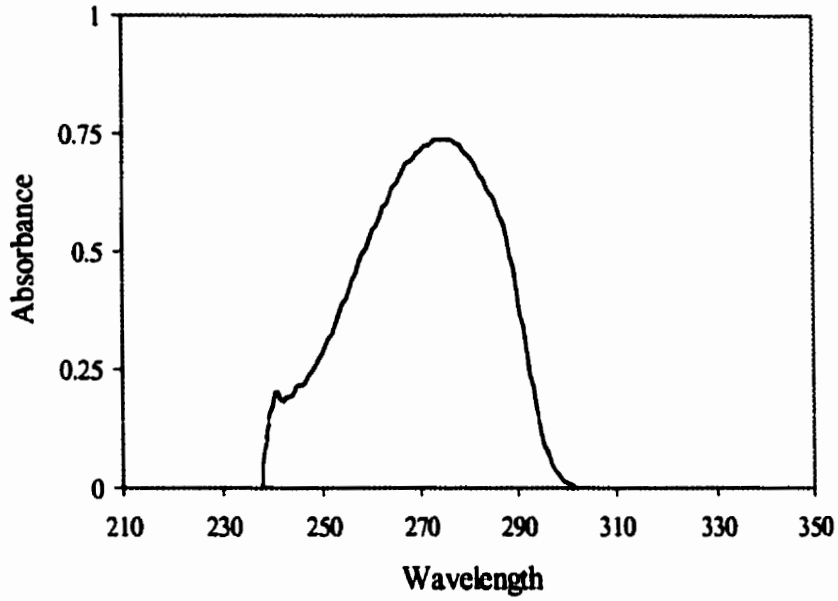

Figure A.15: UV spectrum of 10 µg/mL theophylline in chloroform.

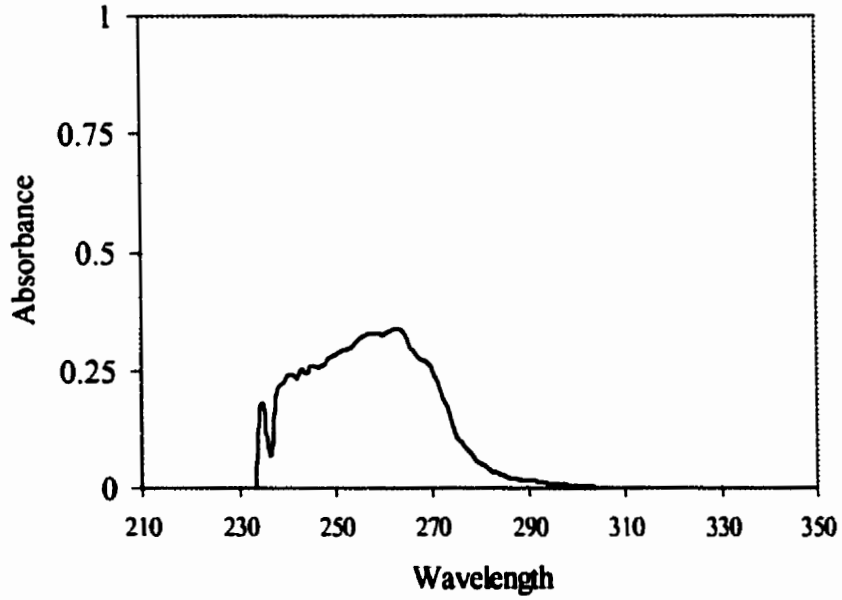

Figure A.16: UV spectrum of 10 µg/mL nicotine in chloroform.

Appendix B

Chemical	Supplier Name and Location
acetaminophen	Health Canada (Ottawa, ON)
acetic acid	Anachemica (Montreal, QC)
acetone	Caledon (Georgetown, ON)
acetonitrile	Caledon (Georgetown, ON)
AIBN	Pfaltz & Bauer (Waterbury, CT)
2-aminopyridine	Sigma (St. Louis, MO)
3-aminopyridine	Sigma (St. Louis, MO)
4-aminopyridine	Sigma (St. Louis, MO)
aniline	Sigma (St. Louis, MO)
β-hydroxyethyltheophylline	Health Canada (Ottawa, ON)
BSA	Sigma (St. Louis, MO)
caffeine	Sigma (St. Louis, MO)
chloroform	Caledon (Georgetown, ON)
dyphylline	Health Canada (Ottawa, ON)
EDMA	Pfaltz & Bauer (Waterbury, CT)
ethanol	Caledon (Georgetown, ON)
FB_1	Sigma (St. Louis, MO)
hydrochlorothiazide	Health Canada (Ottawa, ON)
MAA	Pfaltz & Bauer (Waterbury, CT)
methanol	Caledon (Georgetown, ON)
methylene chloride	Caledon (Georgetown, ON)
4-methylpyrazine	Sigma (St. Louis, MO)
myosmine	Sigma (St. Louis, MO)
nicotine	Sigma (St. Louis, MO)
nicotinic acid	Health Canada (Ottawa, ON)
phenylbutazone	Health Canada (Ottawa, ON)
phosphatidylcholine	Sigma (St. Louis, MO)
2-picoline	Sigma (St. Louis, MO)
4-picoline	Sigma (St. Louis, MO)
1-propranol	Caledon (Georgetown, ON)
2-propranol	Caledon (Georgetown, ON)
sodium chloride	Sigma (St. Louis, MO)
sodium dihydrogen orthrophosphate	Sigma (St. Louis, MO)
TEA	Sigma (St. Louis, MO)
TFA	Sigma (St. Louis, MO)

Chemical	Supplier Name and Location
theobromine	Health Canada (Ottawa, ON)
theophylline	Sigma (St. Louis, MO)
TRIM	Sigma (St. Louis, MO)
Tween 20	Sigma (St. Louis, MO)
xanthine	Health Canada (Ottawa, ON)